Revitalizing polymers:

Repolymerization of mechanochemically activated waste polymers utilizing RAFT-capable agents & ball mill grinding

MSc Thesis

Endino Gieske

Delft University of Technology

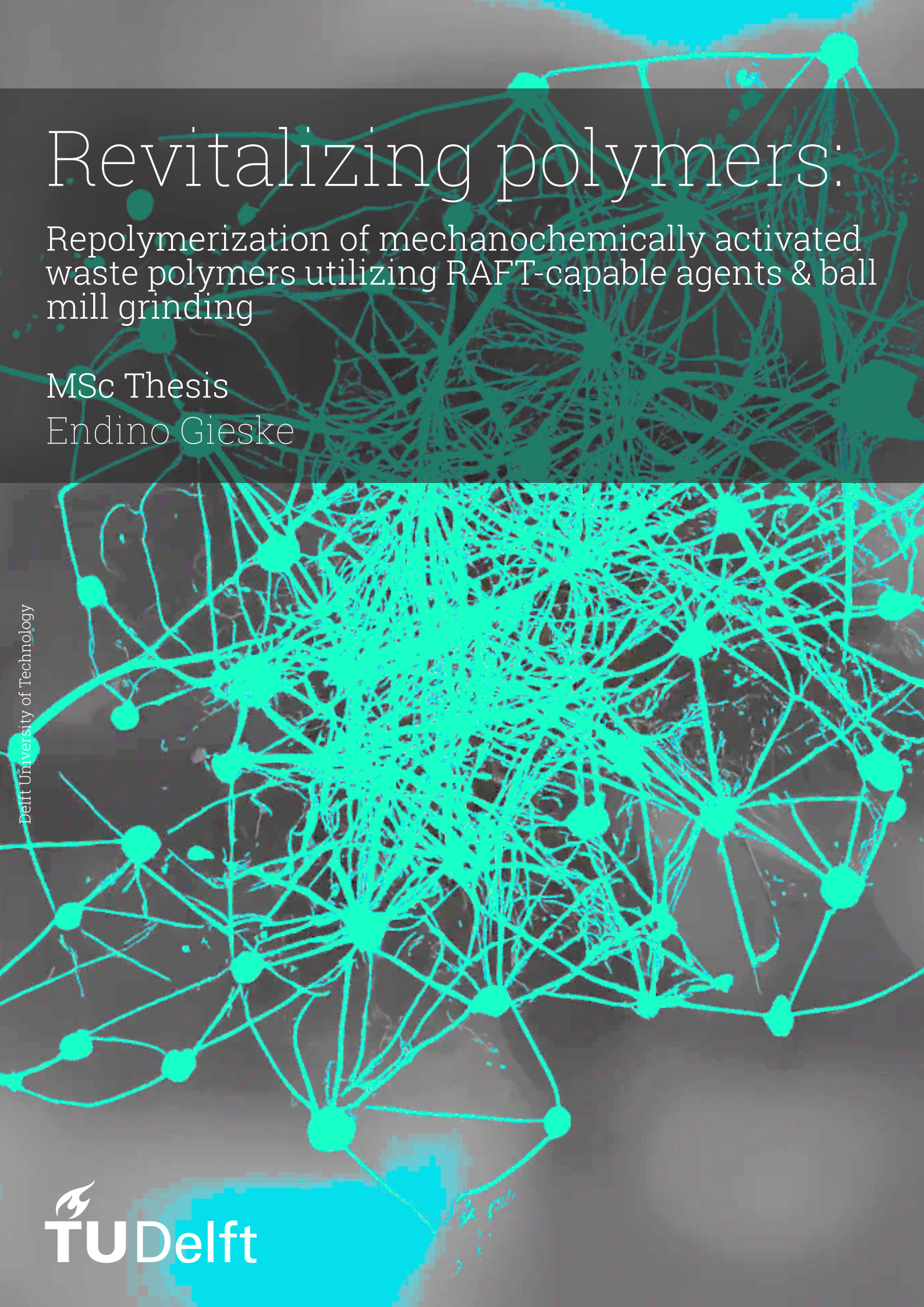

TU Delft

Revitalizing polymers:

Repolymerization of mechanochemically activated waste polymers utilizing RAFT-capable agents & ball mill grinding

by

Endino Gieske

Student Name	Student Number
Endino Gieske	5186137

Supervisor: Georgy A. Filonenko
Committee members: Evgeny A. Pidko, Stephen J. Picken & Rienk Eelkema
Project Duration: July, 2023 - January, 2024
Faculty: Faculty of Chemical Engineering, Delft

Cover: Revitalized ”living” polymer network

TU Delft

Preface

”Man cannot survive except through his mind. He comes on earth unarmed. His brain is his only weapon. Animals obtain food by force. Man has no claws, no fangs, no horns, no great strength of muscle. He must plant his food or hunt it. To plant, he needs a process of thought. To hunt, he needs weapons, and to make weapons - a process of thought. From this simplest necessity to the highest religious abstraction, from the wheel to the skyscraper, everything we are and everything we have comes from a single attribute of man - the function of his reasoning mind.”

”But the mind is an attribute of the individual. There is no such thing as a collective brain. There is no such thing as a collective thought. An agreement reached by a group of men is only a compromise or an average drawn upon many individual thoughts. It is a secondary consequence. The primary act - the process of reason - must be performed by each man alone.”

”And only by living for himself was he able to achieve the things which are the glory of mankind. Such is the nature of achievement.” -Howard Roark in The Fountainhead by Ayn Rand.

A challenging many months,
Mired by confusion in the blurry unknown,
A brave new world one confronts,
The unravelling of knowledge and setting it into stone.

Endino Gieske
Delft, April 2024

Summary

Highlights

- PMMA & PS undergo segmentation, resulting in low molecular weight and moderate dispersity.
- The generation of polymer radical species is observed, and these radicals rapidly engage in reactions to form new end groups.
- Termination of polymer chain end groups into ”living” RDRP capable polymers.
- Terminated polymer chains undergo repolymerization and copolymerization toward regenerated polymers or copolymers, respectively.

Abstract

Plastics are a common material used in everyday life due to their desirable mechanical properties and affordability. However, their utilization pose challenges at the end of their lifecycle, leading to environmental pollution. Therefore the valorization of waste plastics is very important. In order to address this, we propose a mechanochemical approach to activate inert polymers found in common plastics, transforming them into reactive polymers suitable for high-value product synthesis. With the use of ball mill grinding, common polymers such as PMMA and PS underwent chain scission and their molecular weight distribution and functional groups were analyzed. Segmentation of polymers asymptotically reach a minimum molecular weight and dispersity. The chain scission of these polymers can form radicals which rapidly undergo reactions to form new groups such as alkenes. In the presence of radical scavengers, these polymeric radicals are terminated towards RAFT capable polymers. PMMA and PS are successfully terminated with trithiocarbonate and dithiobenzoate groups, followed by repolymerization and copolymerization with respective monomers and comonomers into regenerated polymers or block copolymers. Several factors affect the effective termination of the polymers toward RAFT capable polymers, warranting further optimization. The method explored in this work offers an avenue for the complete recycling and upcycling of waste plastics into high value products, which can be a technologically feasible method to tackle the global problem of plastic waste.

Contents

1

Introduction

Amidst the rapid economic expansion witnessed over the past century, the role of plastics in fostering this growth must not be underestimated. Plastics, renowned for their cost-effectiveness, lightweight nature and durability, have become commonplace in applications ranging from packaging and construction to various consumer goods. Plastic production, which amounted to 2 million metric tons in 1950 [1], has undergone remarkable growth, reaching a staggering 459 million metric tons by 2019. This astonishing surge represents a 230-fold increase over the span of 69 years. Nevertheless, this growth in production has resulted in an increase of plastic waste, presenting substantial environmental challenges [2, 3]. The damaging effects of plastic pollution extend beyond environmental concerns. Plastics lead to the formation of micro and nanoplastics that infiltrate soil, groundwater, and eventually make their way into the food chain [4]. These minuscule plastic particles, in consequence, give rise to detrimental health effects, spanning developmental, reproductive, locomotor, immunotoxic, genotoxic, and cytotoxic effects [5]. Certain polymers may have negative health impacts on humans, as illustrated by the genotoxicity of polyethylene (PE), the cytotoxicity of polypropylene (PP) and more [6]. Polystyrene (PS), the primary constituent in styrofoam, stands out as one of the most toxic polymers, owing to its monomer styrene, a recognized toxicant. Polymethyl methacrylate (PMMA), a widely used thermoplastic, demonstrates notable toxicity such as inducing spleen enlargement in mice [6]. In light of these concerns, the need to actively engage in the sustainable recycling of waste plastics and mitigate plastic pollution becomes apparent.

There are various methods available for plastic recycling; however, they currently still fall short of effectively managing all plastic waste. There is an increasing level of awareness regarding the consequences of plastic pollution and importance of recycling, particularly among well-educated and younger demographics [7]. Despite the notable emphasis on plastic recycling, globally only 8.3% of the plastic produced in 2022 underwent post-consumer recycling [8]. Noteworthy is the leadership of the Netherlands in plastic recycling during the same period, achieving a recycling rate of 45% for post-consumer plastic, while the remaining portion underwent incineration. The methodologies employed for plastic recycling can be broadly categorized into two primary types: mechanical and chemical recycling [9]. Mechanical recycling, a straightforward technique, typically involve shredding, melting, and extrusion applied to plastic waste streams. However, it often results in the degradation of the material properties and is limited to specific plastics. Additionally, the mechanical shredding process is known to generate considerable amounts of micro and nanoplastics [10]. In contrast, chemical recycling seeks to transform waste plastics into valuable products which can be different from plastics themselves [9, 11]. Chemical recycling or upcycling encompass various methods, such as incineration, gasification, solvolysis, and pyrolysis.

Methods for chemical recycling have several benefits over mechanical recycling, however also pose their own unique challenges. Incineration emerges as an economically attractive approach for valorizing waste plastics, leveraging the energy released from plastic combustion to generate power [11]. Nevertheless, its viability is hindered by its harmful gas emissions, such as SO_x, NO_x, and N_2O. Gasification, operating at elevated temperatures (700-1200 °C), prioritizes the production of syngas (a blend

of CO and H_2) that can be further utilized for the generation of hydrocarbons [11, 12]. Gasification is valued for its flexibility in handling various inputs, extending beyond plastic waste to include biomass, sewage sludge, and industrial waste. This flexibility enables the efficient management of heavily contaminated plastic waste streams. Solvolysis is a plastic waste valorization technique which involves the recovery of the polymer's constituent monomers at relatively moderate temperatures. This process utilizes a solvent that acts as a catalyst, inducing the depolymerization of the polymer [9]. Solvolysis facilitates the retrieval of monomers while separating additives. The retrieval of the monomers allows for subsequent polymerization back to the original polymer. However, its functionality is confined to specific chemical bonds, limiting its applicability to certain types of plastics. Lastly, pyrolysis, operating at high temperatures (300-1300 °C) and under an inert atmosphere, yields a diverse array of products similar to those obtained from crude oil [9], sometimes referred to as plastic oil, consisting primarily of hydrocarbons [11, 13]. Despite the potential demonstrated by these recycling technologies, each face unique technical and economic challenges. In light of these impediments, there is a need to investigate innovative approaches for transforming plastic waste streams into high-value products.

The majority of commonly used plastics undergo synthesis through Free Radical Polymerization (FRP), a process reliant on a radical source to react with a monomer to initiate the polymerization reaction. The polymerization progresses as the radical reacts with additional monomers until it recombines with another radical, thereby terminating the polymerization reaction. Once a polymer synthesized via FRP has undergone termination, the polymer ceases to grow and is therefore considered a "dead" polymer. While FRP offers a straightforward method for synthesizing large polymers, it lacks precise control over chain length and the distribution of polymer chain lengths. The variation in chain lengths is referred to as dispersity and quantified by the Poly Dispersity Index (PDI). The inherent characteristics of FRP-based polymers, such as the high PDI, contribute to sub-optimal mechanical properties and can potentially limit its applicability. These limitations have led researchers to explore alternative methods for polymer synthesis.

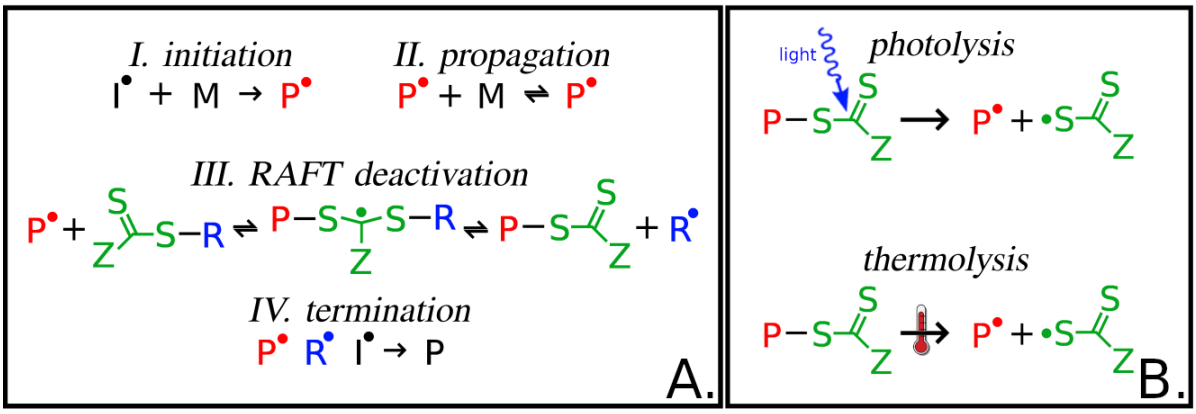

Figure 1.1: A: Mechanism of the Reversible Addition-Fragmentation Chain Transfer (RAFT) polymerization reaction. I.) Initation step via a source of radicals $I^{\bullet}$ reacting with a monomer M, II.) Propagation step, whereby polymer chain $P^{\bullet}$ is extended, III.) RAFT deactivation step, in which a RAFT agent captures a propagating polymer radical and is able to reversibly deactivate the propagating radical, IV.) Termination step, whereby a polymeric macroradical recombines with another radical to form a "dead" and inert polymer, terminating the polymerization reaction. **B:** (reversible) Lysis of the RAFT end group via photons (photolysis) or via thermal excitation (thermolysis).

Controlled Radical Polymerization (CRP), more accurately termed Reversible Deactivation Radical Polymerization (RDRP), is a method employed for precise control over the polymerization process. A key feature of RDRP is its ability to halt (deactivate) polymerization, yet this deactivation is reversible, allowing for subsequent polymerization. In RDRP, the concentration of active radicals is kept low by reversibly deactivating them with the aid of a chain transfer agent. This reversible deactivation imparts a "living" nature to RDRP-based polymers, as the low radical concentration significantly suppresses the undesired termination reaction. Various RDRP-based chemistries exist including Nitroxide-Mediated Polymerization (NMP) [14], Atom Transfer Radical Polymerization (ATRP) [15], iodine based degenerative chain transfer [16], catalytic chain transfer [17] and Reversible Addition-Fragmentation Chain

Transfer (RAFT) [18, 19]. Of particular relevance to this study is RAFT polymerization, where a chain transfer agent, typically comprising dithioesters or trithiocarbonates groups, mediates the radical polymerization process. The mechanism of RAFT polymerization is illustrated in Figure 1.1. Initiating RAFT polymerization requires an initiator, typically an agent that thermally decomposes into radicals. These radicals then initiate the propagation reaction by reacting with nearby monomers (I. & II.). The resulting propagating radical is subsequently captured by the RAFT agent (III.), which contains groups acting as radical scavengers (e.g. dithioesters/trithiocarbonates). This interaction forms a RAFT-terminated end group on a polymer chain. Importantly, the RAFT-terminated end group can be re-activated, leading to its dissociation (fragmentation) from the polymer chain and the generation of a new propagating macroradical, extending the polymer chain as it comes in contact with monomers. Reactivation of the end group can occur through its reaction with a radical, or at sufficiently elevated temperatures (thermolysis) [18], or through activation using photons (photolysis) [20, 21], particularly blue and green visible light (Figure 1.1). However, the existence of the undesired termination reaction (IV.) is still present in RAFT polymerization, which leads to a small portion of the polymers becoming inert. Irrespective of the termination reaction, ”living” polymers offer significant functionality, allowing the ability to halt and resume the polymerization reaction.

The ”living” nature of RDRP-based polymers extends beyond standard polymerization, involving copolymerization, de-polymerization, and end group transformation. After synthesizing a polymer with monomer A using, for example, RAFT polymerization, the polymer chain can be further elongated with monomer B to produce a block copolymer such as AB, ABA, or any desired copolymer configuration [22]. Depending on the properties of monomers A and B, diverse polymers can be tailored to achieve a wide range of products, such as surfactants and adhesives. Polymeric radicals can undergo de-polymerization, as the polymerization reaction operates in equilibrium between propagation and de-propagation, dependent on factors such as monomer type, monomer concentration, solvent choice, and temperature. Reversed Controlled Polymerization (RCP) is a technique applied to induce de-polymerization in CRP/RDRP-synthesized polymers [23]. Due to thermodynamics, de-propagation typically occurs above a specific temperature, known as the ceiling temperature. Nevertheless, researchers have observed de-polymerization occurring well below the ceiling temperature [23, 24, 25], and even accelerated de-polymerization reactions with the use of photons [26]. End group transformation represents a specific application of RDRP wherein the end group is fragmented to terminate the polymer with a functional group, such as an isocyanate-terminated polymer capable of binding to organic tissue in the presence of water, serving medical adhesive purposes [27]. The capabilities of RDRP-based polymers are considerable; however, the majority of contemporary plastics are the inert FRP-based polymers, lacking the diverse functionalities typical of RDRP polymers. It is therefore intriguing to investigate whether inert FRP-synthesized polymers can be transformed into highly functional RDRP-capable polymers.

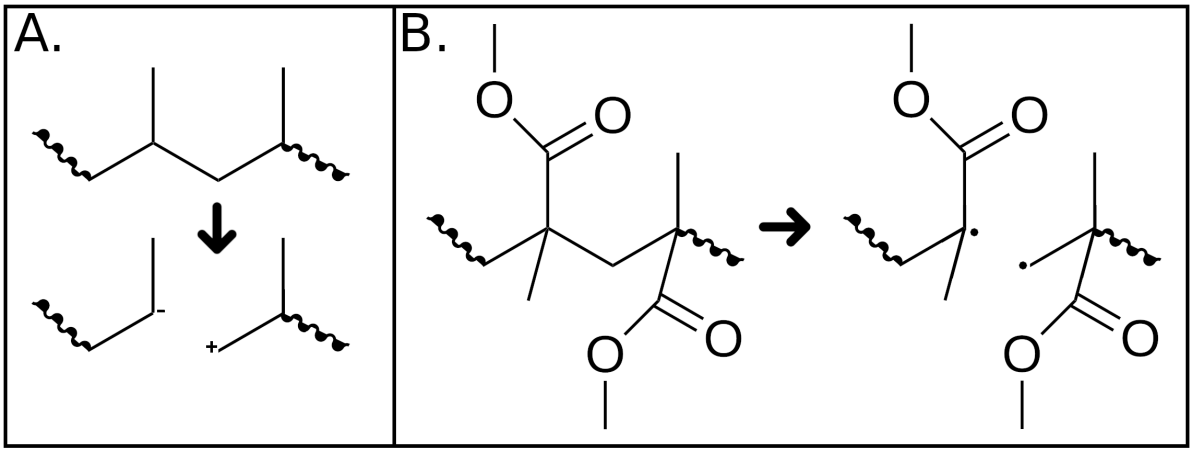

Figure 1.2: A: Heterolytic cleavage of polypropylene, forming an anion and cation pair. **B:** Homolytic cleavage of polymethyl methacrylate, forming two carbon-centered radicals.

Despite the inert nature of FRP polymers, they can participate in certain reactions under ambient conditions. All polymers have the ability to undergo chain scission, where a polymer is cleaved to form two separate polymers. Chain scission can be achieved mechanically by stretching/extending the polymer chain such that the backbone fractures [28]. These polymers can undergo two different types of scission: heterolytic cleavage and homolytic cleavage. In heterolytic chain scission the electrons of the dissociated bond arrange themselves to form an anion and a cation pair [29, 30]. Conversely, in homolytic chain scission, the electrons form two carbon-centered radicals [31, 32], illustrated in Figure 1.2.

Various methods can induce polymeric chain scission, with notable techniques including high-energy radiation [33], thermal degradation [34, 35], and mechanical degradation [32, 36]. Mechanical degradation, a straightforward approach, functions by applying external stress to the polymer, causing it to fracture and segment into multiple chains. Polymer segmentation can be achieved through methods such as extrusion [37], ultrasonication [38], shear flow [39, 40], and ball mill grinding [41, 42]. Chain scission enables previously inert polymers to undergo reactions at ambient conditions. In the case of homolytic cleavage, two radicals are formed, capable of participating in radical reactions. Choi et al. reported the depolymerization of poly(α-methyl styrene) through ball grinding under mild conditions, yielding 64% of its monomers [43]. Balema et al. achieved depolymerization of PS under ambient conditions, yielding 8% of the monomers [44]. Interestingly, when milling was performed using silicon nitride (Si_3N_4) milling chambers and balls, the depolymerization was significantly suppressed, suggesting metals catalyze the depolymerization reaction. Other studies demonstrated that solid-state polymerization from monomers was achievable using ball mill grinding [45, 46]. Mechanochemical activation of inert polymers allows for the termination of the polymer end group with a chemical moiety, introducing a new functional group. This approach was employed by Weber et al. [47], who terminated PMMA macroradicals through ultrasonication in the presence of a molecule containing a nitroxide radical moiety, forming an end group capable of Nitroxide-Mediated Polymerization. They have therefore shown that inert FRP based polymers can be converted into highly functional RDRP-capable polymers.

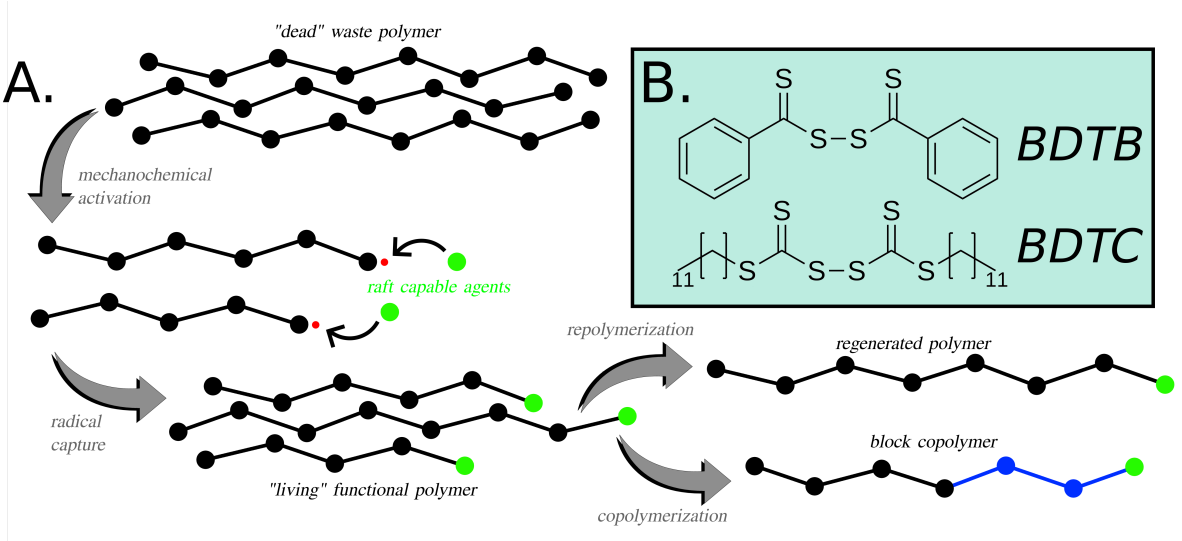

Figure 1.3: A: Simplified schematic of the objective of this study; the mechanochemical activation of inert RDRP based polymers, capturing of the radicals with the use of RCA, whereafter reactivity experiments are performed in order to regenerate the polymer or to form block copolymers. **B:** Structure of bis (dithio benzoate) (BDTB) and structure of bis (dodecyl trithiocarbonate) (BDTC).

The objective of this study is to research whether the mechanochemical activation of FRP-synthesized PMMA and PS in the presence of RCA towards the functionalization of these polymers is possible (illustrated in Figure 1.3A). The approach involves investigating the segmentation of both PS and PMMA through ball mill grinding, referred to simply as milling, and assessing the impact on their end groups. Secondly, the study explores the effects of milling in the presence of two RCA, namely bis (dodecyl trithiocarbonate) (BDTC) and bis (dithio benzoate) (BDTB), shown in Figure 1.3B. These compounds

are typically used as precursors for RAFT agent synthesis. The choice of precursors over the standard RAFT agents allows for the utilization of the two RCA present in the precursors, resulting in a theoretical RCA usage of 100% instead of 50%. In the third phase, the chemical reactivity of the newly functionalized PS and PMMA is evaluated by conducting re-polymerization in the presence of native and co-monomers. This step allows for the re-extension of the milled polymers and the synthesis of block copolymers.

2

Materials & Methods

Materials: Sodium Hydride (NaH, Aldrich, 90.0%) was stored under argon at room temperature. Methyl acrylate ($C_4H_6O_2$, Tokyo Chemical Industry, >99.0%), tert-butyl acrylate ($C_7H_{12}O_2$, Tokyo Chemical Industry, >98.0%), methyl methacrylate ($C_5H_8O_2$, Tokyo Chemical Industry, >99.8%) and styrene (C_8H_8, Aldrich, >99.0%) were all degassed and stored under argon prior to use. Azobisisobutyronitrile (AIBN) ($C_8H_{12}N_4$, Aldrich) was dissolved in diethylether and recrystallized prior to use. Polymethyl methacrylate (PMMA) ($(C_5H_8O_2)_n$, Tokyo Chemical Industry) was filtered to obtain particle sizes between 50-250 µm. Polystyrene (PS) ($(C_8H_8)_n$, Acros Organics) pellets were first ground with a blade grinder, and afterwards filtered to obtain particle sizes between 50-250 µm. 1-dodecanethiol ($C_{12}H_{25}SH$, Aldrich, >98.0%), carbon disulfide (CS_2, Tokyo Chemical Industry, >98.0%) and phenylmagnesium chloride THF solution (C_6H_5MgCl, Aldrich, 2 mol L^{-1}) were used without further processing.

Synthesis: *bis (dodecyl trithiocarbonate) (BDTC)*; For the synthesis of bis (dodecyl trithiocarbonate) (BDTC, $C_{26}H_{50}S_6$), we follow the procedure provided by Abel & Cormick [48], a stirred suspension of sodium hydride (1.68 g, 70.0 mmol) in anhydrous diethyl ether (350 mL) was made under an inert (Ar) environment. Dropwise, 1-dodecanethiol (15 g, 88 mmol) was added over 30 minutes, whereby gentle bubbling was observed (hydrogen evolution reaction). The reaction mixture was allowed to react for 12 hours at room temperature. Carbon disulfide (5.64 g, 74.1 mmol) was added slowly over 15 minutes, and allowed to react for 60 minutes whilst stirring at room temperature. The mixture was diluted with 100 mL of pentane, vacuum filtered and lastly stripped on a rotary evaporator to yield a yellow solid. The solids were re-dissolved in diethyl ether (250 mL), whereby excess solid iodine (I_2) (9.33 g, 77.9 mmol) was added over 5 minutes and subsequently left to react for 60 minutes at room temperature. The formed sodium iodine salt (NaI) was vacuum filtrated. The filtrate was washed in a separatory funnel using a solution of 5 wt-% sodium dithionite ($Na_2S_2O_4$) until all the excess I_2 was removed. It was thereafter washed with water (H_2O) and brine (H_2O saturated with NaCl). Magnesium sulfate ($MgSO_4$) was chosen as a drying agent, the formed suspension was filtered and lastly the solvent was stripped under vacuum to yield a orange oil, which solidified at -10 °C to produce a yellow solid (11.32 g, purity >93% (^{1}H-NMR), yield 55%).

2-cyano-2-propyldodecyl trithiocarbonate (CPDTC); Following the procedure from Abel & Cormick [48], a 250 mL ethyl acetate solution containing AIBN (2.07 g, 12.6 mmol) and bis (dodecyl trithiocarbonate) (6.98 g, 12.6 mmol) were stirred and purged with argon prior to heating to 77 °C for 12 hours. Another 250 mL ethyl acetate solution was prepared, containing AIBN (2.07 g, 12.6 mmol). The solution was added to the reaction mixture and allowed to react at 77 °C for another 12 hours. The mixture was purified via column chromatography (95:5 hexane:ethyl acetate as solvent) and solidified when cooled to -20 °C (6.81 g, purity >97% (^{1}H-NMR), yield 57%).

bis (dithio benzoate) (BDTB); For the synthesis of BDTB, we follow a modified version of the procedure provided by Sanderson et al. [49], starting from phenylmagnesium chloride (C_6H_5MgCl) solution in THF. The C_6H_5MgCl solution (110 mL, 220 mmol) with 50 mL THF were stirred and cooled down to 0 °C. Dropwise, dried carbon disulfide (16.75 g, 220 mmol) was added to the stirred solution, thereafter

it was allowed to react for 2 hours at room temperature. After adding water and 20 g of K_2CO_3, the mixture was filtered to separate the formed salts. An excess of iodine (25.6 g, 101 mmol) was added and left to react overnight, whereafter the solution was washed in a separatory funnel using a solution of 5 wt-% sodium dithionite ($Na_2S_2O_4$) until all the excess I_2 was removed. It was thereafter washed with water (H_2O) and brine (H_2O saturated with NaCl). It was then dried and dissolved in toluene and crystallized at -20 °C to yield a purple solid (purity >90% (^{1}H-NMR)).

Milling: The Retsch MM 400 was used for the ball mill grinding experiments utilizing milling chambers of 10 mL and balls with a diameter of 7 mm. Stainless steel and zirconia (ZrO_2) ceramic milling chambers and balls were obtained from Retsch. All milling experiments were performed under an inert environment (Ar) by degassing the milling chambers with use of a glovebox and by fitting the milling chambers with neoprene gaskets. 300 mg of polymer (PMMA & PS) was milled with two balls at specific frequencies and milling times, with or without the addition of BDTC or BDTB. Polymers were milled for 8 hours at 30 Hz with or without any additives, whereby the milled material was dissolved in chloroform and was purified through an alumina (Al_2O_3) column to separate the micro-particles of stainless steel or zirconia formed through ball mill grinding. THF was used to remove the PMMA stuck to the alumina. The obtained polymer solution was subsequently precipitated in pentane and further washed in pentane to remove any unreacted BDTC, BDTB or potential side products. The pentane was decanted and the remaining was stripped under vacuum to yield the milled polymer.

Polymerization: 50 milligrams of milled polymer were dissolved in a solvent comprising a 1:1 ratio of 750 µL THF and 750 µL monomer. The RAFT polymerization reaction took place within an inert argon environment. To initiate the polymerization reaction, the samples were exposed to blue LED light for photo-initiation or thermally initiated with the use of Azobisisobutyronitrile (AIBN) at 70 °C. Sampling intervals were set at 0, 1, 2, 3, 4, and 24 hours, with each sample collection consisting of 60 µL.

Characterization: All proton nuclear magnetic resonance (^{1}H-NMR) measurements were performed on the Agilent 400-MR DD2 using deuterated chloroform ($CDCl_3$) as solvent. Ultraviolet/Visible absorption spectra were measured on the PerkinElmer UV/Vis Lambda 365. Polymer molecular weights distributions were determined with the use of Gel Permeation Chromatography (GPC) (Shimadzu Prominence). The mobile phase used to operate the GPC is N,N-dimethylformamide (DMF) as it passes through an Agilent PLgel GPC/SEC column. The GPC was fitted with an Refractive Index (RI) detector and a Ultraviolet/Visible (UV/Vis) absorption detector set at a wavelength of 325 nm. Differential Scanning Calorimetry (DSC) analysis was perfomed on the PerkinElmer Diamond DSC. DSC measurements were performed from -30 °C to 170 °C at a scan rate of 10 °C min^{-1}. The polymer films were spin casted using toluene on a silicon wafer in order to perform Atomic Force Microscopy (AFM).

3

Results & Discussion

3.1. Segmentation

3.1.1. Standard Milling

PMMA and PS were milled in a series of experiments at various frequencies and various times. The normalized GPC trace results using the Refractive Index (RI) detector are shown in Figure 3.1 & Figure 3.2. The results were normalized to the highest peak value towards a value of 1, as precise and consistent control over the injection concentration proved challenging. Large polymer chains take less time to elute through the GPC column, meaning a shorter retention time corresponds to a larger polymer. With the use of PMMA and PS calibration standards, the retention time can be converted to molecular weight (number averaged molecular weight (M_n) and weight averaged molecular weight (M_w)), which are shown together with the PDI (= $\frac{M_w}{M_n}$) in Table 3.1.

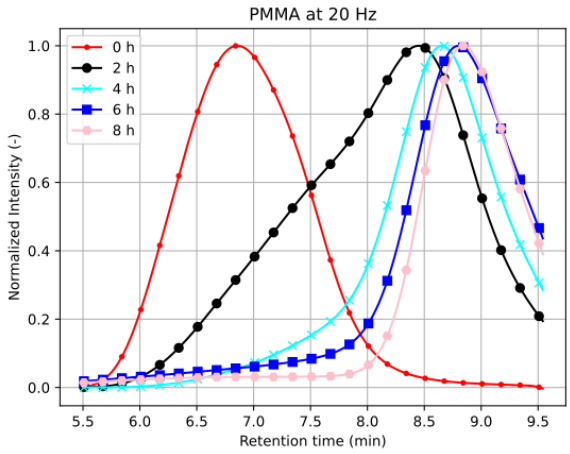

Figure 3.1: Normalized GPC trace of PMMA milled at 20 Hz at several timesteps. Illustrated here is the segmentation of large polymer chains into smaller chains over 8 hours. The molecular weight distribution broadens at t = 2 h, however upon further milling the distribution become narrow, signifying a decrease in PDI.

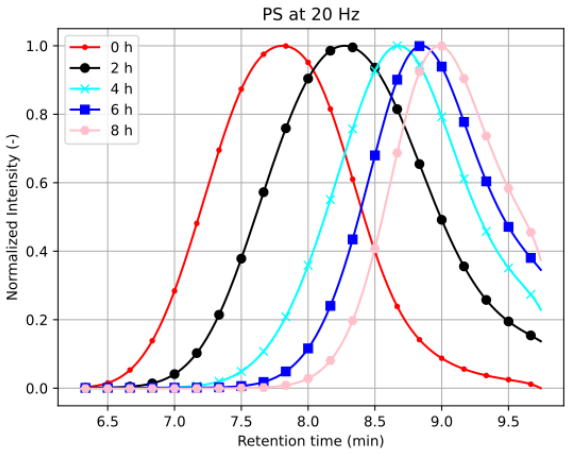

Figure 3.2: Normalized GPC trace of PS milled at 20 Hz at several timesteps. Illustrated here is the segmentation of large polymer chains into smaller chains over 8 hours. Similar to the milling of PMMA, the molecular weight distribution is broad at t = 2 h, however upon further milling the distribution become narrow, signifying a decrease in PDI.

PMMA 20 Hz	0 h	2 h	4 h	6 h	8 h
M_n (kDa)	318.6	18.8	10.8	8.2	7.8
M_w (kDa)	1070.5	203.2	55.4	24.0	11.5
PDI (-)	3.36	10.81	5.13	2.93	1.48

PS 20 Hz	0 h	2 h	4 h	6 h	8 h
M_n (kDa)	123.5	39.0	25.3	20.2	17.6
M_w (kDa)	272.9	83.9	41.5	28.9	23.1
PDI (-)	2.21	2.15	1.64	1.43	1.31

Table 3.1: Molecular weight (M_n & M_w) evolution of PMMA and PS milled at 20 Hz. During the milling procedure, the molecular weight decreases. For PMMA, the dispersity temporarily increases with a subsequent decrease.

All results presented are based on the RI detector, unless stated otherwise. Each data point corresponds to a new experiment, as incremental sampling interrupts the milling process and reduces the amount of sample being milled, both of which can potentially affect the results significantly. The temporary increase in the PDI (molecular weight distribution broadening) is likely due to the partial (incomplete) segmentation of all the polymer chains during the milling process. As milling continues for longer periods, the majority of the polymer chains are cleaved into smaller chains, leading to a decrease in the PDI (molecular weight distribution narrowing). Plotting the results of Table 3.1 yields Figure 3.3 & Figure 3.4:

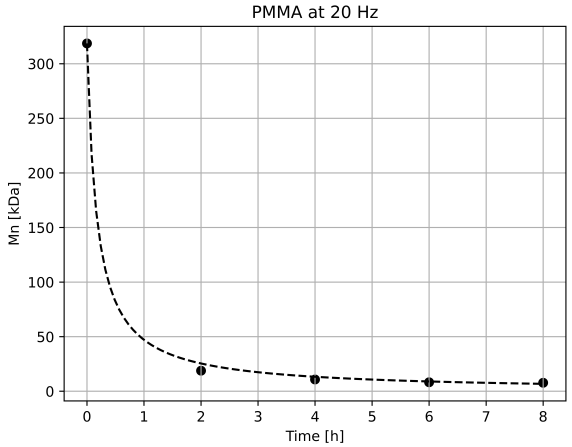

Figure 3.3: Number averaged molecular weight (M_n) evolution of PMMA throughout the milling process at 20 Hz. M_n decreases rapidly and asymptotically towards a limiting molecular weight (M_{lim}). The dots signify the measured values, meanwhile the dashed line shows the fitted kinetic model (k = 18.1 · 10^{-3}).

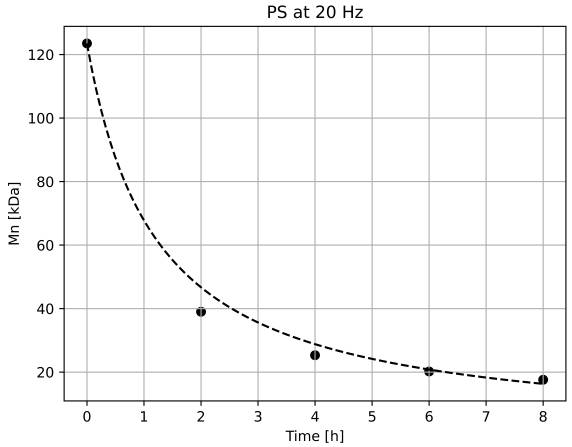

Figure 3.4: Number averaged molecular weight (M_n) evolution of PS throughout the milling process at 20 Hz. M_n decreases asymptotically towards a limiting molecular weight (M_{lim}). The dots signify the measured values, meanwhile the dashed line shows the fitted kinetic model (k = 6.65 · 10^{-3}).

The molecular weight of both PMMA and PS decrease rapidly throughout the milling process, which was fitted using least squares regression to a simple kinetic model developed by Sato & Nalepa [50] which strongly resembles 2nd order kinetics:

$$\begin{aligned} \frac{1}{M_n(t)} &= kt + \frac{1}{M_n(t=0)} \\ M_n(t) &= \frac{1}{kt + M_n(t=0)^{-1}} \end{aligned} \tag{3.1}$$

Whereby $M_n(t)$ is the number averaged molecular weight at time t, k is the segmentation/degradation rate constant and $M_n(t=0)$ is the number averaged molecular weight at t = 0. The fitted rate constants k for the kinetic model are shown in Appendix C. The M_n of both PMMA and PS decrease asymptotically to a minimum value, the limiting molecular weight M_{lim}. Beyond this molecular weight, the chosen method to supply mechanical energy becomes ineffective and segmentation does not occur by mechanical degradation. Any further chain scission is likely caused by thermal degradation leading to random and chain-end scission [34]. Despite PS starting at a lower molecular weight than PMMA (123.5 and 318.6 kDa, respectively), at t = 2 h PS has a higher molecular weight than PMMA (39.0 and 18.8 kDa, respectively). This can be evidence for two phenomena. Firstly, it has been reported that longer chains have a higher scission rate [42]. This is explained by longer polymer chains being easier to extend until breakage [28], meaning a higher probability of scission [39]. When milling, the impact of the balls can lead to compression and extension of the polymers, with the latter being the likely cause of segmentation in ball mill grinding. Therefore, the PMMA starting from a larger M_n means the early segmentation rate is much higher than that of PS. However this does not fully explain why the PMMA segmentation rate is much higher than that of PS, which is seen by the one order of magnitude difference in the degradation rate k. The second phenomena is that the glass transition temperature T_g correlates well with the milling degradation rate [42]. The higher the glass transition temperature, the less viscoelastic energy dissipation of the polymeric material (polymer cushioning effect), allowing for

an enhanced rate of chain scission. PMMA polymers have a higher T_g than PS polymers of the same chain length, leading to a faster degradation rate.

Milling at different frequencies can lead to different mechanical energies being supplied to the polymers, altering the segmentation rate. The milling of PMMA and PS at 10, 20 and 30 Hz is shown in Figure 3.5 & Figure 3.6. The raw data for 10 and 30 Hz is shown in Table 3.2 & Table 3.3. By milling at a lower frequency, less energy is supplied to the polymeric material, leading to a slower degradation rate. This is clearly shown by the M_n evolution at 10 Hz. Conversely, by milling at 30 Hz, far more energy is transferred to the polymers, leading to a faster degradation rate. Milling at 30 Hz shows a similar asymptotic decreasing behaviour as is with 20 Hz, however at 10 Hz, the degradation rate is too small to reach the asymptotic M_{lim} value in 8 hours. Interestingly, milling at 10 Hz leads to a significant broadening of the molecular weight distribution, yielding a PDI of 13.5 and 2.33 at 8 hours for PMMA and PS, respectively. This is once again the partial segmentation noticed when milling at 20 Hz, however this is absent when milling at 30 Hz. Partial segmentation is like to be observed between 0 and 2 h at 30 Hz. The PDI when milling at 30 Hz reaches a value of 1.43 for PMMA and 1.19 for PS, which is lower than the 1.48 and 1.31 at 20 Hz for PMMA and PS, respectively. The imprecise fit is likely because model used to describe the segmentation rate is too simple to describe the M_n evolution of the milled samples with very high accuracy. The GPC trace results for all the experiments are shown in Appendix A.

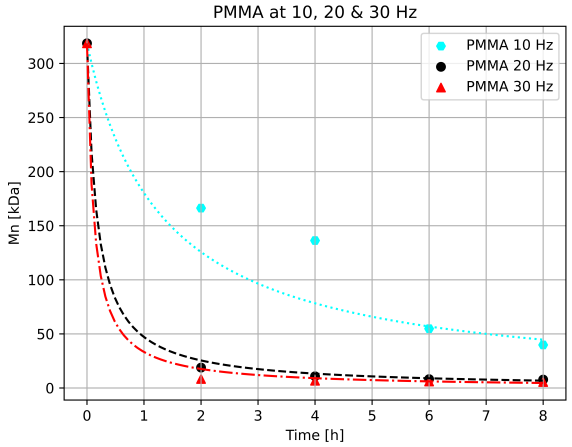

Figure 3.5: Number averaged molecular weight (M_n) evolution of PMMA throughout the milling process at 10, 20 and 30 Hz. The degradation rate at higher frequency is considerably higher.

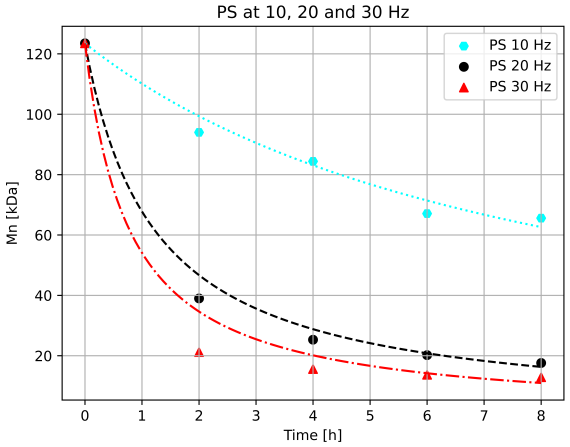

Figure 3.6: Number averaged molecular weight (M_n) evolution of PS throughout the milling process at 10, 20 and 30 Hz. The degradation rate at higher frequency is considerably higher.

PMMA 10 Hz	0 h	2 h	4 h	6 h	8 h
M_n (kDa)	318.6	166.3	136.3	54.8	39.8
M_w (kDa)	1070.5	974.5	774.2	648.8	537.3
PDI (-)	3.36	5.86	5.68	11.84	13.5

PS 10 Hz	0 h	2 h	4 h	6 h	8 h
M_n (kDa)	123.5	94.0	84.4	67.1	65.6
M_w (kDa)	272.9	221.8	205.9	171.8	152.8
PDI (-)	2.21	2.36	2.44	2.56	2.33

Table 3.2: Molecular weight (M_n & M_w) evolution of PMMA and PS milled at 10 Hz. During the milling procedure, the molecular weight decreases. At this frequency, the dispersity increases during the milling procedure, with PMMA reaching a peak PDI at t = 8 h and PS at t = 6 h.

PMMA 30 Hz	0 h	2 h	4 h	6 h	8 h
M_n (kDa)	318.6	8.3	6.7	6.0	5.5
M_w (kDa)	1070.5	15.6	9.7	8.52	7.9
PDI (-)	3.36	1.88	1.45	1.42	1.43

PS 30 Hz	0 h	2 h	4 h	6 h	8 h
M_n (kDa)	123.5	21.2	15.6	13.7	12.9
M_w (kDa)	272.9	29.0	19.2	16.6	15.4
PDI (-)	2.21	1.37	1.23	1.21	1.19

Table 3.3: Molecular weight (M_n & M_w) evolution of PMMA and PS at 30 Hz. During the milling procedure, the molecular weight rapidly decreases, leading to a low dispersity at t = 8 h.

Performing NMR analysis on PMMA and PS milled at 30 Hz for eight hours reveals that during the milling process, many new groups are formed. Shown in Figure 3.7A & Figure 3.7B are the ^{1}H-NMR spectra of the polymer milled at 30 Hz for t = 0 h and t = 8 h.

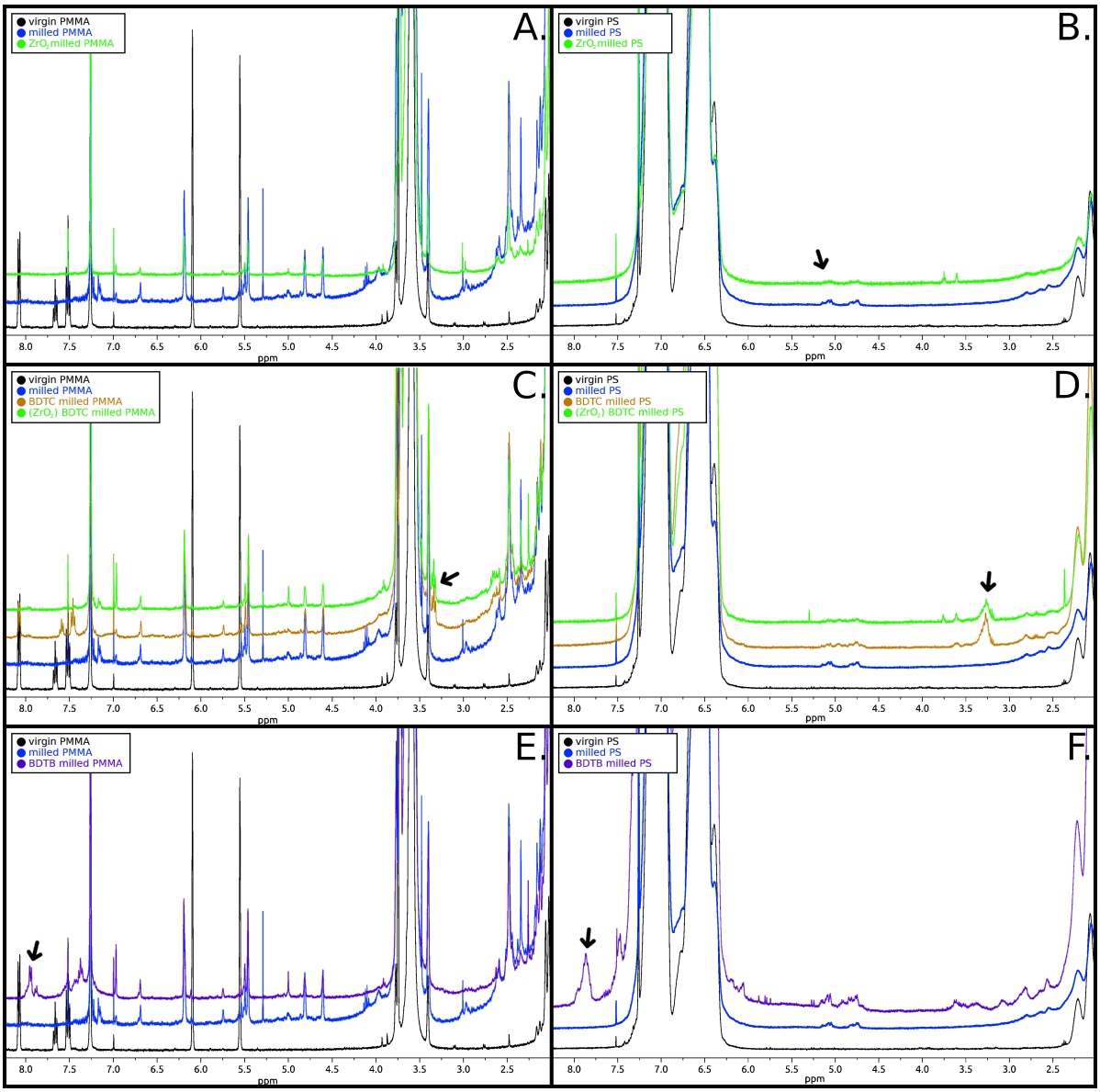

Figure 3.7: ^{1}H-NMR of milled polymers in $CDCl_3$. **A:** PMMA; Virgin, bare milled and bare milled using ZrO_2. **B:** PS; Virgin, bare milled and bare milled using ZrO_2. Arrow indicates alkene group formation. **C:** PMMA; Virgin, bare milled, BDTC milled and BDTC milled using ZrO_2. Arrow indicates TC terminated end group. **D:** PS; Virgin, bare milled, BDTC milled and BDTC milled using ZrO_2. Arrow indicates TC terminated end group. **E:** PMMA; Virgin, bare milled, BDTB milled and BDTB milled using ZrO_2. Arrow indicates DB terminated end group. **F:** PS; Virgin, bare milled, BDTB milled and BDTB milled using ZrO_2 Arrow indicates DB terminated end group. All samples are milled using stainless steel unless mentioned otherwise.

Unmilled (virgin) PMMA inherently contains minor impurities like the monomer MMA and solvent toluene. After milling, the characteristic groups associated with these impurities are no longer detectable, however there is a notable emergence of new groups. Milled PS exhibits similar behaviour, however fewer new groups form. There primarily appears to be the formation of alkene groups (approx. 4.5 to 6.5 ppm) for both polymer samples. When milling polymeric material, the polymer is homolytically cleaved to form two radicals (see Figure 3.8). From the literature it is known that for PMMA, the tertiary macroradical (I) is relatively stable around room temperature meanwhile the primary macroradical (II) is highly unstable as it is no longer measured above -60 °C via Electron Spin Resonance (ESR) spectroscopy [31]. In

this context, the term ”stable” is used to signify that the radical is sufficiently stable to be measured and captured at the operating temperature. It does not imply that the radical is not transient. In the case of PS, the primarily macroradical (III) is highly unstable even at cryogenic temperatures, meanwhile the secondary macroradical (IV) in close proximity of the benzene ring is relatively stable [51]. The unstable radicals will very rapidly undergo side reactions, such as H-transfer towards the formation of double bonds [52]. It is also possible for some of the chain scission to lead to ions via heterogenous cleavage, forming an anion and cation pair [29]. It has been shown that PTFE, PE, PP & PVDF can form ionic end groups, with their heterolytic yields differing due to the difference in electronegativity of the newly formed end groups [30]. These ionic products (carbanions and carbocations) are electro or nucleophiles, which can react and form new groups. Considering the milling process occurs in a stainless steel chamber with stainless steel balls, the polymers come in contact with the metals iron (Fe) and chromium (Cr) and their oxidized states. These metals can potentially react with the macroradicals and catalyze side reactions to form new groups. Added to that, very low concentrations of oxygen can still be present during milling, which rapidly reacts with the carbon-centered radicals to form peroxy radicals [31, 51]. The peroxy radicals can then undergo different side reaction to form new groups.

The vast array of potential side reactions make it particularly challenging to propose proper reaction pathways towards the formation of the groups shown in Figure 3.7A & Figure 3.7B. The possibility of the metals in stainless steel catalyzing the side reactions for the formation of the side groups shown in ^{1}H-NMR spectra lead to a small investigation of the role of the milling chamber material when milling polymeric samples. Therefore, the polymers were milled in a zirconia (ZrO_2) chamber with zirconia balls. PMMA and PS were milled for 8 hours at 30 Hz to produce segmented polymers with an M_n of 5.8 kDa (PDI=1.42) and 15.2 kDa (PDI=1.29), respectively. The ^{1}H-NMR spectra of PMMA and PS milled in zirconia for 8 hours at 30 Hz are shown in Figure 3.7A & Figure 3.7B by the color lime. Despite zirconia being a relatively inert ceramic, the zirconium (Zr) present in the ceramic is a known catalyst and can therefore still catalyze similar or other side reactions [53], which is exactly what is seen in the ^{1}H-NMR results. Although not performed in this work, the investigating the fate of radicals formed through milling using metal free material (e.g. silicon nitride) is of interest in understanding the role of the milling chamber material. The full ^{1}H-NMR spectra of all species can be found in Appendix E.

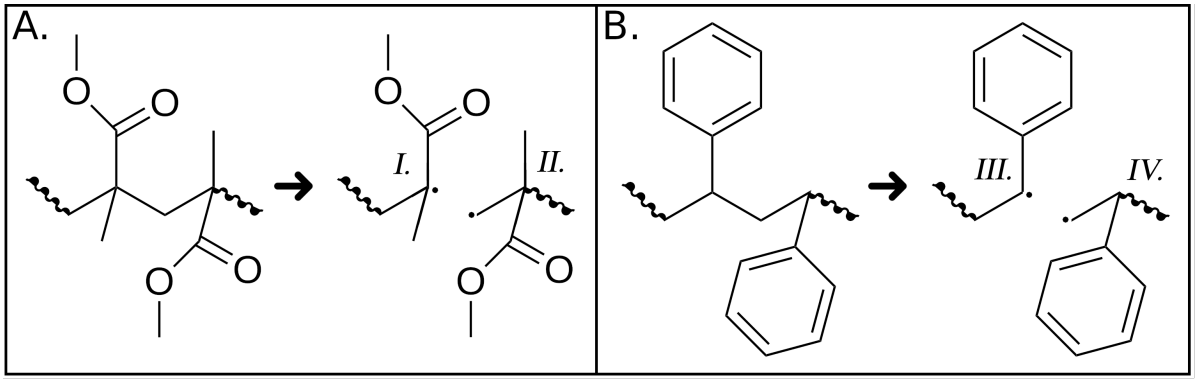

Figure 3.8: Structure of PMMA and PS after homolytic chain scission. **A:** PMMA: stable tertiary macroradical (I) and unstable primary macroradical (II). **B:** PS: stable secondary macroradical (III) and unstable primary macroradical (IV).

3.1.2. Milling with RAFT Capable Agents

The incorporation of radical scavengers during the milling process has the capability to mitigate side reactions by capturing transient macroradicals. This aspect is investigated in this section. If a polymer with an arbitrary chain length of 100 undergoes segmentation into 10 chains of length 10 at the end of the milling procedure, we can estimate that $2 \cdot 10 - 2 = 18$ radicals are formed (2 radicals formed for every new chain, minus 2 chain ends from the initial chain). In this scenario, each molecule of BDTC/BDTB can theoretically capture two radicals and terminate the end group. Therefore, a minimum of 9 molecules of RCA are required to terminate every radical formed during the milling procedure. Utilizing the data from subsection 3.1.1, we can determine the M_{lim} and therefore how many radicals are formed during the segmentation of PMMA and PS. For BDTC (M_w = 555.0 g mol^{-1}), this amounted to approximately 20 mg of BDTC for 300 mg PMMA and 33 mg of BDTC for 300 mg PS. For BDTB (M_w

= 306.5 g mol^{-1}), this amounted to approximately 10 mg of BDTB for 300 mg PMMA and 20 mg of BDTC for 300 mg PS. In practice, it was found that BDTC had a significant impact on the degradation rate of PMMA, meanwhile a minor effect was noticed with PS. Therefore, PS was milled with 50 mg of BDTC, 1.5 times the minimum theoretical amount. The results of milling with BDTC and BDTB at 20 Hz for several time steps are shown in Figure 3.9 & Figure 3.10, with the data tabulated in Table 3.4 & Table 3.5. Adding RCA in the earlier mentioned quantities had a negligible effect on the degradation rate for PMMA. Similarly for PS, the addition of RCA to the milling chamber had little effect on the segmentation rate. Of particular note is the lower dispersity of PS when milling using RCA in comparison to milled without any additives.

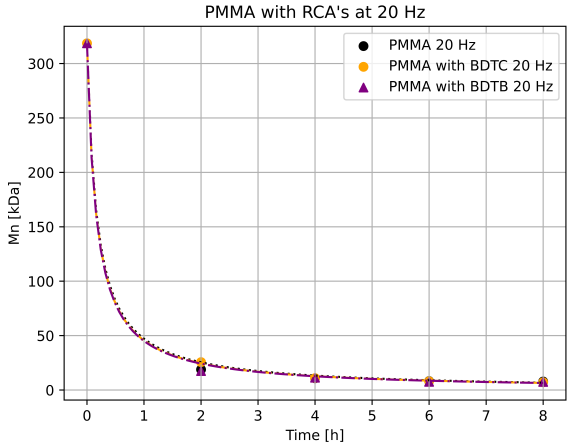

Figure 3.9: Number averaged molecular weight (M_n) evolution of PMMA milled alone, with BDTC or with BDTB at 20 Hz. The quantity of RCA added negligibly affected the degradation rate of PMMA.

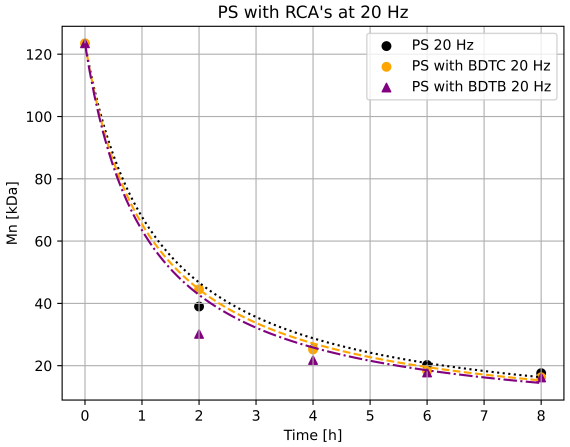

Figure 3.10: Number averaged molecular weight (M_n) evolution of PS milled alone, with BDTC or with BDTB at 20 Hz. The quantity of RCA added had a negligible impact on the degradation rate of PS, with a potential improvement in the degradation rate observed with the addition of BDTB.

BDTC PMMA	0 h	2 h	4 h	6 h	8 h
M_n (kDa)	318.6	25.6	10.9	8.0	7.1
M_w (kDa)	1070.5	464.9	88.2	12.9	10.4
PDI (-)	3.36	18.16	8.09	1.61	1.46

BDTC PS	0 h	2 h	4 h	6 h	8 h
M_n (kDa)	123.5	44.5	25.2	18.2	16.3
M_w (kDa)	272.9	126.8	51.4	23.7	20.2
PDI (-)	2.21	2.85	2.04	1.30	1.24

Table 3.4: Molecular weight (M_n & M_w) evolution of PMMA and PS milled with BDTC at 20 Hz.

BDTB PMMA	0 h	2 h	4 h	6 h	8 h
M_n (kDa)	318.6	17.4	11.3	7.5	7.4
M_w (kDa)	1070.5	208.8	66.9	14.2	10.8
PDI (-)	3.36	12.00	5.92	1.89	1.46

BDTB PS	0 h	2 h	4 h	6 h	8 h
M_n (kDa)	123.5	30.2	21.8	17.8	16.2
M_w (kDa)	272.9	52.9	28.6	21.0	19.2
PDI (-)	2.21	1.75	1.31	1.18	1.19

Table 3.5: Molecular weight (M_n & M_w) evolution of PMMA and PS milled with BDTB at 20 Hz.

Up to this point, all GPC trace results and the corresponding evolution of molecular weight have been obtained using the Refractive Index (RI) detector, which indiscriminately measures all molecules eluted through the GPC column. The incorporation of the UV/Vis absorption detector enables the specific detection of UV-interactive compounds. Both BDTC and BDTB are UV-absorbing molecules, with BDTC having a maximum absorption wavelength (λ_{max}) of approximately 310 nm and BDTB having a λ_{max} of 300 nm [54]. The use of the UV-Vis absorption detector thus enables the detection of polymer chains that have been terminated with an RCA. While PMMA has a weak UV signal in this range, PS contains phenyl groups that absorb significant amounts of UV light, with a λ_{max} of 270 nm [55]. Consequently, to detect RAFT-terminated polymer chains, the detector wavelength needs to be set at an appropriate value that minimizes PS absorption, yet captures the UV signal from the RCA. To determine an appropriate wavelength, UV-Vis absorption spectra were recorded of PMMA, PS, RAFT-terminated PMMA

and RAFT-terminated PS. The results can be found in Appendix F. The investigation revealed that the terminated polymers exhibited high activity in the range of 290 nm to 340 nm. In contrast, the un-terminated polymers demonstrated very low absorption. Consequently, the chosen wavelength for detecting the RAFT-terminated polymers was set at 325 nm. The normalized GPC trace results using the UV/Vis absorption detector of PMMA and PS milled with BDTC are shown in Figure 3.11 & Figure 3.12. The GPC trace results for milling PMMA and PS with BDTB are shown in Appendix A. By utilizing PS calibration standards, the signal of the UV/Vis absorption detector could be converted to molecular weights. Nevertheless, it's essential to acknowledge that PMMA and PS have distinct hydrodynamic radii due to the considerable differences in their monomer radii. As a result, the accuracy when using PS calibration when applied to the analysis of PMMA is severely diminished. This discrepancy is evident in the calibration outcomes, where a PMMA sample with an M_n of 5.8 kDa (analyzed using PMMA calibration on the RI detector) has an M_n of 17.8 kDa when analyzed using PS calibration on the RI detector. By calculating the ratio between these two values, it becomes possible to approximate the M_n of RAFT-terminated PMMA on the UV-Vis detector using PS standards. These results are presented in Table 3.6 & Table 3.7. Considering that only RAFT-terminated polymers are detectable, the results suggest that the termination during the milling process primarily involves shorter-chain polymers. A continuous decrease in PDI was expected and observed for both BDTC and BDTB, however BDTB has a higher M_n and a lower PDI than BDTC. A plausible explanation for this phenomenon is steric hindrance, where BDTC is a bulkier molecule than BDTB. As a result, BDTB is able to terminate slightly larger chains than BDTC.

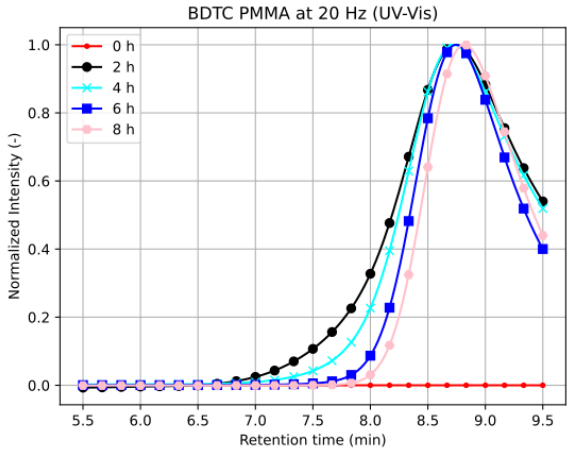

Figure 3.11: Normalized GPC trace of PMMA milled with BDTC at 20 Hz at several timesteps using a UV-Vis absorption detector at 325 nm. Primarily small chains are observed.

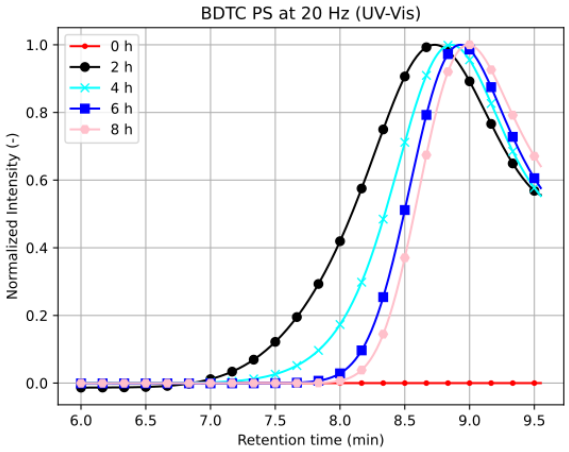

Figure 3.12: Normalized GPC trace of PS milled with BDTC at 20 Hz at several timesteps using a UV-Vis absorption detector at 325 nm. Primarily small chains are observed.

BDTC PMMA	0 h	2 h	4 h	6 h	8 h
M_n (kDa)	0.0	5.5	5.9	5.7	5.3
M_w (kDa)	0.0	12.1	9.5	7.5	6.9
PDI (-)	0.0	2.20	1.62	1.32	1.31

BDTC PS	0 h	2 h	4 h	6 h	8 h
M_n (kDa)	0.0	19.2	15.5	14.3	13.9
M_w (kDa)	0.0	38.4	24.6	19.0	17.4
PDI (-)	0.0	2.00	1.59	1.33	1.25

Table 3.6: Molecular weight (M_n & M_w) evolution of BDTC terminated PMMA and PS at 20 Hz using the UV-Vis absorption detector. Given that only RAFT-terminated polymers are detectable, the results indicate that predominantly short-chain polymers undergo termination during the milling procedure.

BDTB PMMA	0 h	2 h	4 h	6 h	8 h
M_n (kDa)	0.0	7.4	7.5	6.4	6.3
M_w (kDa)	0.0	12.1	10.1	7.9	7.6
PDI (-)	0.0	1.63	1.34	1.24	1.20

BDTB PS	0 h	2 h	4 h	6 h	8 h
M_n (kDa)	0.0	21.5	19.2	16.6	15.0
M_w (kDa)	0.0	28.6	24.0	19.4	17.7
PDI (-)	0.0	1.33	1.25	1.17	1.18

Table 3.7: Molecular weight (M_n & M_w) evolution of BDTB terminated PMMA and PS at 20 Hz. Given that only RAFT-terminated polymers are detectable, the results indicate that predominantly short-chain polymers undergo termination during the milling procedure.

An ^{1}H-NMR analysis was performed on PMMA and PS milled with RCA for 8 hours at 30 Hz. The NMR spectra of PMMA and PS milled with BDTC are shown in Figure 3.7C & Figure 3.7D. Milling with BDTC seems to repress certain side reactions when comparing the polymer milled by itself (blue) and the polymer milled with BDTC (brown). Indicated by the black arrows is the CH_2 group of the dodecyl chain directly next to the trithiocarbonate group, indicating that the polymer chain had been terminated. After milling PMMA and PS with BDTC in the zirconia chamber at 30 Hz for 8 hours, they too were analyzed using ^{1}H-NMR. These results are also shown in Figure 3.11C & Figure 3.7D by the color lime. Milling with zirconia yields no substantial difference compared to milling with stainless steel.
Similarly to BDTC, PMMA and PS were milled in the presence of BDTB, illustrated in Figure 3.7E & Figure 3.7F. The characteristic peak for a BDTB terminated end group is indicated by the black arrows. BDTB is difficult to purify to a high purity, therefore the impurities might potentially react with macroradicals formed during milling and lead to undesired end groups.

3.2. Reactivity

To validate the RAFT termination of the polymer end-group, repolymerization reactions are conducted on the milled samples. The chosen method for RDRP involves the photo-initiation of the RAFT end group using blue LED light [20]. All samples are milled at a frequency of 30 Hz and a duration of 8 hours to achieve a low PDI and M_n prior to repolymerization.

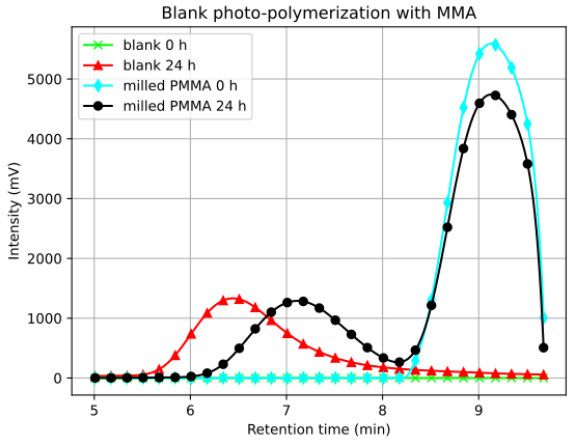

Figure 3.13: GPC trace of the blank polymerization of pure MMA in THF (blank) and milled PMMA in MMA and THF (milled PMMA) after 0 and 24 hours. Both scenarios show a degree of polymerization, but the molecular weight distribution of the two newly formed polymer peaks differs.

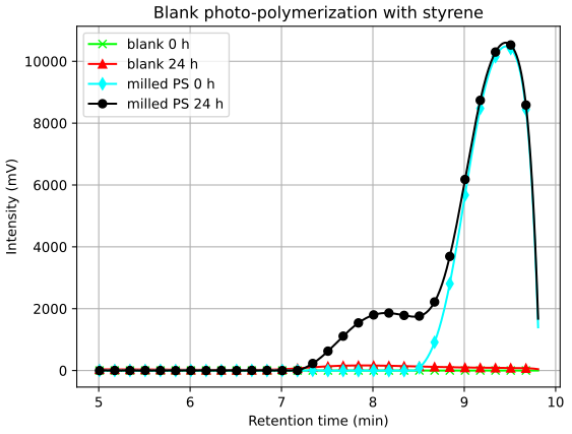

Figure 3.14: GPC trace of the blank polymerization of pure styrene in THF (blank) and milled PS in styrene and THF (milled PS) after 0 and 24 hours. The pure styrene case exhibits little to no polymerization, whereas the milled PS case shows a small degree of polymerization.

3.2.1. Repolymerization

In this section, the aim is to extend the RAFT-terminated polymer chain using native monomers to assess both termination and the regenerative potential of the milled polymer. Initially, a blank experiment was conducted with a 1:1 volumetric ratio of THF to monomer, subjected to blue light under an inert atmosphere. Another blank experiment was performed by dissolving 50 mg of milled polymer (milled without any additives) in THF along with its native monomer and exposed to blue light under an inert atmosphere. The GPC trace results of these two blank experiments, performed with the monomers MMA and styrene, are collectively depicted in Figure 3.13 and Figure 3.14. The sampling for the GPC

trace results of polymerization remained consistent at 60 µL of reaction solution and 1 mL of DMF, eliminating the need for normalization to compare results.

The polymerization using MMA shows that both the pure MMA and milled PMMA experiments polymerize. However, there is a difference in the molecular weight distribution between these two experiments, with pure MMA leaning towards higher molecular weights. The polymerization of pure styrene shows a negligible degree of polymerization, however when milled PS is used for polymerization, observable polymerization is noted. Free from a source of radicals, none of these samples are capable of undergoing radical polymerization. Photo-polymerization without any photo-initiating molecule using blue LED lights may seem strange. However, considering the bond dissociation energy of the π orbital in the vinyl functional group in MMA is approximately 272 kJ mol^{-1} [56], utilizing the Planck-Einstein relation ($E = \frac{hc}{\lambda}$), we calculate the wavelength required to excite the π orbital to the π^* anti-bonding orbital, weakening the bond such that radicals are formed. That wavelength is approximately 430 nm. Blue LED light is capable of producing a small amount of light at this wavelength. Therefore, the observed polymerization in Figure 3.13 and Figure 3.14 is attributed to Free Radical Polymerization induced by the blue LED light. Trithiocarbonates absorb blue light effectively [20], and as a result, the intensity displayed in the GPC trace results of RAFT polymerization should be significantly higher than in the blank experiments, indicating more polymerization reactions. This aspect was investigated via the photo-polymerization of PMMA and PS milled with BDTC in THF and their respective native monomers. The results are depicted in Figure 3.15 & Figure 3.16.

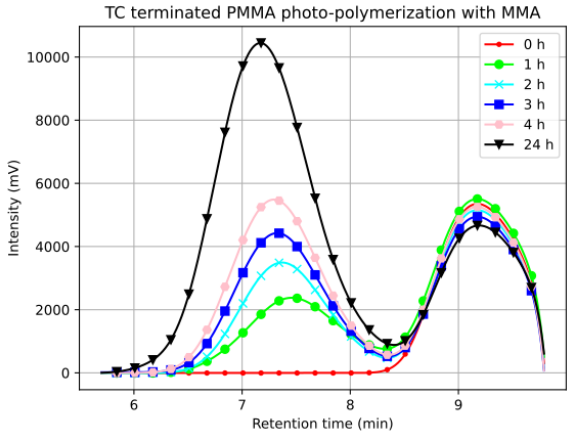

Figure 3.15: GPC trace of trithiocarbonate (TC)-terminated PMMA photo-polymerized with MMA in THF after 0, 1, 2, 3, 4 and 24 hours, showing the emergence of a new peak at t = 7.4 minutes, while the original peak at t = 9.2 minutes undergoes a gradual reduction. After 24 hours, the newly formed peak becomes prominent, but the original peak persists.

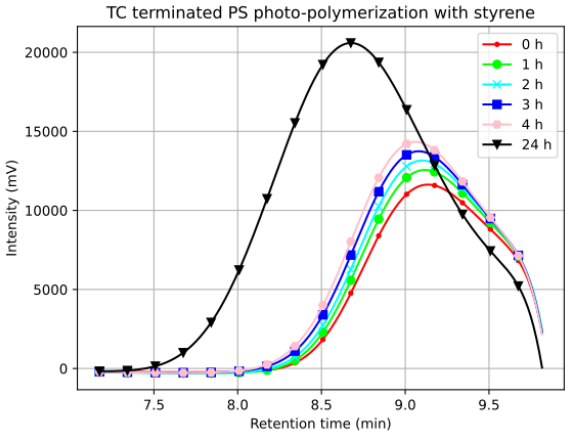

Figure 3.16: GPC trace of trithiocarbonate (TC)-terminated PS photo-polymerized with styrene in THF after 0, 1, 2, 3, 4 and 24 hours, showing slow polymerization of PS. The molecular weight distribution appears to move in its entirety with time, which is not observed in the case of TC-terminated PMMA.

Both PMMA and PS terminated with trithiocarbonate (TC) were able to undergo photo-polymerization with their native monomers, albeit at different rates. The signal intensity suggests a different polymerization reaction than simply FRP, most likely RAFT-mediated polymerization, as the signal is significantly stronger than the newly formed peaks in the blank case (one order of magnitude difference), meanwhile the PDI remains similar (Table 3.8). PMMA with MMA exhibited a considerably faster reaction than PS with styrene, potentially due to the bulky nature of styrene, causing steric hindrance and slowing down the polymerization process. Interestingly, in the case of TC-terminated PMMA (Figure 3.15), high molecular weight polymers are formed during polymerization. However, the original polymer (between retention time 8.3 - 9.8 min) shows a slow decrease in intensity, persisting even after 24 hours of polymerization. This suggests that a portion of the PMMA milled with trithiocarbonate (TC) did undergo scission, however the RAFT end group is not being activated by blue light or the macroradical had undergone side reactions and was therefore not terminated. In the following section, we explore the potential enhancement of termination efficiency. The incomplete RAFT end group activation is discussed soon thereafter.

For the purposes of discussion, we posit that the unreacted tail represents unterminated polymer chains. Two plausible explanations for this are: end group thermolysis or mass transfer limitations. Ball mill grinding is an energy-intensive process that generates heat, reaching temperatures of up to 60 °C during the milling procedure, consistent with the reported temperature (60-65 °C) by Balema et al. [44]. The potential existence of transient hot spots during milling, with temperatures up to 1000 K, has been suggested by Sievers et al. [57]. Both trithiocarbonate and dithiobenzoate end groups are known to undergo thermolysis at high temperatures [58]. Irrespective of the presence of hot spots during milling, it remains plausible that a portion of the TC-terminated PMMA underwent thermolysis, as the global temperature reached approximately 60 °C. Alternatively, despite milling being effective at solid-state mixing, there may be mass transfer limitations due to insufficient RCA being present at the site of the polymer cleavage. Depending on whether the chain scission occurred on the surface of the particle containing the polymers or within the particle, solid-state diffusion might also be required to reach the radical [59, 60]. For PS milled with BDTC, the degree of polymerization was too small to accurately determine whether all the milled PS polymers had been terminated by BDTC or not. In order to investigate whether thermolysis or mass transfer limitations affect the termination of the polymer end-group, two experiments were carried out. The ball mill grinding setup currently does not allow for temperature control, therefore to reduce the exposure time to high temperatures PMMA was milled with BDTC at 20 Hz for four hours (in comparison to the standard 30 Hz for 8 hours). This sample was then subjected to blue light, where the GPC trace results (found in Appendix A) showed little difference to the standard case. To investigate whether mass transfer limitations signficantly affected the RAFT end group termination, PMMA was milled with an excess of BDTC (30 milligrams instead of the standard 20 milligrams, meaning 1.5x the standard amount) for both 4 hours at 20 Hz and 8 hours at 30 Hz. The GPC trace results are illustrated by Figure 3.17 & Figure 3.18. When milled with excess BDTC at 20 Hz for 4 hours, the polymer produced has a very broad molecular weight distribution at t = 0 h (a PDI of 9.03 in comparison to a PDI of 5.13 when milled without any BDTC at 20 Hz (Table 3.1)). Considering RCA primarily terminates short polymer chains, this means that the longer chains have not been terminated as of yet and are unlikely to participate in the polymerization reaction. After 24 hours of polymerization, the intensity of the smaller chains decrease significantly, suggesting the majority have been extended and formed long chains. However a small tail at high retention times persist, suggesting thermolysis is unlikely to be the cause of the dead tail. Upon milling for 8 hours at 30 Hz with excess BDTC and subsequent polymerization, the resulting GPC trace shows minimal deviation from the standard case for PMMA (as depicted in Figure 3.15 and Figure 3.18). This suggests that if mass transfer limitations are to be present, increasing the concentration when milling has little effect on the termination efficiency. Milling with zirconia showed no significant difference to milling with stainless steel (see in Appendix A).

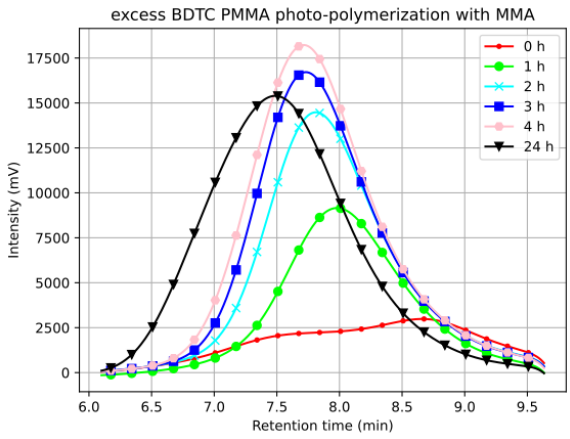

Figure 3.17: GPC trace of PMMA milled with excess BDTC at 20 Hz for 4 hours, photo-polymerized with MMA in THF after 0, 1, 2, 3, 4 and 24 hours. There is a very broad molecular weight distribution at t = 0, however, the short chains decrease rapidly and vanish almost entirely after 24 hours of polymerization.

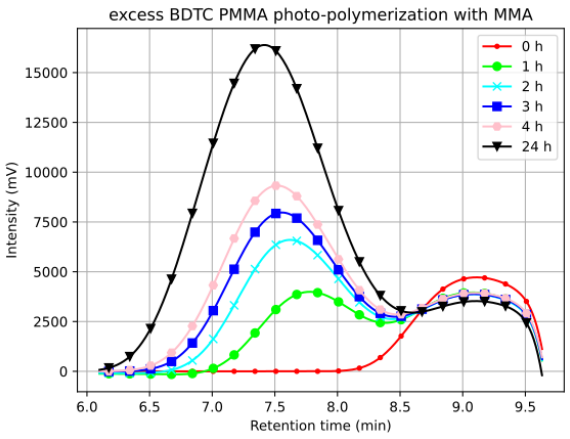

Figure 3.18: GPC trace of PMMA milled with excess BDTC at 30 Hz for 8 hours, photo-polymerized with MMA in THF after 0, 1, 2, 3, 4 and 24 hours. The results are very similar to the standard case (20 mg BDTC, see Figure 3.15).

As mentioned earlier in the report, the use of the UV/Vis absorption detector allows for the detection of UV responsive compounds. This means that chains that have been terminated are visible, meanwhile unterminated polymer chains are not visible. The GPC trace results for the photo-polymerization of TC terminated PMMA and PS with their native monomers using the UV/Vis absorption detector are shown in Figure 3.19 & Figure 3.20. Both PMMA and PS show a change in their molecular weight distribution to larger polymer chains, however similar to the case of the RI detector, a portion remains at high retention times. For PMMA, the low molecular weight polymers behave very similar when measured using the RI detector, a decrease in intensity of the original peak and the formation of a new peak. The fact that the original peak remains on the UV/Vis absorption detector even after 24 hours suggests either that the RAFT end group has not being activated or that milling with BDTC incorporates a UV absorbing group that is not capable of RAFT polymerization.

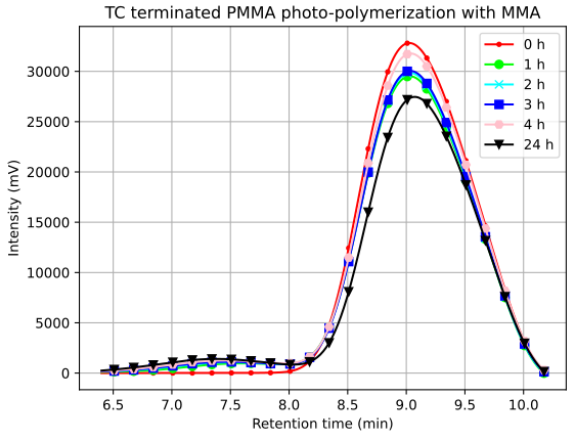

Figure 3.19: GPC trace of trithiocarbonate (TC)-terminated PMMA photo-polymerized with MMA in THF after 0, 1, 2, 3, 4 and 24 hours measured using a UV/Vis absorption detector at 325 nm. A slow reduction in the original peak at retention time of 9 minutes suggests minimal repolymerization of the small chains.

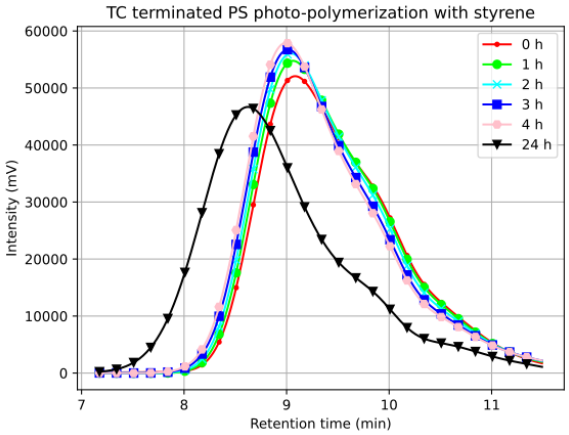

Figure 3.20: GPC trace of trithiocarbonate (TC)-terminated PS photo-polymerized with styrene in THF after 0, 1, 2, 3, 4 and 24 hours measured using a UV/Vis absorption detector at 325 nm. Simiarly to the GPC trace using the RI detector, the entire distribution appears to shift to lower retention times.

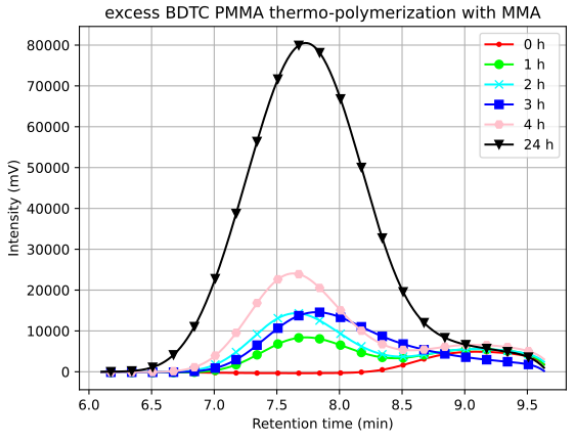

Figure 3.21: GPC trace of PMMA milled with excess BDTC at 30 Hz for 8 hours, thermo-polymerized with MMA in THF after 0, 1, 2, 3, 4 and 24 hours. The thermal polymerization reactions occurs similarly to the photo polymerization reaction, however at a much quicker rate.

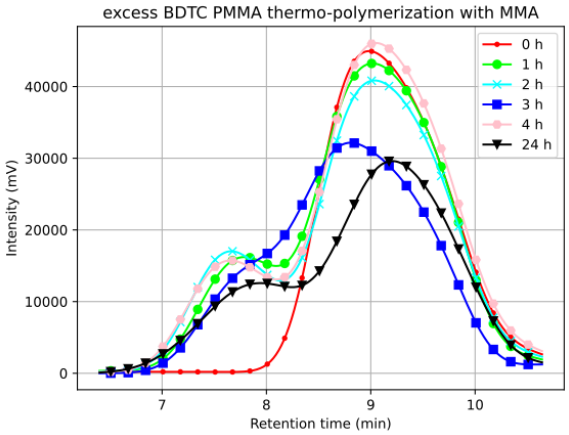

Figure 3.22: GPC trace of PMMA milled with excess BDTC at 30 Hz for 8 hours, thermo-polymerized with MMA in THF after 0, 1, 2, 3, 4 and 24 hours measured using a UV/Vis absorption detector at 325 nm. The steady and relatively rapid decrease in intensity suggests a moderate portion of the polymers have been terminated with a RAFT end group. The results strongly resemble other GPC trace results of PMMA polymerization (found in Appendix A).

To ascertain whether the polymer chains had been terminated, however are not responsive to blue light activation (or potentially undergo photo-degradation [61]), we conduct a polymerization experi-

ment utilizing a thermal initiator. Azobisisobutyronitrile (AIBN) undergoes decomposition at elevated temperatures, generating two radicals that can effectively activate and initiate the RAFT polymerization reaction for all the RAFT end groups. The GPC trace of the thermal polymerization experiment of TC terminated PMMA with MMA at 70 °C with the use of AIBN over a period of 24 hours is shown in Figure 3.21 & Figure 3.22. Both the RI & UV/Vis detector results are displayed. Due to the polymerization rate and conditions of the thermal polymerization experiment, the reaction mixture became viscous such that uncertainties were introduced during sampling and by extent the measured intensity. The initial polymers at t = 0 do disappear with time, however similar to the photo polymerization case, a certain portion remain with time. This suggests that there are polymers that contain a UV responsive group, but are unable to undergo RAFT polymerization. It is possible that the RCA itself undergoes side reactions which forms radical scavenging groups that are UV absorbing yet RAFT incapable. These RAFT incapable groups can undergo parasitic side reactions which terminate radical end groups towards ”dead” polymer chains.

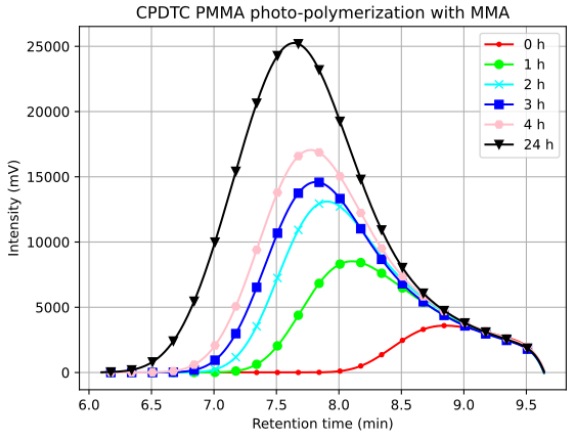

Figure 3.23: GPC trace of CPDTC milled PMMA photo-polymerized with MMA in THF after 0, 1, 2, 3, 4 and 24 hours. Instead of forming two different peaks, the polymerization reaction forms one very broad molecular weight distribution.

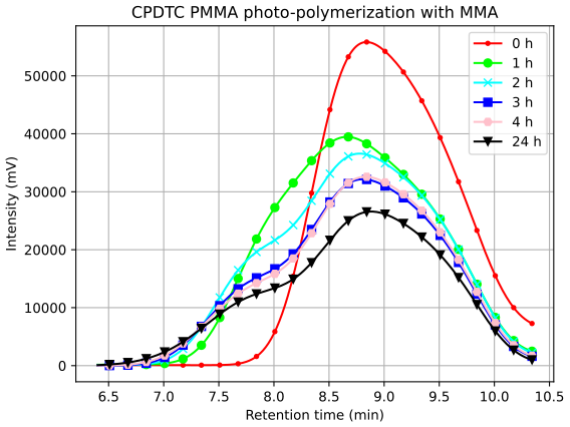

Figure 3.24: GPC trace of CPDTC milled PMMA photo-polymerized with MMA in THF after 0, 1, 2, 3, 4 and 24 hours measured using a UV/Vis absorption detector at 325 nm. Similarly to Figure 3.22, the steady and relatively rapid decrease in intensity suggests a moderate portion of the polymers have been terminated with a RAFT end group.

PMMA was milled in the presence of another RCA, namely 2-cyano-2-propyldodecyl trithiocarbonate (CPDTC) (refer to the chemical structure in Appendix D), a chain transfer agent utilized for RAFT polymerization. It’s essential to note that the maximum theoretical efficiency of CPDTC is 50%, as the AIBN-derived moiety dissociates from the TC moiety as a tertiary radical and cannot terminate another radical to form a RAFT end group. Milling 300 mg PMMA with 42 mg CPDTC at 30 Hz for eight hours results in PMMA with an M_n of 7.1 kDa and a PDI of 1.52. Subsequently, this PMMA sample undergoes photo-polymerization, and the outcomes are illustrated in Figure 3.23 & Figure 3.24. Interestingly, despite undergoing the same conditions as TC-terminated PMMA with MMA, the GPC traces of the RI and UV/Vis absorption detectors are dissimilar. Particularly when comparing Figure 3.19 and Figure 3.24, significant differences emerge. The distribution in CPDTC-milled PMMA changes intensely from t = 0 h to t = 1 h, suggesting a larger portion of the polymers have been terminated when milling with CPDTC rather than BDTC. CPDTC is a liquid at room temperature, implying that throughout the milling procedure with CPDTC, the polymer particles were coated and soaked in the RAFT agent. Similar behaviour was observed when using BDTC and CPDTC, suggesting that having a molecule with two radical scavenging moieties is not necessary.

Similar analysis could not be performed on the DB-terminated polymers, because dithiobenzoates are not very effective at photo-polymerization and therefore the polymerization occurs at a far slower rate than trithiocarbonates [20]. The use of thermally initiated radicals (with the use of e.g. AIBN) might be necessary to further investigate the termination efficiency of BDTB, which is not performed in this work. However, polymerization of DB-terminated PMMA is observed on both detectors even when

using photo-initiation, suggesting that some chains are terminated. The GPC trace results for the photo-polymerization of dithiobenzoate (DB)-terminated PMMA and PS with their native monomers can be found in Appendix A. A table containing the values of all the molecular weights and PDI of all the polymerization experiments is provided as Table 3.8 (and its UV/Vis variant can be found in Appendix C). Further optimization is required in order to achieve a greater degree of radical end group termination towards ”living” polymers. There are several possible phenomena present that reduce the effective radical capture such as macroradical stability, end group thermolysis, mass transfer limitations and parasitic radical scavengers. Strategies to optimize of handle each phenomena separately is discussed briefly. The stability of the radical, especially the primary macroradical (see Figure 3.8) can be enhanced by cryomilling, however this can adversely affect the segmentation of the polymers [41]. End group thermolysis can be reduced by keeping the temperature within the milling chamber at room temperature or lower, and potentially by optimizing the milling times to not subject the polymers unnecessary transient hot spots. Mass transfer limitations can be ameliorated in several ways, namely by increasing the concentration of RCA or by having the RCA be in the liquid phase. It should be noted that both of these can adversely affect the segmentation rate of the polymers. The parasitic radical scavengers can be avoided by using stabler radical scavengers, for example 2,2,6,6-Tetramethylpiperidine 1-oxyl (TEMPO) or 4-hydroxy-2,2,6,6-tetramethylpiperidin-1-oxyl (TEMPOL) which are both chain transfer agents used for Nitroxide-Mediated Polymerization.

	0 h	1 h	2 h	3 h	4 h	24 h
TC-PMMA 1	4.9 (1.32)[a]	136.2 (1.63)	146.6 (1.79)	171.3 (1.78)	167.2 (1.91)	209.8 (2.05)
TC-PMMA 2	10.0 (1.83)	22.0 (3.02)	26.5 (3.72)	30.8 (4.03)	29.0 (4.81)	51.2 (5.30)
TC-PMMA 3	14.8 (9.03)	28.8 (2.96)	31.4 (4.10)	35.4 (3.68)	39.9 (3.38)	68.7 (4.07)
TC-PMMA 4	5.9 (1.30)[a]	72.3 (1.49)	89.5 (1.70)	98.5 (1.87)	102.4 (2.00)	121.5 (2.43)
TC-PMMA 5	5.7 (1.39)[a]	75.2 (1.44)	85.5 (1.55)	90.9 (1.57)	87.3 (1.61)	73.4 (2.04)
TC-PMMA 6	5.9 (1.30)[a]	119.2 (1.40)	136.3 (1.56)	145.6 (1.62)	149.6 (1.76)	176.0 (1.97)
TC-PMMA 7	5.0 (1.32)[a]	67.7 (1.48)	70.5 (1.54)	69.0 (1.59)	68.8 (1.59)	50.9 (1.78)
TC-PMMA 8	7.1 (1.52)	15.6 (2.61)	19.9 (3.13)	23.4 (3.35)	24.5 (3.75)	35.7 (4.43)
DB-PMMA 9	4.8 (1.34)[a]	34.1 (1.12)	40.2 (1.16)	44.2 (1.16)	49.7 (1.31)	94.7 (1.48)
TC-PS 10	17.0 (1.28)	17.5 (1.29)	17.9 (1.30)	18.3 (1.31)	18.7 (1.33)	29.3 (1.56)
TC-PS 11	19.3 (1.27)	19.5 (1.27)	19.9 (1.27)	20.1 (1.28)	20.5 (1.29)	29.3 (1.50)
TC-PS 12	15.6 (1.21)	16.2 (1.25)	17.3 (1.29)	18.3 (1.31)	18.9 (1.38)	27.3 (1.83)
DB-PS 13	13.6 (1.16)	13.4 (1.16)	13.4 (1.16)	13.6 (1.16)	13.6 (1.15)	13.8 (1.16)
TC-ePS 14	16.5 (1.23)	16.8 (1.22)	17.2 (1.21)	17.3 (1.26)	17.7 (1.23)	27.5 (1.41)
TC-ePS 15	16.2 (1.20)	17.6 (1.22)	18.9 (1.25)	19.8 (1.28)	20.7 (1.32)	29.7 (1.85)
pure MMA	0 (-)	- (-)	- (-)	- (-)	- (-)	1124.4 (1.99)
PMMA 16	5.5 (1.34)[a]	- (-)	- (-)	- (-)	- (-)	214.7 (2.41)
pure styrene	0 (-)	- (-)	- (-)	- (-)	- (-)	0 (-)
PS 17	13.2 (1.12)	- (-)	- (-)	- (-)	- (-)	14.9 (1.66)
pure tBuA	0 (-)	- (-)	- (-)	- (-)	- (-)	74.0 (1.40)
pure MA	0 (-)	- (-)	- (-)	- (-)	- (-)	76.3 (1.94)

Table 3.8: Molecular weight evolution of all polymerization experiments measured on the RI detector, displaying the Mn (in kDa) with the PDI in parenthesis. All experiments are photo polymerization unless mentioned explicitly otherwise. 1: PMMA with MMA, 2: (4 h 20 Hz milled) PMMA with MMA, 3: (excess BDTC 4 h 20 Hz) PMMA with MMA, 4: (excess BDTC) PMMA with MMA, 5: (thermally initiated, excess BDTC) PMMA with MMA, 6: (ZrO_2 milled) PMMA with MMA, 7: PMMA with MA, 8: (CPDTC milled) PMMA with MMA, 9: PMMA with MMA, 10: PS with styrene, 11: (ZrO_2 milled) PS with styrene, 12: PS with tBuA, 13: PS with styrene, 14: e-PS with styrene, 15: e-PS with tBuA, 16: (bare milled) PMMA with MMA, 17: (bare milled) PS with styrene. [a] M_n and PDI of the original peak at t = 0, the subsequent data is of the newly formed peak.

3.2.2. Copolymerization

Polymer chain extension with the use of the native monomers of PMMA and PS milled in the presence of an RCA has been displayed in the previous section. Now, it is of interest to determine if it is possible to extend the chain with the use of different monomers to create block copolymers. TC-terminated PMMA was photo-polymerized with the comonomer methyl acrylate (MA), and TC-terminated PS was photo-polymerized with the comonomer t-butyl acrylate (tBuA). Their molecular weight evolution is reported in Table 3.8 as TC-PMMA 7 and TC-PS 12, respectively, while their GPC trace results can be found in Appendix A. It should be noted that calculating the molecular weight distribution of copolymers

can be slightly inaccurate due to the differing structures of the monomers within the copolymer. The use of calibration standards in such cases may introduce uncertainty into the molecular weight calculations. TC-terminated PMMA polymerizes rapidly with MA, forming a broad molecular weight distribution after 24 hours of polymerization. TC-terminated PS undergoes a quick polymerization with tBuA, quicker than when it is polymerized with styrene. After 24 hours, a broad polymer chain length distribution is formed, with a significant tail at lower molecular weights. After the 24 hours of polymerization, the polymer solution was precipitated in methanol and brine, thereafter it was redissolved in chloroform, dried with magnesium sulfate, and filtered. Then it was cast onto a PTFE film, and the solvent was allowed to dry overnight. This was done to acquire a sample usable for DSC analysis, which was performed on the block copolymers. PS-b-PtBuA is extremely static after casting, rendering it practically impossible to manipulate and analyze, therefore it was redissolved in chloroform and pipetted in the DSC pan, after which the solvent was allowed to evaporate overnight. The DSC measurements (found in Appendix G) show that PMMA-b-PMA has a glass transition temperature (T_g) at 20.5 °C, which is approximately 11 degrees above the T_g of MA [62]. PS-b-PtBuA had a T_g at 48.0 °C and at 99.7 °C, in line with their homopolymer values.

Furthermore, Atomic Force Microscopy (AFM) analysis was performed on both copolymers. Their height measurements are displayed in Figure 3.25 & Figure 3.26. The nanoindentation results can be found in Appendix H. It should be noted that the modulus was estimated using the Derjaguin-Muller-Toporov (DMT) model, which relies on certain assumptions that might affect the accuracy of the results. No phase separation is detected for the PMMA-b-PMA copolymer, the results only show noise, especially the modulus results. This makes sense, as both both MMA and MA only differ by one methyl group, and therefore would interact favorably with one another. The PS-b-PtBuA copolymer however, does exhibit phase separation, with small domains of approximately 150 nm and larger domains surrounding it. Similar results can be seen in the modulus map. Styrene and tBuA differ significantly and therefore would interact less favorably with each other than with it's own monomer, leading to phase separation.

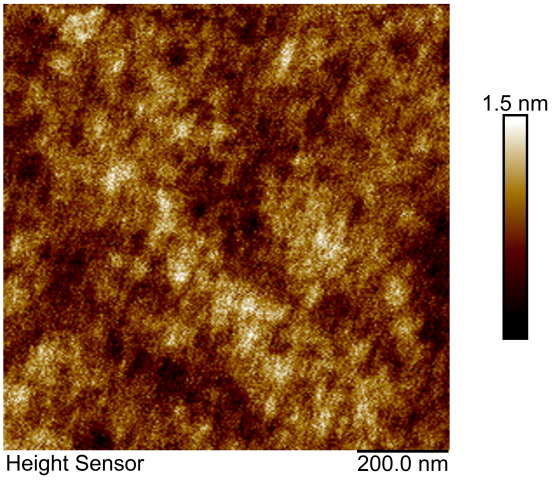

Figure 3.25: Atomic Force Microscopy (AFM) height results for the PMMA-b-PMA block copolymer at a 1 µm scale. The depth height differences are very small. No significant domains are seen, especially when viewing the modulus map (Appendix H).

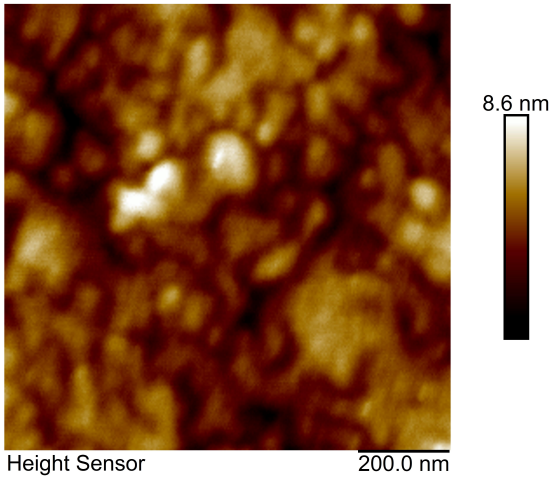

Figure 3.26: Atomic Force Microscopy (AFM) height results for the PS-b-PtBuA block copolymer at a 1 µm scale. There are small domains formed of approximately 150 nm in size, with larger domains surrounding it. This is indicative of phase separation.

3.2.3. e-PS

We have demonstrated that the mechanochemical activation of FRP-synthesized polymers is possible, converting them into RDRP-capable polymers. However, the polymers used in this study were lab-grade polymeric materials. To investigate the applicability of the process to commercially used materials, we employed Expanded Polystyrene (e-PS), a commonly used packaging material known by its brand name Styrofoam. Due to its primarily air-filled composition, e-PS is voluminous yet lightweight. e-PS is typically contaminated with additives like colorants, and the presence of these contaminants

can be seen in the proton NMR spectrum, found in Appendix E. Due to the lightweight and expanded nature of e-PS, it is challenging to work with. First, the sample was compacted under a hydraulic press, followed by grinding in a blade grinder to produce small particles.

GPC analysis of the e-PS after compression and grinding revealed an M_n of 70.4 kDa and a PDI of 2.28. After milling bare e-PS for 8 hours at 30 Hz, the M_n and PDI were 12.3 kDa and 1.16, respectively. Subsequently, a new batch of 300 mg e-PS was milled with 50 mg BDTC at 30 Hz for 8 hours (yielding an M_n of 16.6 kDa with a PDI of 1.24), purified via an alumina column chromatography, and then precipitated in pentane. 50 milligrams of the TC-terminated e-PS was dissolved in 1.5 mL 1:1 THF:monomer and photo-polymerized under blue light for 24 hours. Two separate experiments were conducted; the first using styrene as monomer, and the second using tBuA. The GPC trace results can be found in Appendix A, and the molecular weight evolution of both experiments with e-PS is displayed in Table 3.8 as TC-ePS 14 & TC-ePS 15. This demonstrates the feasibility of mechanochemically activating commercial Styrofoam and converting it into a block copolymer or regenerating it into long-chain PS.

4

Conclusion

Our discoveries showcase the mechanochemical activation of ”dead” (inert) polymers, leading to the integration of new functional end groups, transforming them into ”living” Reversible Deactivation Radical Polymerization-capable polymers. In a ball mill grinder, PMMA and PS underwent chain scission, generating macroradicals that readily engage in radical reactions, resulting in the introduction of new groups such as alkenes. Characterizing the polymers involved evaluating the newly formed groups and monitoring the molecular weight distribution during milling. Initially, the Free Radical Polymerization polymers exhibit high dispersity, but as the polymers undergo segmentation, the dispersity and polymer chain length significantly decrease, yielding relatively uniform short polymer chain lengths.

The introduction of radical scavengers, specifically RAFT-Capable Agents in this study, captures macroradicals and terminates the polymer chain with a RAFT end group. Our research reveals that the addition of RCA influences the segmentation behavior of both PMMA and PS, slowing down the segmentation rate and altering the resulting molecular weight distribution. Although RCA termination suppresses side reactions, it does not entirely prevent the formation of new groups. We observe that smaller chains are the primary target of the radical scavengers. Furthermore, after the end group termination, we show repolymerization and copolymerization of the mechanochemically activated polymers by extending PMMA and PS polymer chains. However, the reactivity of the polymer chains is dependent on the efficiency of radical termination, influenced by factors such as radical lifetime, thermolysis of the RAFT end group, mass transfer limitations of the radical scavenger, or the presence of parasitic radical scavengers. Further optimization is necessary for effective macroradical capture towards RDRP-capable polymers. Additionally, our study demonstrates that e-PS, a common form of PS synthesized using FRP, can be mechanochemically activated into ”living” RAFT-capable polymers.

The combination of radical formation during the mechanical processing of waste polymers with RDRP-capable radical scavengers offers a pathway for the complete recycling or upcycling of waste plastics into high-value products. The insights gained from this work provide a foundation for further optimization towards a technologically feasible method to address the growing problem of plastic waste.

Recommendations for future work

Further optimizations are required for the technological feasibility of the mechanochemical activation of waste polymers. Particularly, the use of NMP or ATRP based radical scavengers can potentially be more effective than that of RAFT polymerization. Temperature control during milling, either at room temperature or cryogenic temperatures can potentially further optimize the macroradical capture. Milling with the use of a liquid radical scavenger can potentially mitigate mass transfer limitations and improve the radical capture. These warrant further research.

Acknowledgements

We extend our gratitude to Evgeny Pidko for allowing us to make use of the Inorganic Systems Engineering Lab. Gratitude is extended to Georgy Filonenko for his valuable knowledge and guidance.

References

[1] H. Ritchie, V. Samborska, and M. Roser. *Plastic Pollution | Our World In Data*. 2023. URL: https://ourworldindata.org/plastic-pollution.

[2] F. D. de Sousa. "Plastic effects on marine and freshwater environments". In: *Water Biology and Security* (2023), p. 100228. ISSN: 2772-7351. DOI: https://doi.org/10.1016/j.watbs.2023.100228.

[3] N. Casagrande et al. "Ecotoxicity effect factors for plastic additives on the aquatic environment: a new approach for life cycle impact assessment". In: *Environmental Pollution* 341 (2024), p. 122935. ISSN: 0269-7491. DOI: https://doi.org/10.1016/j.envpol.2023.122935.

[4] J. Xu et al. "Nano- and micro-plastic transport in soil and groundwater environments: Sources, behaviors, theories, and models". In: *Science of The Total Environment* 904 (2023), p. 166641. ISSN: 0048-9697. DOI: https://doi.org/10.1016/j.scitotenv.2023.166641.

[5] J. Bhagat et al. "Zebrafish: An emerging model to study microplastic and nanoplastic toxicity". In: *Science of The Total Environment* 728 (2020), p. 138707. ISSN: 0048-9697. DOI: 10.1016/j.scitotenv.2020.138707.

[6] K. Kadac-Czapska, E. Knez, and M. Grembecka. "Food and human safety: the impact of microplastics". In: *Critical Reviews in Food Science and Nutrition* 0.0 (2022), pp. 1–20. DOI: 10.1080/10408398.2022.2132212.

[7] I. Miguel et al. "Knowledge, concerns and attitudes towards plastic pollution: An empirical study of public perceptions in Portugal". In: *Science of The Total Environment* 906 (2024), p. 167784. ISSN: 0048-9697. DOI: https://doi.org/10.1016/j.scitotenv.2023.167784.

[8] *Plastics - The Facts 2022 | Plastics Europe*. 2022. URL: https://plasticseurope.org/knowledge-hub/plastics-the-facts-2022/.

[9] I. Vollmer et al. "Beyond Mechanical Recycling: Giving New Life to Plastic Waste". In: *Angewandte Chemie International Edition* 59.36 (2020), pp. 15402–15423. DOI: https://doi.org/10.1002/anie.201915651.

[10] M. J. Stapleton et al. "Evaluating the generation of microplastics from an unlikely source: The unintentional consequence of the current plastic recycling process". In: *Science of The Total Environment* 902 (2023), p. 166090. ISSN: 0048-9697. DOI: https://doi.org/10.1016/j.scitotenv.2023.166090.

[11] Q. Qian and J. Ren. "From plastic waste to potential wealth: Upcycling technologies, process synthesis, assessment and optimization". In: *Science of The Total Environment* 907 (2024), p. 167897. ISSN: 0048-9697. DOI: https://doi.org/10.1016/j.scitotenv.2023.167897.

[12] K. Q. Tan et al. "Valorization of hazardous plastic wastes into value-added resources by catalytic pyrolysis-gasification: A review of techno-economic analysis". In: *Renewable and Sustainable Energy Reviews* 182 (2023), p. 113346. ISSN: 1364-0321. DOI: https://doi.org/10.1016/j.rser.2023.113346.

[13] S. H. Chang. "Plastic waste as pyrolysis feedstock for plastic oil production: A review". In: *Science of The Total Environment* 877 (2023), p. 162719. ISSN: 0048-9697. DOI: https://doi.org/10.1016/j.scitotenv.2023.162719.

[14] L. Tebben and A. Studer. "Nitroxides: Applications in Synthesis and in Polymer Chemistry". In: *Angewandte Chemie International Edition* 50.22 (2011), pp. 5034–5068. DOI: https://doi.org/10.1002/anie.201002547.

[15] K. Matyjaszewski. "Atom Transfer Radical Polymerization (ATRP): Current Status and Future Perspectives". In: *Macromolecules* 45.10 (2012), pp. 4015–4039. DOI: 10.1021/ma3001719.

[16] S. G. Gaynor, J.-S. Wang, and K. Matyjaszewski. “Controlled Radical Polymerization by Degenerative Transfer: Effect of the Structure of the Transfer Agent”. In: *Macromolecules* 28.24 (1995), pp. 8051–8056. DOI: 10.1021/ma00128a012.

[17] J. P. A. Heuts and N. M. B. Smeets. “Catalytic chain transfer and its derived macromonomers”. In: *Polym. Chem.* 2 (11 2011), pp. 2407–2423. DOI: 10.1039/C1PY00224D.

[18] S. Perrier. “50th Anniversary Perspective: RAFT Polymerization—A User Guide”. In: *Macromolecules* 50.19 (2017), pp. 7433–7447. DOI: 10.1021/acs.macromol.7b00767.

[19] G. Moad, E. Rizzardo, and S. H. Thang. “Living Radical Polymerization by the RAFT Process – A Third Update”. In: *Australian Journal of Chemistry* 65.8 (2012), pp. 985–1076. DOI: 10.1071/CH12295.

[20] J. Xu et al. “Catalyst-Free Visible Light-Induced RAFT Photopolymerization”. In: *Controlled Radical Polymerization: Mechanisms*. Vol. 1187. ACS Symposium Series. American Chemical Society, 2015. Chap. 13, pp. 247–267. DOI: https://doi.org/10.1016/j.eurpolymj.2023.112292.

[21] G. Moad, E. Rizzardo, and S. H. Thang. “End-functional polymers, thiocarbonylthio group removal/transformation and RAFT polymerization”. In: *Polymer International* 60.1 (2011), pp. 9–25. DOI: 10.1002/pi.2988.

[22] C. M. Bates and F. S. Bates. “50th Anniversary Perspective: Block Polymers—Pure Potential”. In: *Macromolecules* 50.1 (2017), pp. 3–22. DOI: 10.1021/acs.macromol.6b02355.

[23] G. R. Jones et al. “Reversed Controlled Polymerization (RCP): Depolymerization from Well-Defined Polymers to Monomers”. In: *J. Am. Chem. Soc.* 145.18 (2023), pp. 9898–9915. DOI: 10.1021/jacs.3c00589.

[24] H. S. Wang et al. “Investigating the Effect of End-Group, Molecular Weight, and Solvents on the Catalyst-Free Depolymerization of RAFT Polymers: Possibility to Reverse the Polymerization of Heat-Sensitive Polymers”. In: *ACS Macro Lett.* 11.10 (2022), pp. 1212–1216. DOI: 10.1021/acsmacrolett.2c00506.

[25] H. S. Wang et al. “Reversing RAFT Polymerization: Near-Quantitative Monomer Generation Via a Catalyst-Free Depolymerization Approach”. In: *J. Am. Chem. Soc.* 144.10 (2022), pp. 4678–4684. DOI: 10.1021/jacs.2c00963.

[26] J. B. Young et al. “Photoassisted Radical Depolymerization”. In: *ACS Macro Lett.* 11.12 (2022), pp. 1390–1395. DOI: 10.1021/acsmacrolett.2c00603.

[27] E. J. Beckman et al. “Medical adhesive and methods of tissue adhesion”. US7264823B2. 2007.

[28] S. Wang et al. “Quantitative Adjustment to the Molecular Energy Parameter in the Lake-Thomas Theory of Polymer Fracture Energy”. In: *Macromolecules* 52.7 (2019), pp. 2772–2777. ISSN: 0024-9297. DOI: 10.1021/acs.macromol.8b02341.

[29] M. Sakaguchi et al. “Ionic products from the mechanical fracture of solid polypropylene”. In: *Polymer* 25.7 (1984), pp. 944–946. ISSN: 0032-3861. DOI: 10.1016/0032-3861(84)90077-6.

[30] M. Sakaguchi and H. Kashiwabara. “Mechano-ions produced by mechanical fracture of solid polymers”. In: *Makromolekulare Chemie. Macromolecular Symposia* 27.1 (1989), pp. 299–304. DOI: https://doi.org/10.1002/masy.19890270120.

[31] J. Pilař and K. Ulbert. “An ESR study of PMMA mechanoradicals and of their interaction with oxygen”. In: *Journal of Polymer Science: Polymer Physics Edition* 16.11 (1978), pp. 1973–1982. ISSN: 0098-1273. DOI: 10.1002/pol.1978.180161107.

[32] Martyn C.R. Symons. “Formation of Radicals by Mechanical Processes”. In: *Free Radical Research Communications* 5.3 (1988), pp. 131–139. ISSN: 8755-0199. DOI: 10.3109/10715768809066922.

[33] H. Otaguro et al. “High-energy radiation forming chain scission and branching in polypropylene”. In: *Radiation Physics and Chemistry* 79.3 (2010), pp. 318–324. ISSN: 0969-806X. DOI: 10.1016/j.radphyschem.2009.11.003.

[34] Tomonaga Ueno, Erika Nakashima, and Kunihiko Takeda. “Quantitative analysis of random scission and chain-end scission in the thermal degradation of polyethylene”. In: *Polymer Degradation and Stability* 95.9 (2010), pp. 1862–1869. ISSN: 0141-3910. DOI: 10.1016/j.polymdegradstab.2010.04.020.

[35] G. Madras, J. M. Smith, and B. J. McCoy. “Thermal degradation kinetics of polystyrene in solution”. In: *Polymer Degradation and Stability* 58.1 (1997), pp. 131–138. ISSN: 0141-3910. DOI: 10.1016/S0141-3910(97)00036-0.

[36] Q. Huang, O. Hassager, and J. Madsen. “Spatial Radical Distribution in Fractured Polymer Glasses and Melts Visualized Using a Profluorescent Nitroxide Probe”. In: *Macromolecules* 55.21 (2022), pp. 9431–9441. DOI: 10.1021/acs.macromol.2c01594.

[37] S. V. Canevarolo. “Chain scission distribution function for polypropylene degradation during multiple extrusions”. In: *Polymer Degradation and Stability* 70.1 (2000), pp. 71–76. ISSN: 0141-3910. DOI: https://doi.org/10.1016/S0141-3910(00)00090-2.

[38] P. A. May and J. S. Moore. “Polymer mechanochemistry: techniques to generate molecular force via elongational flows”. In: *Chem. Soc. Rev.* 42 (18 2013), pp. 7497–7506. DOI: 10.1039/C2CS35463B.

[39] B. A. Buchholz et al. “Flow-induced chain scission as a physical route to narrowly distributed, high molar mass polymers”. In: *Polymer* 45.4 (2004), pp. 1223–1234.

[40] R. S. Porter and J. F. Johnson. “A Study of Several Systems of the Type Laminar Flow Degradation of Polyisobutene.” In: *The Journal of Physical Chemistry* 63 (1959), pp. 202–205.

[41] A. P. Smith et al. “High-energy mechanical milling of poly(methyl methacrylate), polyisoprene and poly(ethylene-alt-propylene)”. In: *Polymer* 41.16 (2000), pp. 6271–6283. DOI: 10.1016/S0032-3861(99)00830-7.

[42] G. I. Peterson et al. “Mechanochemical Degradation of Amorphous Polymers with Ball-Mill Grinding: Influence of the Glass Transition Temperature”. In: *Macromolecules* 53 (18 2020), pp. 7795–7802. DOI: 10.1021/acs.macromol.0c01510.

[43] E. Jung et al. “Depolymerization of poly(α-methyl styrene) with ball-mill grinding”. In: *J. Polym. Sci.* 61.7 (2023), pp. 553–560. DOI: 10.1002/pol.20220578.

[44] V. P. Balema et al. “Depolymerization of polystyrene under ambient conditions”. In: *New J. Chem.* 45 (6 2021), pp. 2935–2938. DOI: 10.1039/D0NJ05984F.

[45] I. Simionescu, V. Oprea, and J. Nicoleanu. “Mechanochemically initiated polymerizations—5. Polymerization by vibratory milling of acrylamide and methacrylamide”. In: *European Polymer Journal* 19.6 (1983), pp. 525–528. DOI: 10.1016/0014-3057(83)90204-5.

[46] M. Kuzuya, S. Kondo, and A. Noguchi. “A new development of mechanochemical solid-state polymerization of vinyl monomers: prodrug syntheses and its detailed mechanistic study”. In: *Macromolecules* 24.14 (1991), pp. 4047–4053. DOI: 10.1021/ma00014a013.

[47] G. Schmidt-Naake, M. Drache, and M. Weber. “Combination of Mechanochemical Degradation of Polymers with Controlled Free-Radical Polymerization”. In: *Macromolecular Chemistry and Physics* 203.15 (2002), pp. 2232–2238. DOI: 10.1002/1521-3935(200211)203:15<2232::AID-MACP2232>3.0.CO;2-N.

[48] Brooks A. Abel and Charles L. McCormick. “Mechanistic Insights into Temperature-Dependent Trithiocarbonate Chain-End Degradation during the RAFT Polymerization of N-Arylmethacrylamides”. In: *Macromolecules* 49.2 (2016), pp. 465–474. DOI: 10.1021/acs.macromol.5b02463.

[49] J. J. Vosloo et al. “Controlled Free Radical Polymerization in Water-Borne Dispersion Using Reversible Addition−Fragmentation Chain Transfer”. In: *Macromolecules* 35.13 (2002), pp. 4894–4902. DOI: 10.1021/ma011617j.

[50] T. Sato and D. E. Nalepa. “Shear degradation of cellulose derivatives”. In: *J. Appl. Polym. Sci.* 22.3 (1978), pp. 865–867. DOI: 10.1002/app.1978.070220326.

[51] P. Fordyce, K. L. Devries, and B. M. Fanconi. “Chain Scission and Mechanical Degradation of Polystyrene”. In: *Polymer Engineering & Science* 24.6 (1984), pp. 421–427. DOI: 10.1002/pen.760240606.

[52] K. Kohli et al. “Pyrolytic Depolymerization Mechanisms for Post-Consumer Plastic Wastes”. In: *Energies* 15.23 (2022). ISSN: 1996-1073. DOI: 10.3390/en15238821.

[53] W. Asim et al. “Recent advances in the synthesis of zirconium complexes and their catalytic applications”. In: *Journal of Molecular Structure* 1250 (2022), p. 131925. ISSN: 0022-2860. DOI: 10.1016/j.molstruc.2021.131925.

[54] K. Skrabania et al. “Examining the UV-vis absorption of RAFT chain transfer agents and their use for polymer analysis”. In: *Polym. Chem.* 2.9 (2011), pp. 2074–2083. DOI: 10.1039/C1PY00173F.

[55] T. Li, C. Zhou, and M. Jiang. “UV absorption spectra of polystyrene”. In: *Polymer Bulletin* 25.2 (1991), pp. 211–216. DOI: 10.1007/BF00310794.

[56] S. J. Blanksby and G. B. Ellison. “Bond Dissociation Energies of Organic Molecules”. In: *Accounts of Chemical Research* 36.4 (Apr. 2003), pp. 255–263. DOI: 10.1021/ar020230d.

[57] A. W. Tricker et al. “Hot Spot Generation, Reactivity, and Decay in Mechanochemical Reactors”. In: *Chemical Engineering Journal* 382 (2020), p. 122954. ISSN: 1385-8947. DOI: 10.1016/j.cej.2019.122954.

[58] M. Z. Bekanova et al. “Thermal stability of RAFT-based poly(methyl methacrylate): A kinetic study of the dithiobenzoate and trithiocarbonate end-group effect”. In: *Polymer Degradation and Stability* 164 (2019), pp. 18–27. ISSN: 0141-3910. DOI: https://doi.org/10.1016/j.polymdegradstab.2019.03.017.

[59] N. Ramesh and J. L. Duda. “Diffusion in Polymers below the Glass Transition Temperature: Comparison of Two Approaches Based on Free Volume Concepts”. In: *Korean Journal of Chemical Engineering* 17.3 (2000), pp. 310–317. ISSN: 1975-7220. DOI: 10.1007/BF02699046.

[60] F. Welle. “Diffusion Coefficients and Activation Energies of Diffusion of Organic Molecules in Polystyrene below and above Glass Transition Temperature”. In: *Polymers* 13.8 (2021), p. 1317. DOI: 10.3390/polym13081317.

[61] M. A. Beres et al. “Photoiniferter-RAFT polymerization mediated by bis(trithiocarbonate) disulfides”. In: *Polym. Chem.* (2024). DOI: 10.1039/D3PY01307C.

[62] Sigma-Aldrich. *Thermal Transitions of Homopolymers*. Dec. 2023. URL: https://www.sigmaaldrich.com/NL/en/technical-documents/technical-article/materials-science-and-engineering/polymer-synthesis/thermal-transitions-of-homopolymers.

Abbreviations

^{1}H-NMR proton NMR. 6, 7, 11, 12, 15

AFM Atomic Force Microscopy. 7, 21, 57
AIBN Azobisisobutyronitrile. 6, 7, 19
ATRP Atom Transfer Radical Polymerization. 2, 23

BDTB bis (dithio benzoate). 4, 6, 7, 11–15, 19, 31, 32, 40, 41, 43, 47, 52, 55
BDTC bis (dodecyl trithiocarbonate). 4, 6, 7, 11–20, 22, 31, 32, 34, 37, 40–43, 47, 50, 51, 53, 55

CPDTC 2-cyano-2-propyldodecyl trithiocarbonate. 19, 20, 35, 41, 42, 44, 48, 54
CRP Controlled Radical Polymerization. 2, 3

DB dithiobenzoate. 11, 19, 20, 33, 36
DMF N,N-dimethylformamide. 7
DMT Derjaguin-Muller-Toporov. 21
DSC Differential Scanning Calorimetry. 7, 56

e-PS Expanded Polystyrene. 21–23, 35, 38
ESR Electron Spin Resonance. 11

FRP Free Radical Polymerization. 2–4, 16, 21, 23

GPC Gel Permeation Chromatography. 7, 8

LED Light Emitting Diode. 15, 16

MA Methyl Acrylate. 20, 41, 42

NMP Nitroxide-Mediated Polymerization. 2, 20, 23

PDI Poly Dispersity Index. 2, 8–10, 12–17, 20, 22, 41, 42
PE Polyethylene. 1, 12
PMMA Polymethyl Methacrylate. 1, 6, 7
PP Polypropylene. 1, 12
PS Polystyrene. 1, 6, 7
PTFE Polytetrafluoroethylene. 12, 21
PVDF Polyvinylidene Fluoride. 12

RAFT Reversible Addition-Fragmentation Chain Transfer. ii, 2, 3, 5, 7, 16, 23
RCA RAFT-Capable Agents. 4, 5, 12, 13, 15, 17, 19, 20, 23, 39
RCP Reversed Controlled Polymerization. 3
RDRP Reversible Deactivation Radical Polymerization. ii, 2–4, 15, 21, 23
RI Refractive Index. 7, 8, 13, 18–20, 41

SEC Size Exclusion Chromatography. 7

tBuA tert-Butyl Acrylate. 20–22

TC trithiocarbonate. 11, 16, 18, 19, 33–38
TEMPO 2,2,6,6-Tetramethylpiperidine 1-oxyl. 20
TEMPOL 4-hydroxy-2,2,6,6-tetramethylpiperidin-1-oxyl. 20

UV Ultraviolet. 13
UV/Vis Ultraviolet/Visible. 7, 13, 14, 18–20, 35–38, 42

A

GPC Trace Results

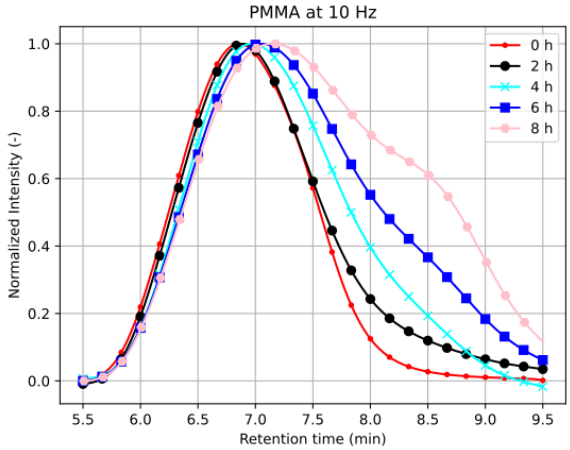

Figure A.1: Normalized GPC trace of PMMA milled at 10 Hz at several timesteps.

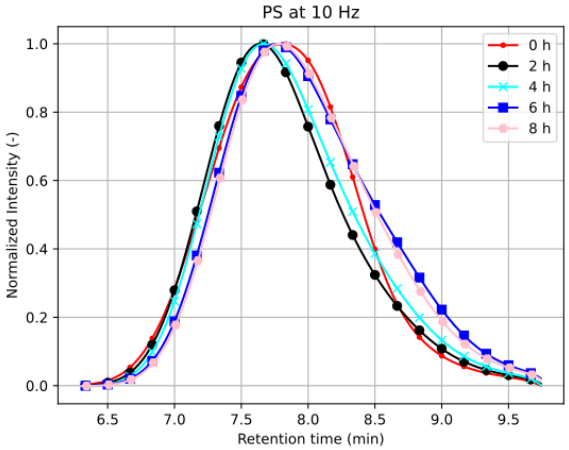

Figure A.2: Normalized GPC trace of PS milled at 10 Hz at several timesteps.

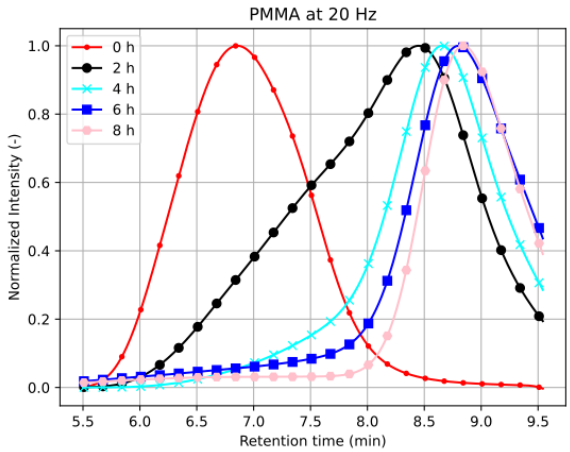

Figure A.3: Normalized GPC trace of PMMA milled at 20 Hz at several timesteps.

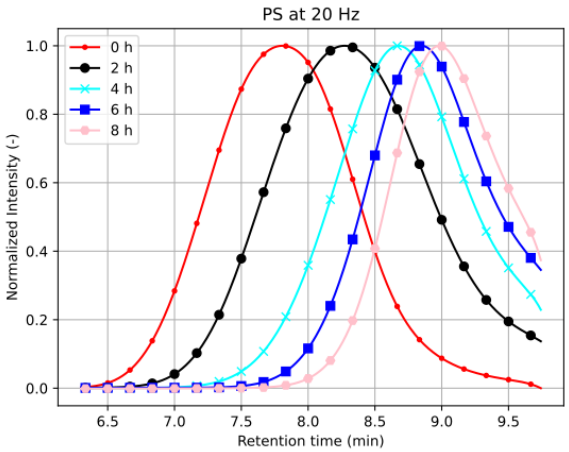

Figure A.4: Normalized GPC trace of PS milled at 20 Hz at several timesteps.

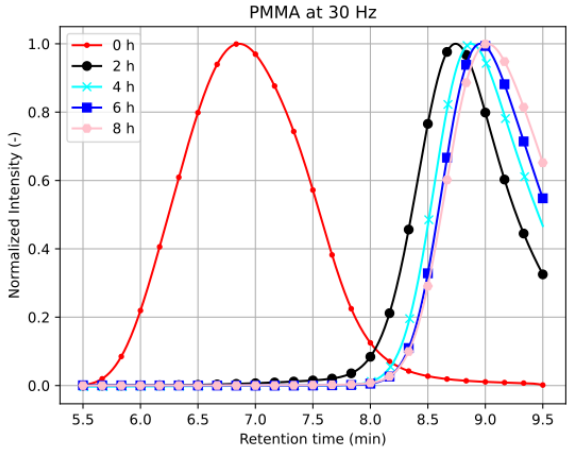

Figure A.5: Normalized GPC trace of PMMA milled at 30 Hz at several timesteps.

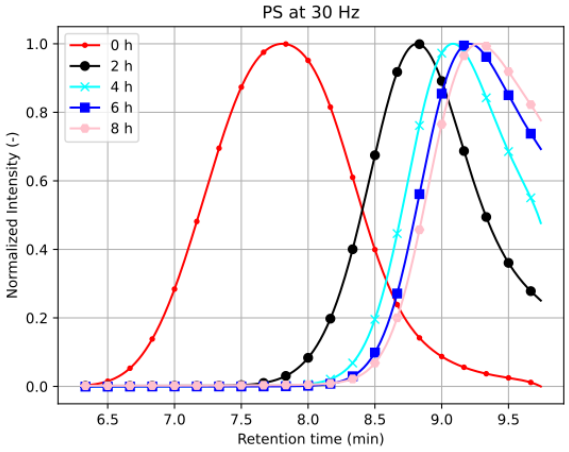

Figure A.6: Normalized GPC trace of PS milled at 30 Hz at several timesteps.

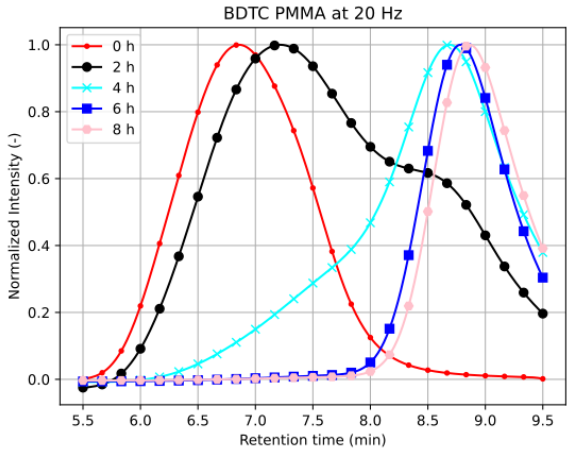

Figure A.7: Normalized GPC trace of PMMA milled with BDTC at 20 Hz at several timesteps.

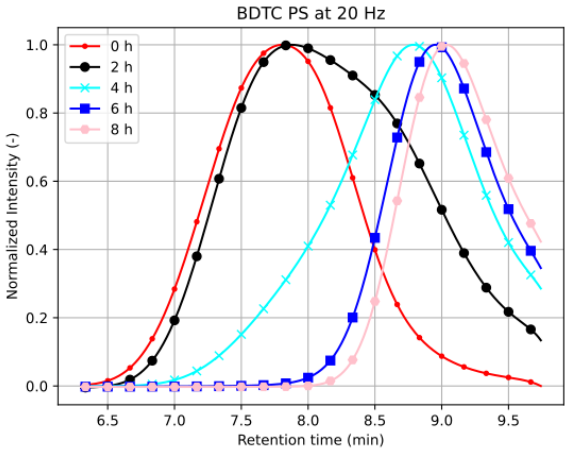

Figure A.8: Normalized GPC trace of PS milled with BDTC at 20 Hz at several timesteps.

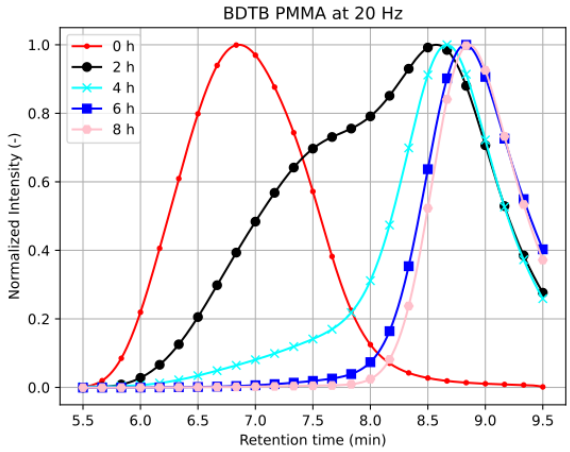

Figure A.9: Normalized GPC trace of PMMA milled with BDTB at 20 Hz at several timesteps.

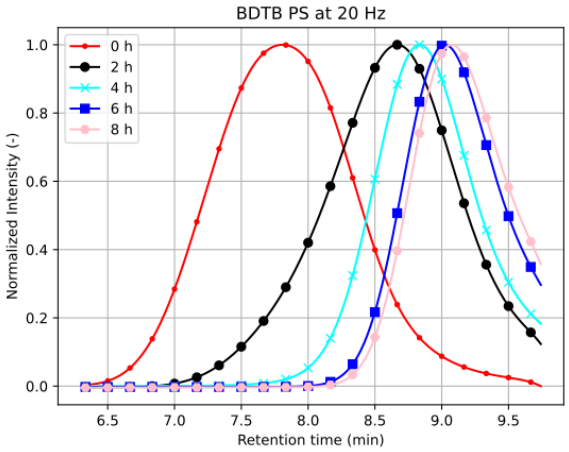

Figure A.10: Normalized GPC trace of PS milled with BDTB at 20 Hz at several timesteps.

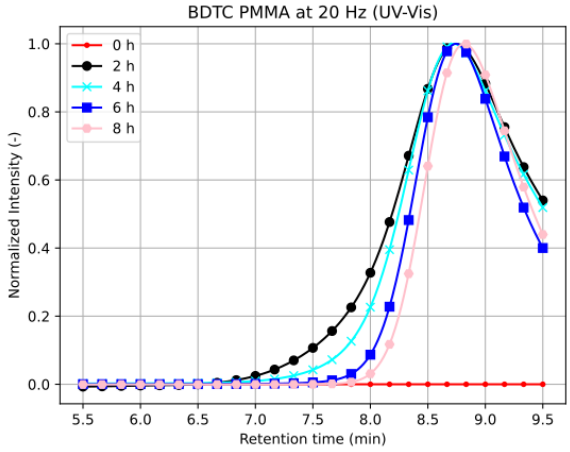

Figure A.11: Normalized GPC trace of PMMA milled with BDTC at 20 Hz at several timesteps using a UV-Vis absorption detector at 325 nm.

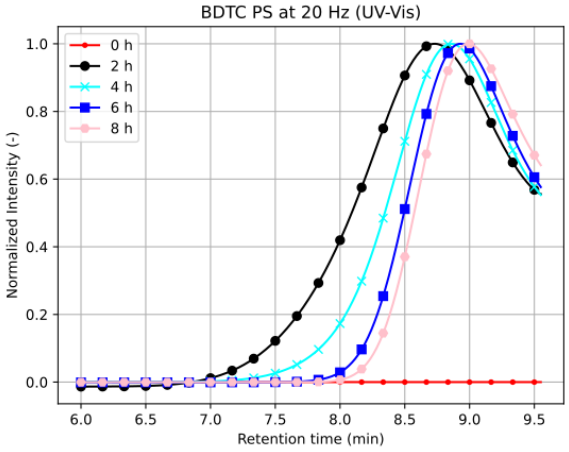

Figure A.12: Normalized GPC trace of PS milled with BDTC at 20 Hz at several timesteps using a UV-Vis absorption detector at 325 nm.

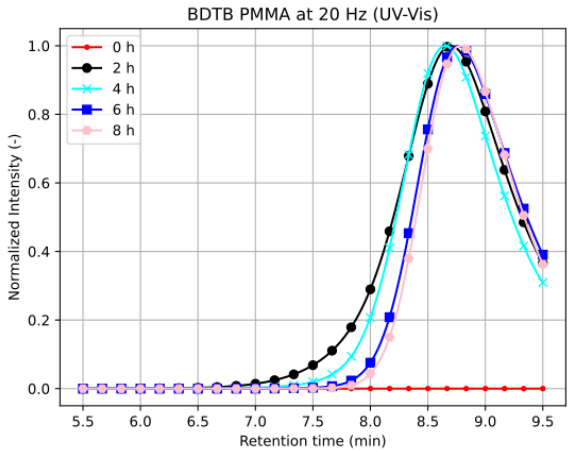

Figure A.13: Normalized GPC trace of PMMA milled with BDTB at 20 Hz at several timesteps using a UV-Vis absorption detector at 325 nm.

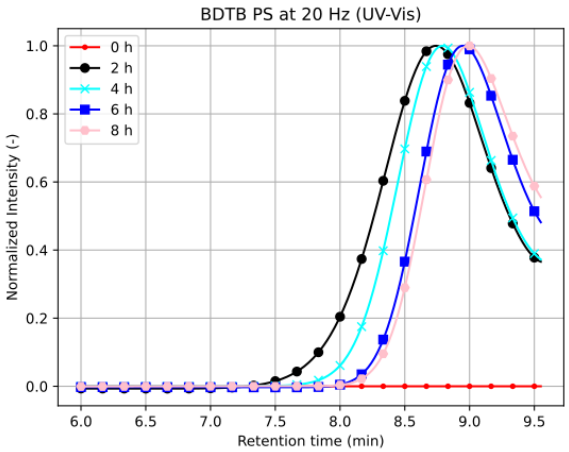

Figure A.14: Normalized GPC trace of PS milled with BDTB at 20 Hz at several timesteps using a UV-Vis absorption detector at 325 nm.

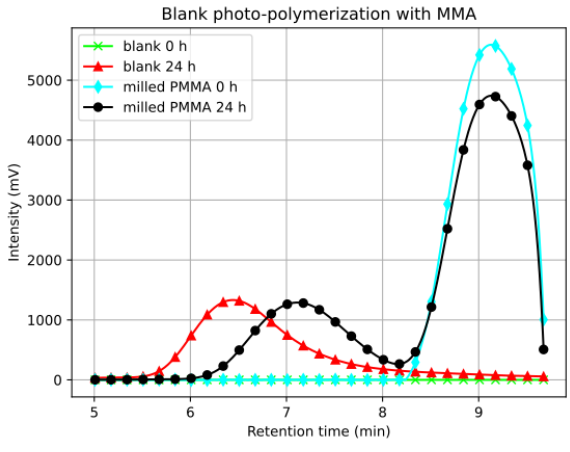

Figure A.15: GPC trace of the blank polymerization of pure MMA in THF (blank) and milled PMMA in MMA and THF (milled PMMA).

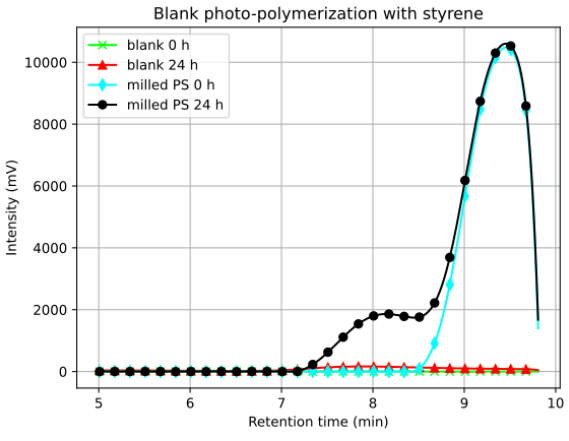

Figure A.16: GPC trace of the blank polymerization of pure styrene in THF (blank) and milled PS in styrene and THF (milled PS).

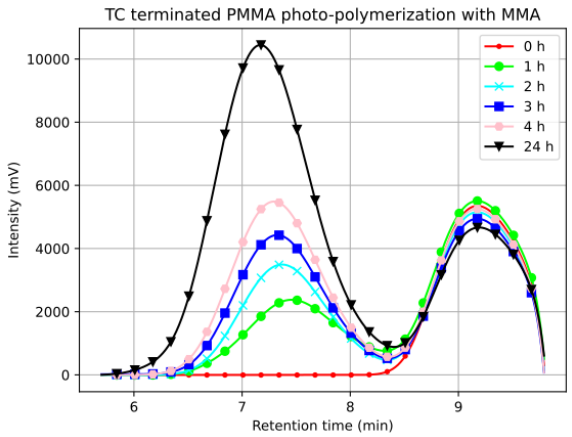

Figure A.17: GPC trace of trithiocarbonate (TC)-terminated PMMA photo-polymerized with MMA in THF after 0, 1, 2, 3, 4 and 24 hours.

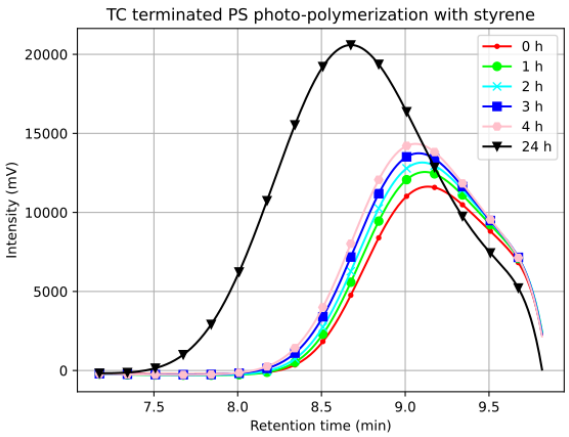

Figure A.18: GPC trace of trithiocarbonate (TC)-terminated PS photo-polymerized with styrene in THF after 0, 1, 2, 3, 4 and 24 hours.

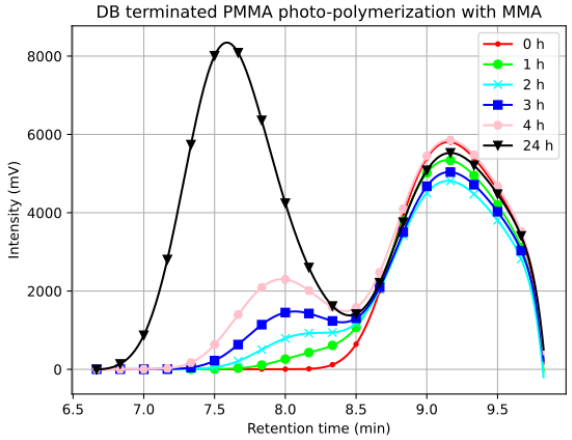

Figure A.19: GPC trace of dithiobenzoate (DB)-terminated PMMA photo-polymerized with MMA in THF after 0, 1, 2, 3, 4 and 24 hours.

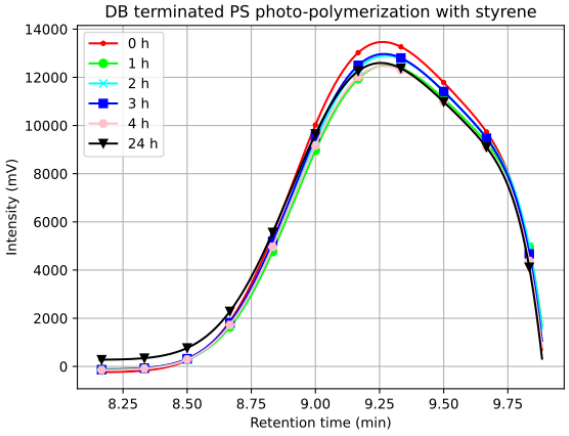

Figure A.20: GPC trace of dithiobenzoate (DB)-terminated PS photo-polymerized with styrene in THF for after 0, 1, 2, 3, 4 and 24 hours.

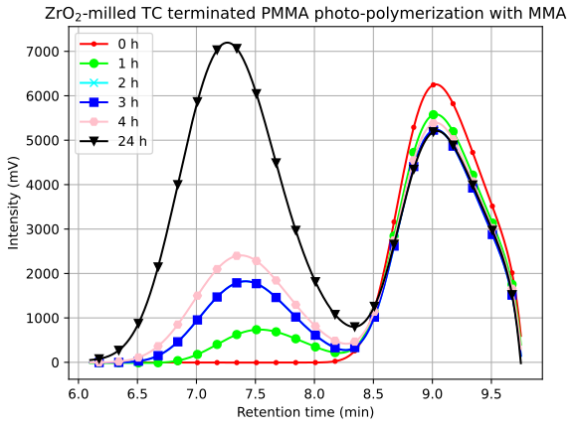

Figure A.21: GPC trace of zirconia milled trithiocarbonate (TC)-terminated PMMA photo-polymerized with MMA in THF after 0, 1, 2, 3, 4 and 24 hours.

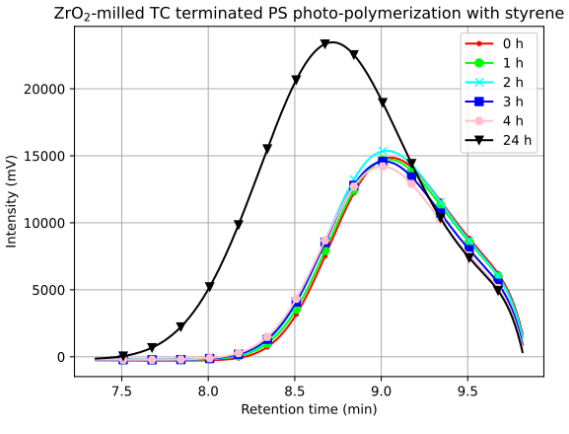

Figure A.22: GPC trace of zirconia milled trithiocarbonate (TC)-terminated PS photo-polymerized with styrene in THF after 0, 1, 2, 3, 4 and 24 hours.

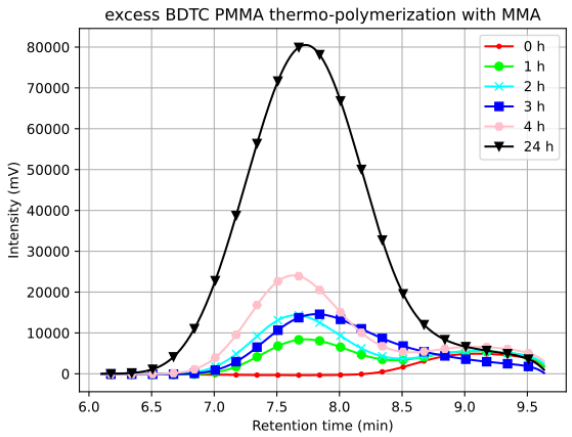

Figure A.23: GPC trace of PMMA milled with excess BDTC at 30 Hz for 8 hours, thermo-polymerized with MMA in THF after 0, 1, 2, 3, 4 and 24 hours.

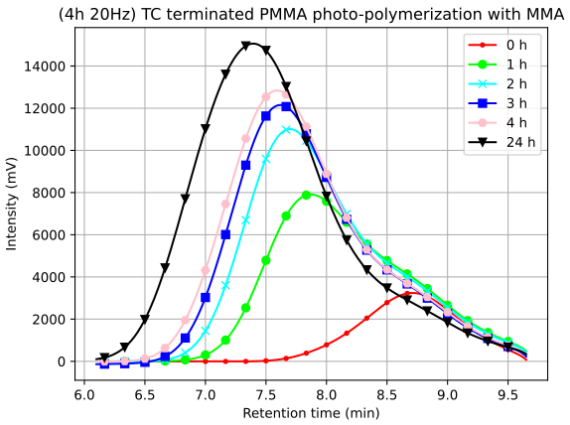

Figure A.24: GPC trace of trithiocarbonate (TC)-terminated PMMA milled at 20 Hz for 4 hours photo-polymerized with MMA in THF after 0, 1, 2, 3, 4 and 24 hours.

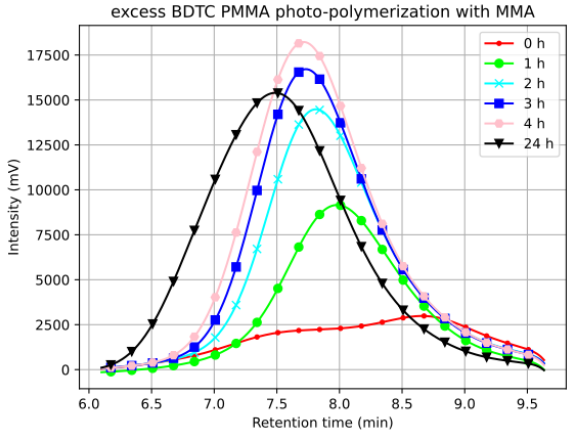

Figure A.25: GPC trace of PMMA milled with excess BDTC at 20 Hz for 4 hours, photo-polymerized with MMA in THF after 0, 1, 2, 3, 4 and 24 hours.

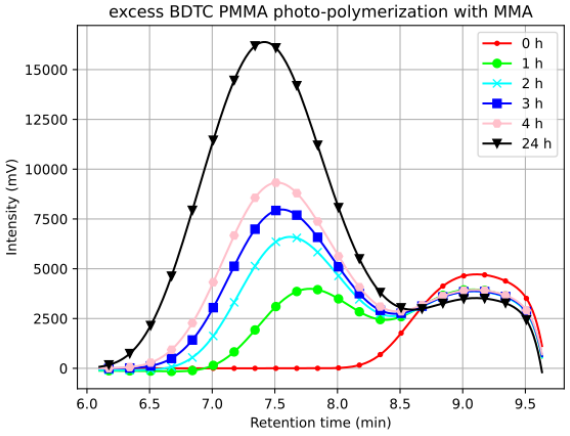

Figure A.26: GPC trace of PMMA milled with excess BDTC at 30 Hz for 8 hours, photo-polymerized with MMA in THF after 0, 1, 2, 3, 4 and 24 hours.

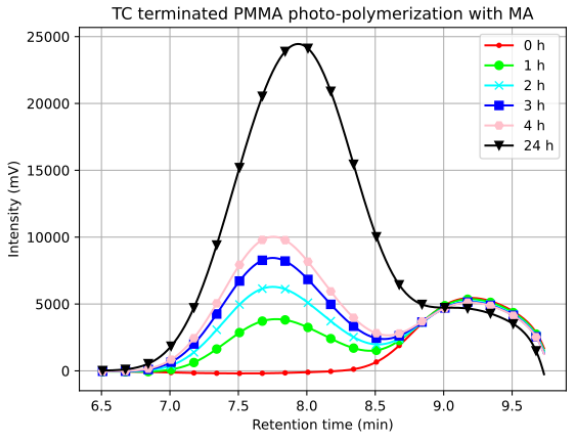

Figure A.27: GPC trace of trithiocarbonate (TC)-terminated PMMA photo-polymerized with MA in THF after 0, 1, 2, 3, 4 and 24 hours.

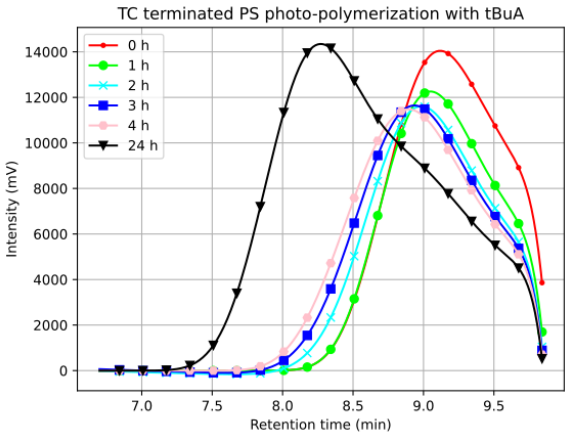

Figure A.28: GPC trace of trithiocarbonate (TC)-terminated PS photo-polymerized with tBuA in THF after 0, 1, 2, 3, 4 and 24 hours.

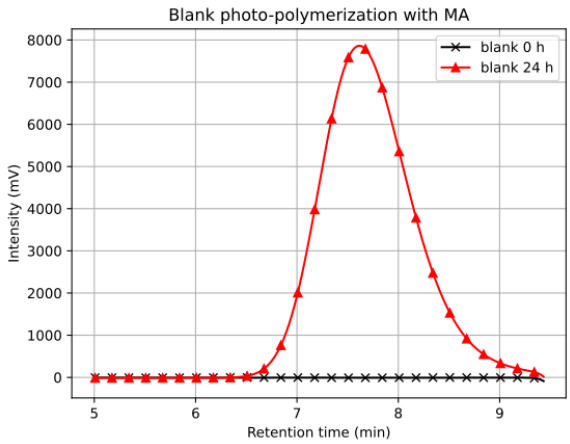

Figure A.29: GPC trace of the blank polymerization of pure MA in THF (blank).

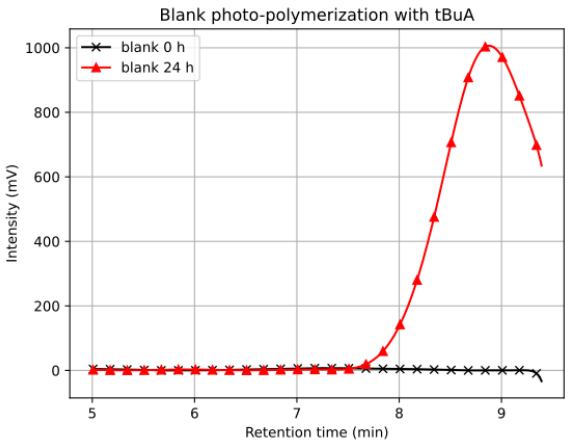

Figure A.30: GPC trace of the blank polymerization of pure tBuA in THF (blank).

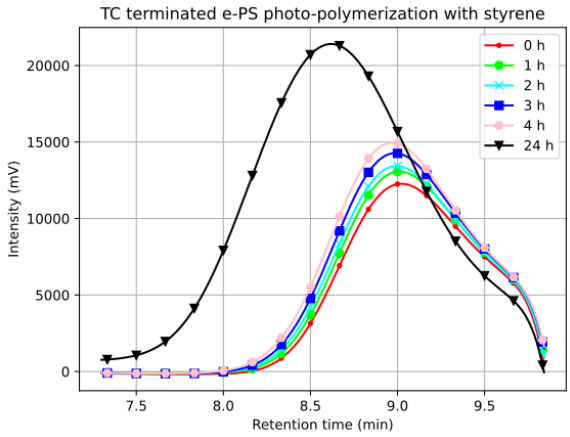

Figure A.31: GPC trace of trithiocarbonate (TC)-terminated e-PS photo-polymerized with styrene in THF after 0, 1, 2, 3, 4 and 24 hours.

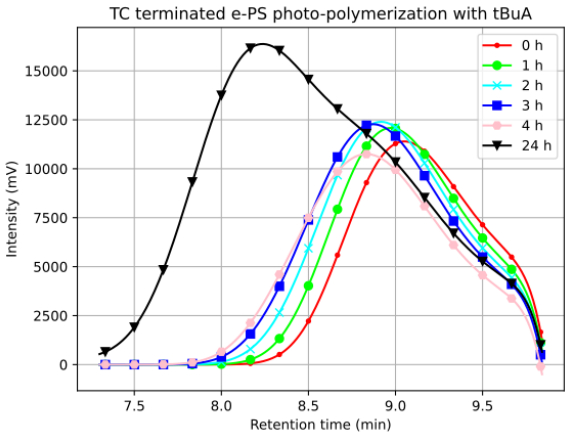

Figure A.32: GPC trace of trithiocarbonate (TC)-terminated e-PS photo-polymerized with tBuA in THF after 0, 1, 2, 3, 4 and 24 hours.

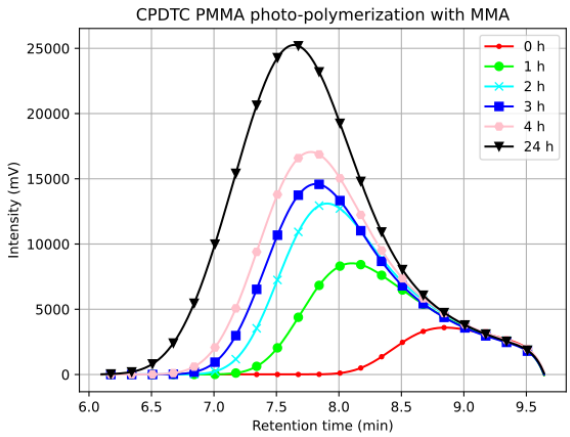

Figure A.33: GPC trace of CPDTC milled PMMA photo-polymerized with MMA in THF after 0, 1, 2, 3, 4 and 24 hours.

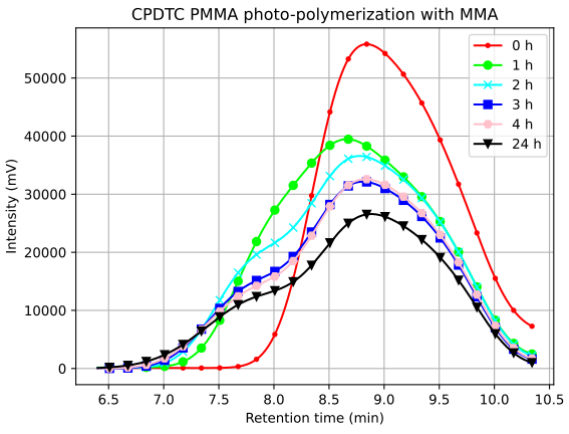

Figure A.34: GPC trace of CPDTC milled PMMA photo-polymerized with MMA in THF after 0, 1, 2, 3, 4 and 24 hours measured using a UV/Vis absorption detector at 325 nm.

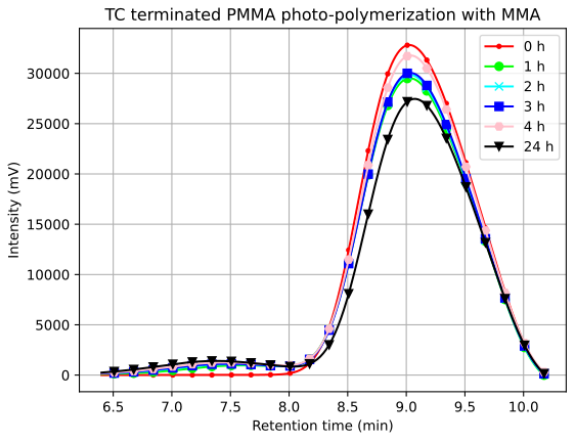

Figure A.35: GPC trace of trithiocarbonate (TC)-terminated PMMA photo-polymerized with MMA in THF after 0, 1, 2, 3, 4 and 24 hours measured using a UV/Vis absorption detector at 325 nm.

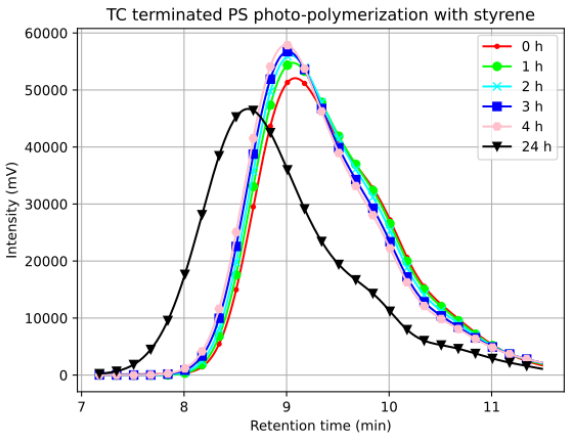

Figure A.36: GPC trace of trithiocarbonate (TC)-terminated PS photo-polymerized with styrene in THF after 0, 1, 2, 3, 4 and 24 hours measured using a UV/Vis absorption detector at 325 nm.

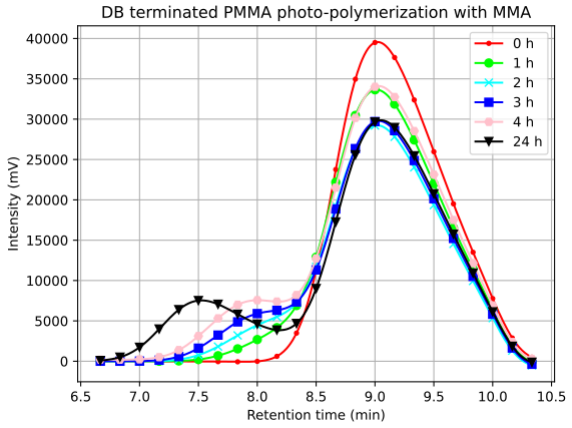

Figure A.37: GPC trace of dithiobenzoate (DB)-terminated PMMA photo-polymerized with MMA in THF after 0, 1, 2, 3, 4 and 24 hours measured using a UV/Vis absorption detector at 325 nm.

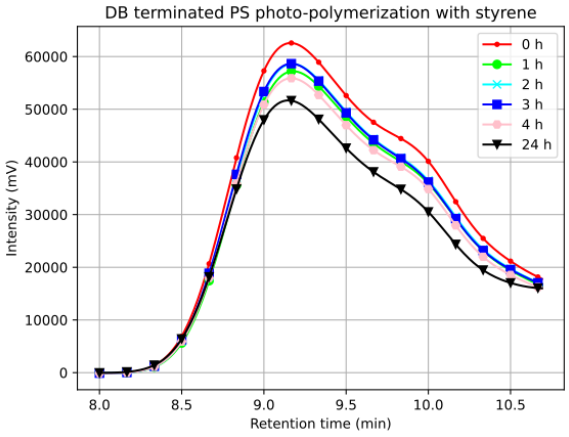

Figure A.38: GPC trace of dithiobenzoate (DB)-terminated PS photo-polymerized with styrene in THF after 0, 1, 2, 3, 4 and 24 hours measured using a UV/Vis absorption detector at 325 nm.

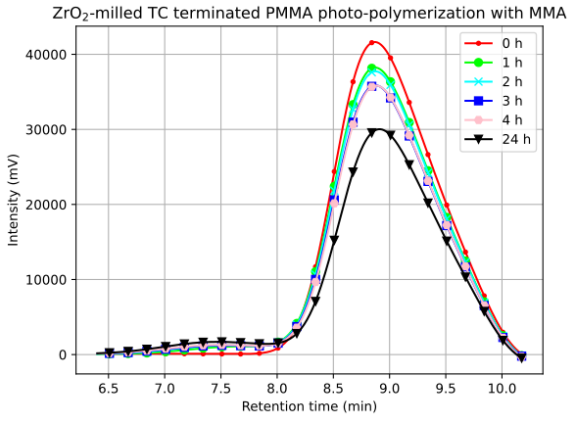

Figure A.39: GPC trace of zirconia milled (TC)-terminated PMMA photo-polymerized with MMA in THF after 0, 1, 2, 3, 4 and 24 hours measured using a UV/Vis absorption detector at 325 nm.

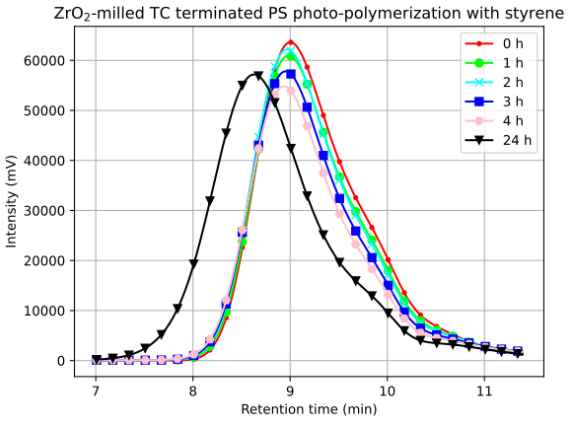

Figure A.40: GPC trace of zirconia milled (TC)-terminated PS photo-polymerized with styrene in THF after 0, 1, 2, 3, 4 and 24 hours measured using a UV/Vis absorption detector at 325 nm.

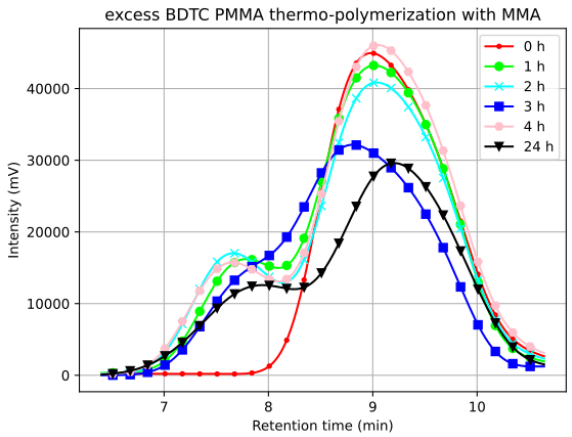

Figure A.41: GPC trace of PMMA milled with excess BDTC at 30 Hz for 8 hours, thermo-polymerized with MMA in THF after 0, 1, 2, 3, 4 and 24 hours measured using a UV/Vis absorption detector at 325 nm.

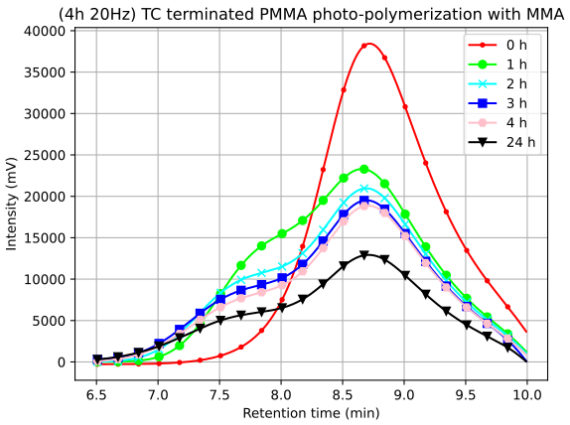

Figure A.42: GPC trace of trithiocarbonate (TC)-terminated PMMA milled at 20 Hz for 4 hours photo-polymerized with MMA in THF after 0, 1, 2, 3, 4 and 24 hours measured using a UV/Vis absorption detector at 325 nm.

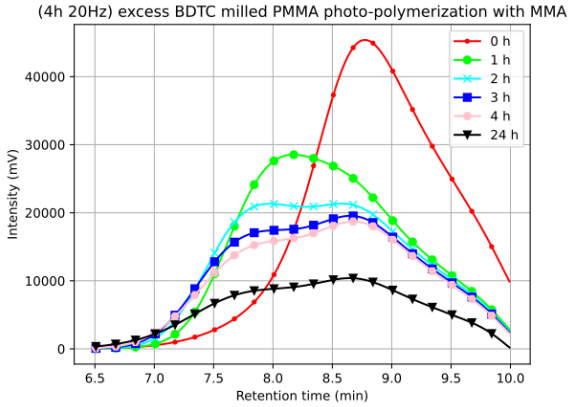

Figure A.43: GPC trace of PMMA milled with excess BDTC at 20 Hz for 4 hours, photo-polymerized with MMA in THF after 0, 1, 2, 3, 4 and 24 hours measured using a UV/Vis absorption detector at 325 nm.

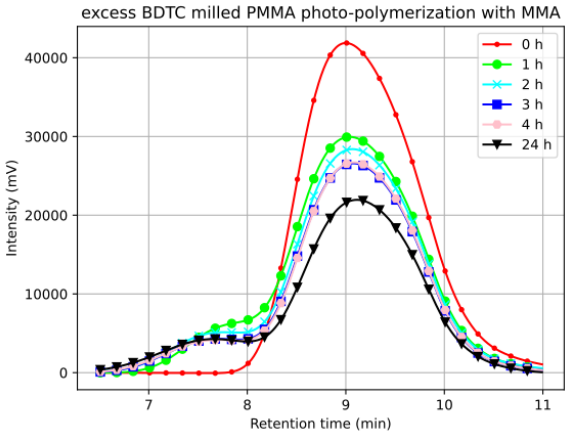

Figure A.44: GPC trace of PMMA milled with excess BDTC at 30 Hz for 8 hours, photo-polymerized with MMA in THF after 0, 1, 2, 3, 4 and 24 hours measured using a UV/Vis absorption detector at 325 nm.

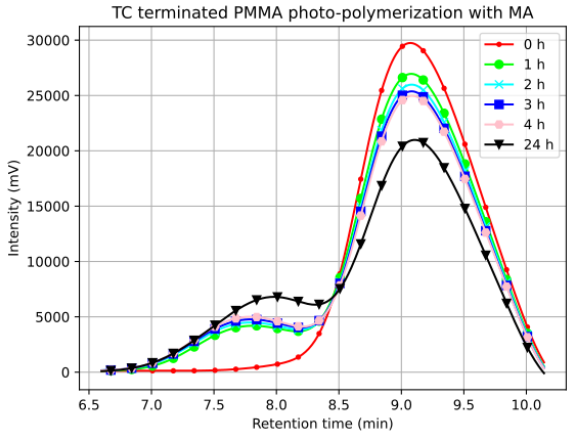

Figure A.45: GPC trace of trithiocarbonate (TC)-terminated PMMA photo-polymerized with MA in THF after 0, 1, 2, 3, 4 and 24 hours measured using a UV/Vis absorption detector at 325 nm.

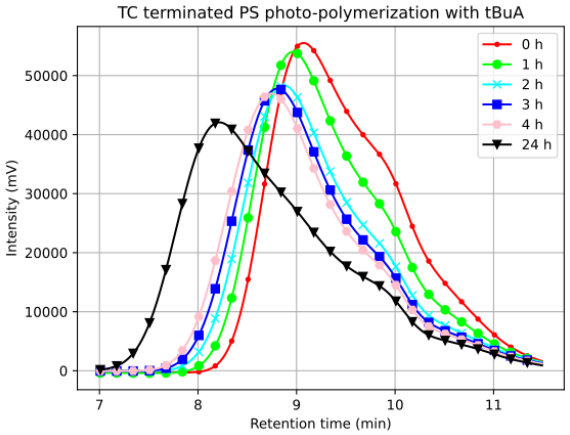

Figure A.46: GPC trace of trithiocarbonate (TC)-terminated PS photo-polymerized with tBuA in THF after 0, 1, 2, 3, 4 and 24 hours measured using a UV/Vis absorption detector at 325 nm.

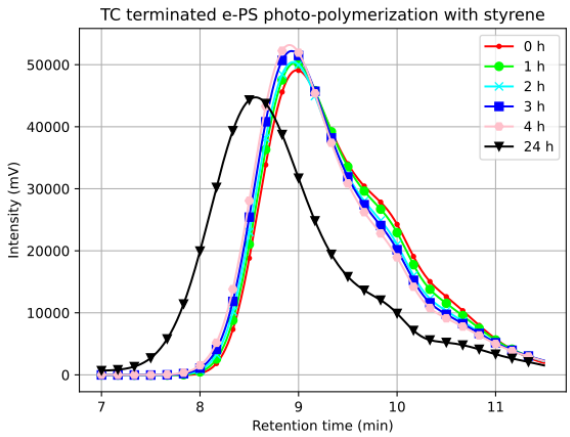

Figure A.47: GPC trace of trithiocarbonate (TC)-terminated e-PS photo-polymerized with styrene in THF after 0, 1, 2, 3, 4 and 24 hours measured using a UV/Vis absorption detector at 325 nm.

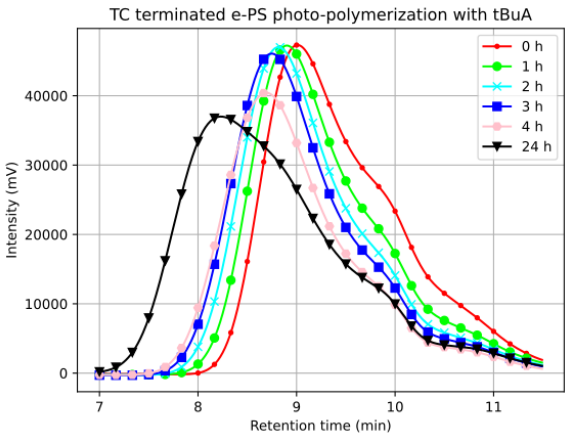

Figure A.48: GPC trace of trithiocarbonate (TC)-terminated e-PS photo-polymerized with tBuA in THF after 0, 1, 2, 3, 4 and 24 hours measured using a UV/Vis absorption detector at 325 nm.

B

Miscellaneous Experiments

This section will very briefly go over experiments we have done to optimize certain phenomena, but have however not yielded satisfactory results to include in the official report. The discussion will be very brief and data is not reported.

Wet milling: We have tried wet milling with the addition of pentane and hexane. The idea behind this was to attempt to increase the mass transfer by having the RCA dissolved in a solvent that does not dissolve the polymers themselves. Wet milling greatly slowed down the segmentation rate and did not appear to have much of a difference at improving the mass transfer.

Monomer milling: We have tried milling with the addition of the polymers native polymer. The idea behind this was to attempt to prolong the lifetime of the radical by having it react with the monomers until it comes in contact with a RCA. At small quantities (10 µL) it had little to no effect at reducing the side group formations. At larger quantities (100 µL) it significantly plasticized PS. PS stuck to one of the sides of the mill and in essence was not segmented during the entire experiment. PMMA segmentation rate was reduced, however even after milling no significant difference was observed than when milled without its native monomer MMA.

Impregnation: We have tried to impregnate the polymers with RCA by dissolving the RCA in pentane, and then submerging the polymer in the solution overnight. This was to allow the RCA to diffuse within the polymer particles. Afterward impregnation, the pentane was allowed to evaporate and then the impregnate polymers were milled. This showed negligible difference.

C

Tables

PMMA 20 Hz	0 h	2 h	4 h	6 h	8 h
M_n (kDa)	318.6	18.8	10.8	8.2	7.8
M_w (kDa)	1070.5	203.2	55.4	24.0	11.5
PDI (-)	3.36	10.81	5.13	2.93	1.48

PS 20 Hz	0 h	2 h	4 h	6 h	8 h
M_n (kDa)	123.5	39.0	25.3	20.2	17.6
M_w (kDa)	272.9	83.9	41.5	28.9	23.1
PDI (-)	2.21	2.15	1.64	1.43	1.31

Table C.1: Molecular weight (M_n & M_w) evolution of PMMA and PS milled at 20 Hz.

PMMA 10 Hz	0 h	2 h	4 h	6 h	8 h
M_n (kDa)	318.6	166.3	136.3	54.8	39.8
M_w (kDa)	1070.5	974.5	774.2	648.8	537.3
PDI (-)	3.36	5.86	5.68	11.84	13.5

PS 10 Hz	0 h	2 h	4 h	6 h	8 h
M_n (kDa)	123.5	94.0	84.4	67.1	65.6
M_w (kDa)	272.9	221.8	205.9	171.8	152.8
PDI (-)	2.21	2.36	2.44	2.56	2.33

Table C.2: Molecular weight (M_n & M_w) evolution of PMMA and PS milled at 10 Hz.

PMMA 30 Hz	0 h	2 h	4 h	6 h	8 h
M_n (kDa)	318.6	8.3	6.7	6.0	5.5
M_w (kDa)	1070.5	15.6	9.7	8.52	7.9
PDI (-)	3.36	1.88	1.45	1.42	1.43

PS 30 Hz	0 h	2 h	4 h	6 h	8 h
M_n (kDa)	123.5	21.2	15.6	13.7	12.9
M_w (kDa)	272.9	29.0	19.2	16.6	15.4
PDI (-)	2.21	1.37	1.23	1.21	1.19

Table C.3: Molecular weight (M_n & M_w) evolution of PMMA and PS at 30 Hz.

BDTC PMMA	0 h	2 h	4 h	6 h	8 h
M_n (kDa)	318.6	25.6	10.9	8.0	7.1
M_w (kDa)	1070.5	464.9	88.2	12.9	10.4
PDI (-)	3.36	18.16	8.09	1.61	1.46

BDTC PS	0 h	2 h	4 h	6 h	8 h
M_n (kDa)	123.5	44.5	25.2	18.2	16.3
M_w (kDa)	272.9	126.8	51.4	23.7	20.2
PDI (-)	2.21	2.85	2.04	1.30	1.24

Table C.4: Molecular weight (M_n & M_w) evolution of PMMA and PS milled with BDTC at 20 Hz.

BDTB PMMA	0 h	2 h	4 h	6 h	8 h
M_n (kDa)	318.6	17.4	11.3	7.5	7.4
M_w (kDa)	1070.5	208.8	66.9	14.2	10.8
PDI (-)	3.36	12.00	5.92	1.89	1.46

BDTB PS	0 h	2 h	4 h	6 h	8 h
M_n (kDa)	123.5	30.2	21.8	17.8	16.2
M_w (kDa)	272.9	52.9	28.6	21.0	19.2
PDI (-)	2.21	1.75	1.31	1.18	1.19

Table C.5: Molecular weight (M_n & M_w) evolution of PMMA and PS milled with BDTB at 20 Hz.

BDTC PMMA	0 h	2 h	4 h	6 h	8 h
M_n (kDa)	0.0	5.5	5.9	5.7	5.3
M_w (kDa)	0.0	12.1	9.5	7.5	6.9
PDI (-)	0.0	2.20	1.62	1.32	1.31

BDTC PS	0 h	2 h	4 h	6 h	8 h
M_n (kDa)	0.0	19.2	15.5	14.3	13.9
M_w (kDa)	0.0	38.4	24.6	19.0	17.4
PDI (-)	0.0	2.00	1.59	1.33	1.25

Table C.6: Molecular weight (M_n & M_w) evolution of BDTC terminated PMMA and PS at 20 Hz using the UV-Vis scattering detector.

BDTB PMMA	0 h	2 h	4 h	6 h	8 h
M_n (kDa)	0.0	7.4	7.5	6.4	6.3
M_w (kDa)	0.0	12.1	10.1	7.9	7.6
PDI (-)	0.0	1.63	1.34	1.24	1.20

BDTB PS	0 h	2 h	4 h	6 h	8 h
M_n (kDa)	0.0	21.5	19.2	16.6	15.0
M_w (kDa)	0.0	28.6	24.0	19.4	17.7
PDI (-)	0.0	1.33	1.25	1.17	1.18

Table C.7: Molecular weight (M_n & M_w) evolution of BDTB terminated PMMA and PS at 20 Hz.

k (kDa^{-1} h^{-1})	Bare 10 Hz	Bare 20 Hz	Bare 30 Hz	BDTC 20 Hz	BDTB 20 Hz
PMMA	$2.41{\cdot}10^{-3}$	$18.1{\cdot}10^{-3}$	$26.9{\cdot}10^{-3}$	$18.8{\cdot}10^{-3}$	$19.1{\cdot}10^{-3}$
PS	$0.98{\cdot}10^{-3}$	$6.65{\cdot}10^{-3}$	$10.4{\cdot}10^{-3}$	$7.18{\cdot}10^{-3}$	$7.66{\cdot}10^{-3}$

Table C.8: Segmentation/degradation rate constant from the simple polymer degradation kinetic model proposed by Sato & Nalepa [50].

	0 h	1 h	2 h	3 h	4 h	24 h
TC-PMMA 1	4.9 (1.32)[a]	136.2 (1.63)	146.6 (1.79)	171.3 (1.78)	167.2 (1.91)	209.8 (2.05)
TC-PMMA 2	10.0 (1.83)	22.0 (3.02)	26.5 (3.72)	30.8 (4.03)	29.0 (4.81)	51.2 (5.30)
TC-PMMA 3	14.8 (9.03)	28.8 (2.96)	31.4 (4.10)	35.4 (3.68)	39.9 (3.38)	68.7 (4.07)
TC-PMMA 4	5.9 (1.30)[a]	72.3 (1.49)	89.5 (1.70)	98.5 (1.87)	102.4 (2.00)	121.5 (2.43)
TC-PMMA 5	5.7 (1.39)[a]	75.2 (1.44)	85.5 (1.55)	90.9 (1.57)	87.3 (1.61)	73.4 (2.04)
TC-PMMA 6	5.9 (1.30)[a]	119.2 (1.40)	136.3 (1.56)	145.6 (1.62)	149.6 (1.76)	176.0 (1.97)
TC-PMMA 7	5.0 (1.32)[a]	67.7 (1.48)	70.5 (1.54)	69.0 (1.59)	68.8 (1.59)	50.9 (1.78)
TC-PMMA 8	7.1 (1.52)	15.6 (2.61)	19.9 (3.13)	23.4 (3.35)	24.5 (3.75)	35.7 (4.43)
DB-PMMA 9	4.8 (1.34)[a]	34.1 (1.12)	40.2 (1.16)	44.2 (1.16)	49.7 (1.31)	94.7 (1.48)
TC-PS 10	17.0 (1.28)	17.5 (1.29)	17.9 (1.30)	18.3 (1.31)	18.7 (1.33)	29.3 (1.56)
TC-PS 11	19.3 (1.27)	19.5 (1.27)	19.9 (1.27)	20.1 (1.28)	20.5 (1.29)	29.3 (1.50)
TC-PS 12	15.6 (1.21)	16.2 (1.25)	17.3 (1.29)	18.3 (1.31)	18.9 (1.38)	27.3 (1.83)
DB-PS 13	13.6 (1.16)	13.4 (1.16)	13.4 (1.16)	13.6 (1.16)	13.6 (1.15)	13.8 (1.16)
TC-ePS 14	16.5 (1.23)	16.8 (1.22)	17.2 (1.21)	17.3 (1.26)	17.7 (1.23)	27.5 (1.41)
TC-ePS 15	16.2 (1.20)	17.6 (1.22)	18.9 (1.25)	19.8 (1.28)	20.7 (1.32)	29.7 (1.85)
pure MMA	0 (-)	- (-)	- (-)	- (-)	- (-)	1124.4 (1.99)
PMMA 16	5.5 (1.34)[a]	- (-)	- (-)	- (-)	- (-)	214.7 (2.41)
pure styrene	0 (-)	- (-)	- (-)	- (-)	- (-)	0 (-)
PS 17	13.2 (1.12)	- (-)	- (-)	- (-)	- (-)	14.9 (1.66)
pure tBuA	0 (-)	- (-)	- (-)	- (-)	- (-)	74.0 (1.40)
pure MA	0 (-)	- (-)	- (-)	- (-)	- (-)	76.3 (1.94)

Table C.9: Molecular weight evolution of all polymerization experiments measured on the RI detector, displaying the Mn (in kDa) with the PDI in parenthesis. All experiments are photo polymerization unless mentioned explicitly otherwise. 1: PMMA with MMA, 2: (4 h 20 Hz milled) PMMA with MMA, 3: (excess BDTC 4 h 20 Hz) PMMA with MMA, 4: (excess BDTC) PMMA with MMA, 5: (thermally initiated, excess BDTC) PMMA with MMA, 6: (ZrO_2 milled) PMMA with MMA, 7: PMMA with MA, 8: (CPDTC milled) PMMA with MMA, 9: PMMA with MMA, 10: PS with styrene, 11: (ZrO_2 milled) PS with styrene, 12: PS with tBuA, 13: PS with styrene, 14: e-PS with styrene, 15: e-PS with tBuA, 16: (bare milled) PMMA with MMA, 17: (bare milled) PS with styrene. [a] M_n and PDI of the original peak at t = 0, the subsequent data is of the newly formed peak.

	0 h	1 h	2 h	3 h	4 h	24 h
TC-PMMA 1	15.0 (1.21)[a]	148.3 (1.81)	160.6 (1.86)	162.0 (1.91)	166.1 (1.93)	175.9 (1.99)
TC-PMMA 2	20.4 (1.37)	26.6 (2.04)	26.4 (2.39)	26.6 (2.65)	25.9 (2.61)	26.9 (3.01)
TC-PMMA 3	17.1 (1.78)	26.7 (2.13)	26.8 (2.53)	26.1 (2.75)	25.7 (2.81)	27.4 (3.39)
TC-PMMA 4	13.7 (1.35)[a]	117.6 (1.31)	134.2 (1.46)	140.7 (1.54)	144.9 (1.58)	148.2 (1.78)
TC-PMMA 5	13.1 (2.37)[a]	108.3 (1.38)	117.8 (1.46)	126.1 (1.48)	124.1 (1.47)	98.6 (1.66)
TC-PMMA 6	16.9 (1.23)[a]	158.0 (1.56)	167.1 (1.64)	163.5 (1.77)	177.0 (1.69)	174.9 (1.71)
TC-PMMA 7	14.3 (1.25)[a]	97.0 (1.49)	96.6 (1.47)	98.0 (1.60)	98.1 (1.58)	84.0 (1.58)
TC-PMMA 8	14.5 (1.45)	19.5 (2.03)	19.2 (2.32)	19.0 (2.47)	18.7 (2.53)	19.0 (2.53)
DB-PMMA 9	13.8 (1.24)[a]	57.4 (1.12)	63.2 (1.15)	69.3 (1.20)	75.6 (1.24)	124.2 (1.50)
TC-PS 10	11.3 (1.49)	11.8 (1.51)	12.1 (1.51)	12.3 (1.55)	12.8 (1.55)	19.0 (1.94)
TC-PS 11	13.3 (1.46)	13.7 (1.46)	14.1 (1.46)	14.4 (1.46)	14.8 (1.48)	21.5 (1.79)
TC-PS 12	13.9 (1.21)	14.8 (1.26)	16.3 (1.31)	17.3 (1.35)	18.2 (1.40)	24.3 (1.86)
DB-PS 13	13.5 (1.15)	13.0 (1.16)	13.0 (1.16)	13.0 (1.17)	13.3 (1.15)	13.1 (1.17)
TC-ePS 14	14.6 (1.23)	14.9 (1.24)	14.9 (1.26)	15.4 (1.26)	15.6 (1.28)	22.7 (1.55)
TC-ePS 15	14.3 (1.23)	15.7 (1.28)	17.2 (1.32)	18.4 (1.36)	19.5 (1.40)	24.5 (1.89)

Table C.10: Molecular weight evolution of all polymerization experiments measured on the UV/Vis scattering detector, displaying the Mn (in kDa) with the PDI in parenthesis. All experiments are photo polymerization unless mentioned explicitly otherwise. PS calibration is used for PMMA without any conversion factor. 1: PMMA with MMA, 2: (4 h 20 Hz milled) PMMA with MMA, 3: (excess BDTC 4 h 20 Hz) PMMA with MMA, 4: (excess BDTC) PMMA with MMA, 5: (thermally initiated, excess BDTC) PMMA with MMA, 6: (ZrO_2 milled) PMMA with MMA, 7: PMMA with MA, 8: (CPDTC milled) PMMA with MMA, 9: PMMA with MMA, 10: PS with styrene, 11: (ZrO_2 milled) PS with styrene, 12: PS with tBuA, 13: PS with styrene, 14: e-PS with styrene, 15: e-PS with tBuA. [a] M_n and PDI of the original peak at t = 0, the subsequent data is of the newly formed peak. Regarding PMMA, it is advised to only view the trend and not the absolute values, as a consistent conversion from PS calibration to PMMA over the whole distribution range proves difficult.

D

Structures of select Molecules

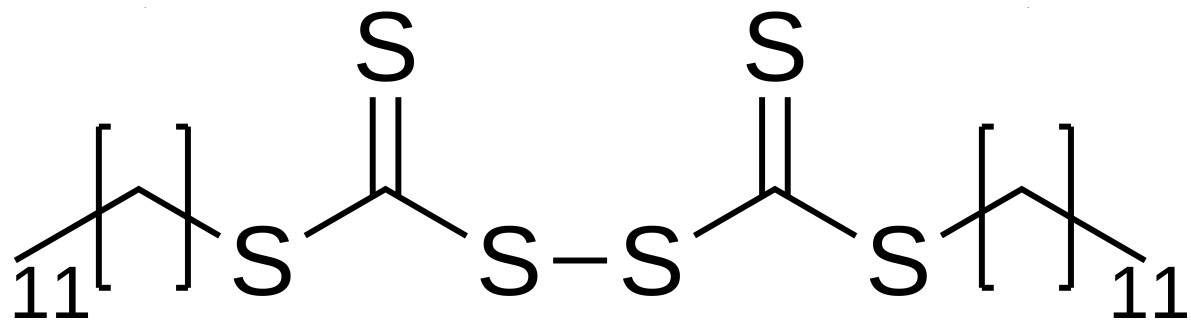

Figure D.1: Molecular structure of bis (dodecyl trithiocarbonate) (BDTC).

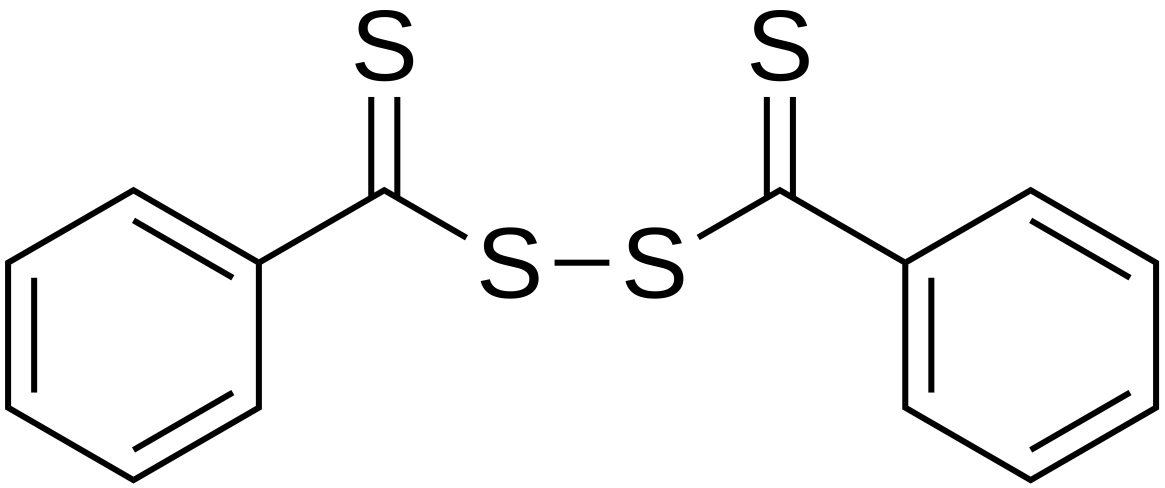

Figure D.2: Molecular structure of bis (dithio benzoate) (BDTB).

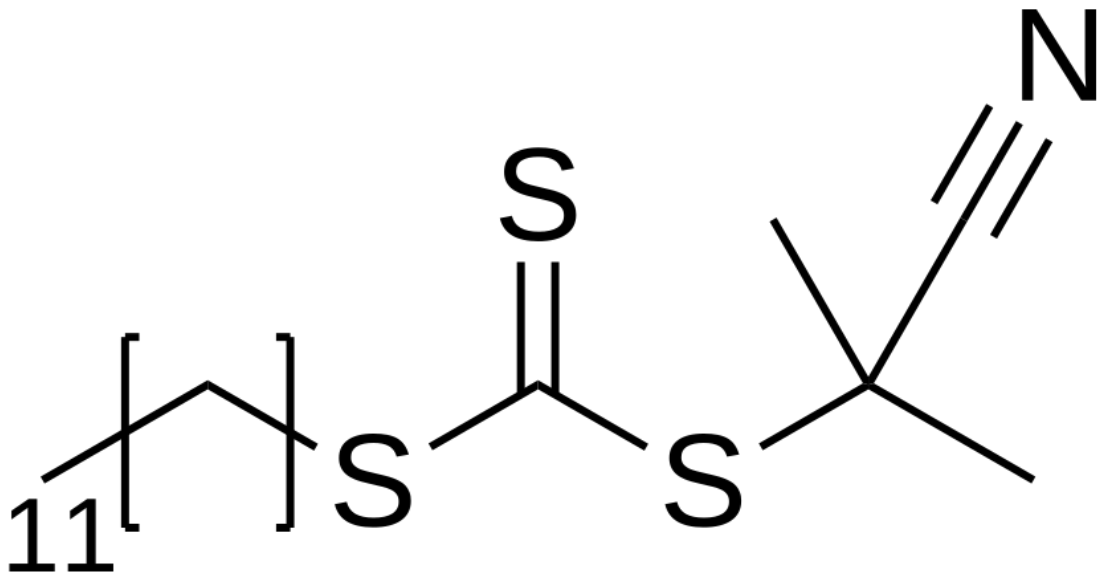

Figure D.3: Molecular structure of 2-cyano-2-propyldodecyl trithiocarbonate (CPDTC).

E

NMR Spectra

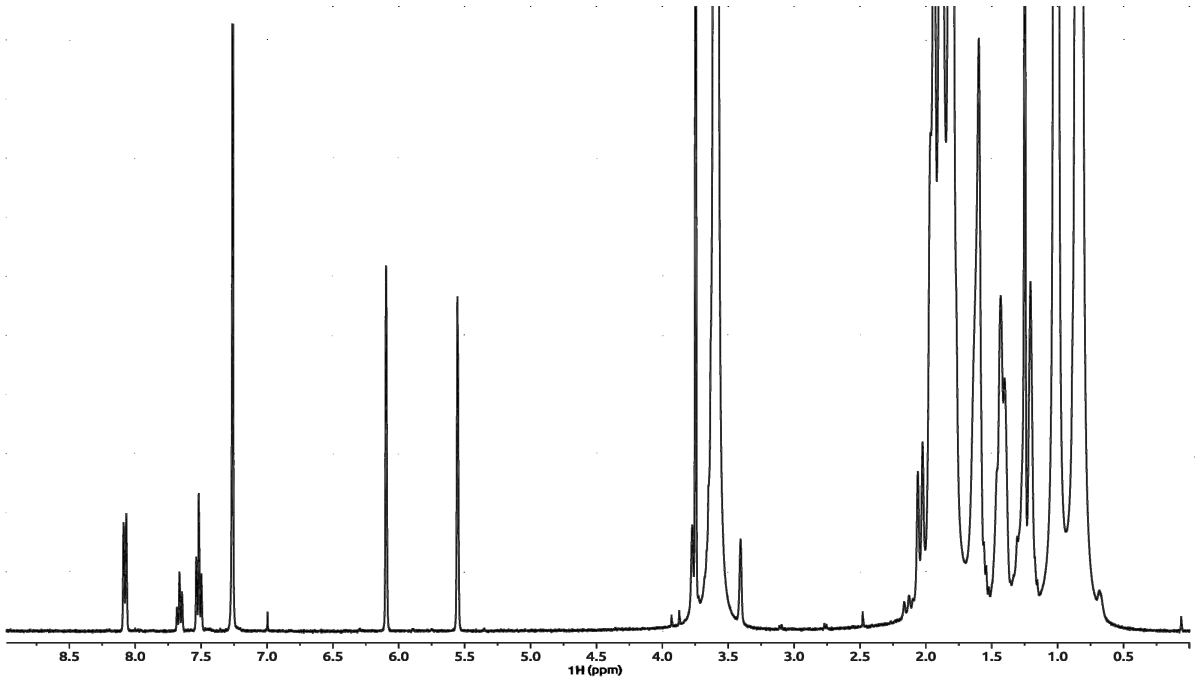

Figure E.1: ^{1}H-NMR spectrum of virgin PMMA.

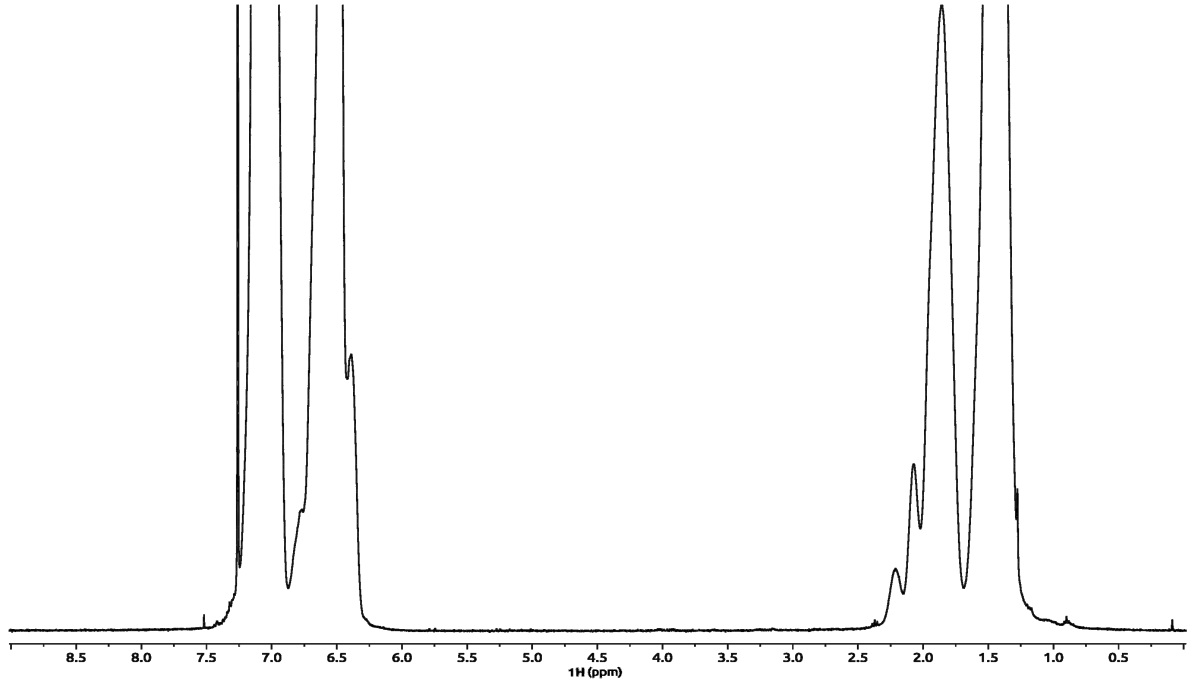

Figure E.2: ^{1}H-NMR spectrum of virgin PS.

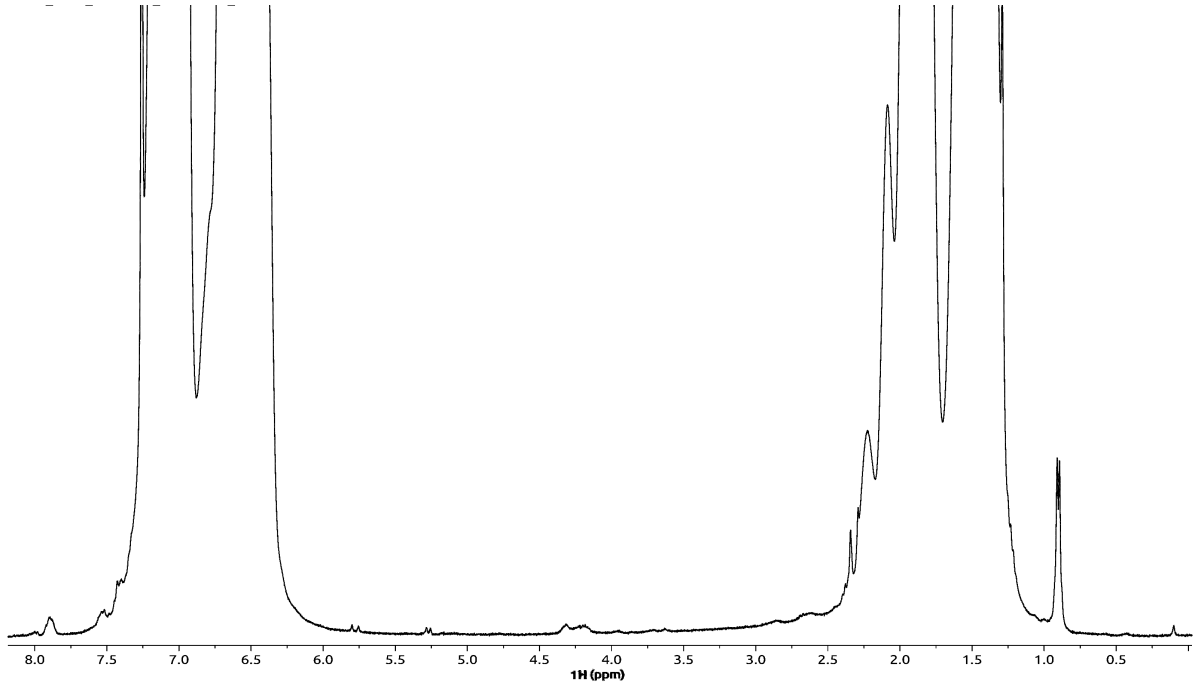

Figure E.3: ^{1}H-NMR spectrum of virgin EPS.

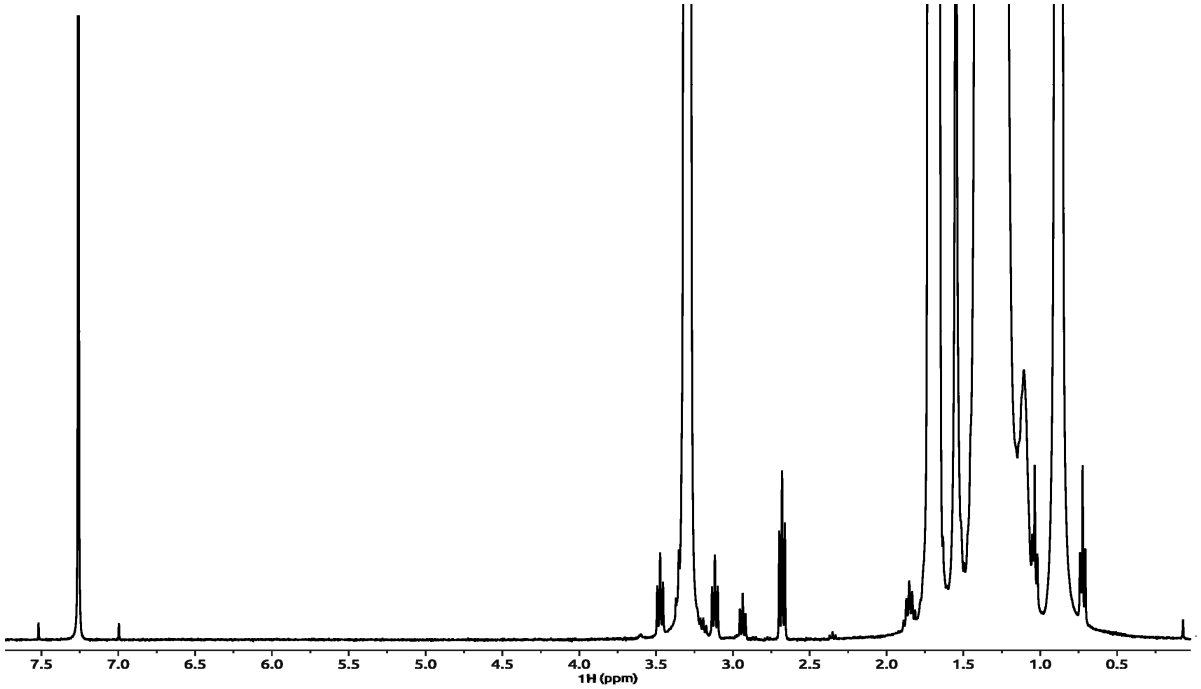

Figure E.4: ^{1}H-NMR spectrum of bis (dodecyl trithiocarbonate) (BDTC).

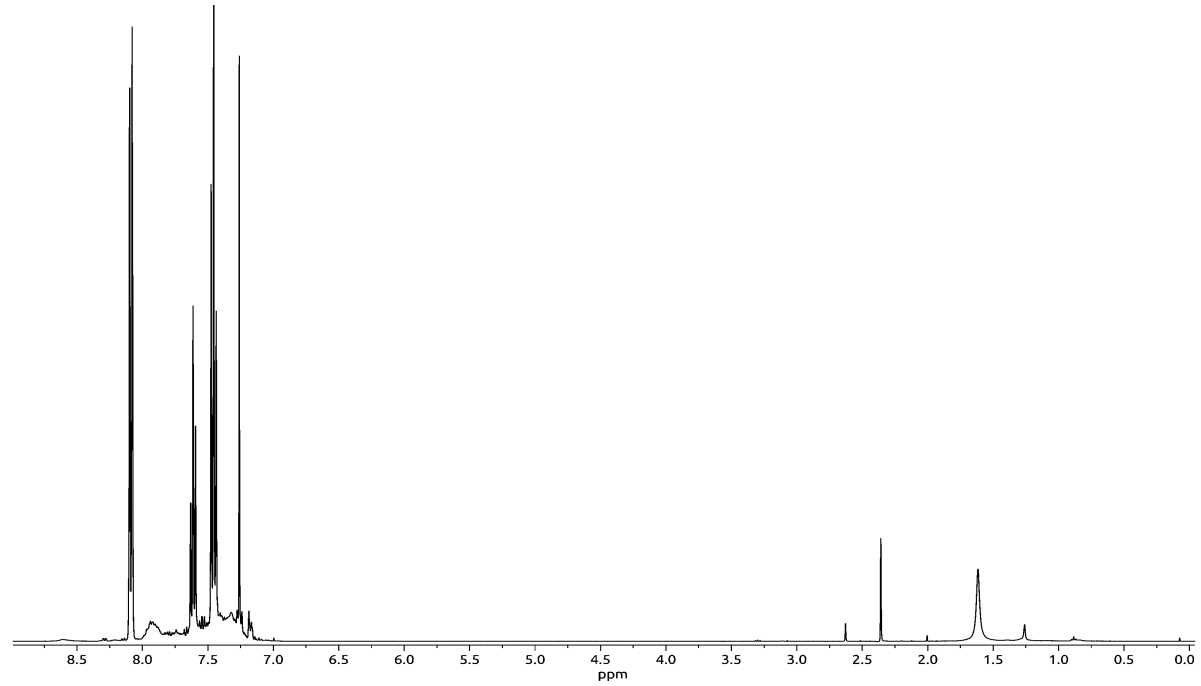

Figure E.5: ^{1}H-NMR spectrum of bis (dithio benzoate) (BDTB).

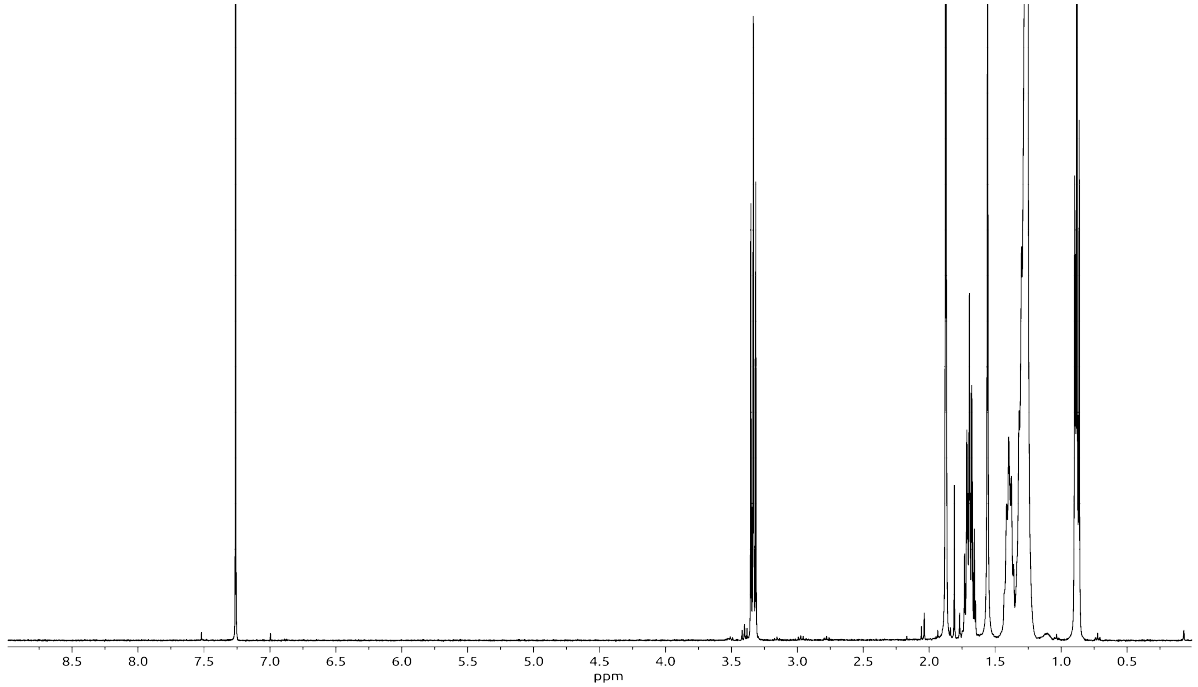

Figure E.6: ^{1}H-NMR spectrum of 2-cyano-2-propyldodecyl trithiocarbonate (CPDTC).

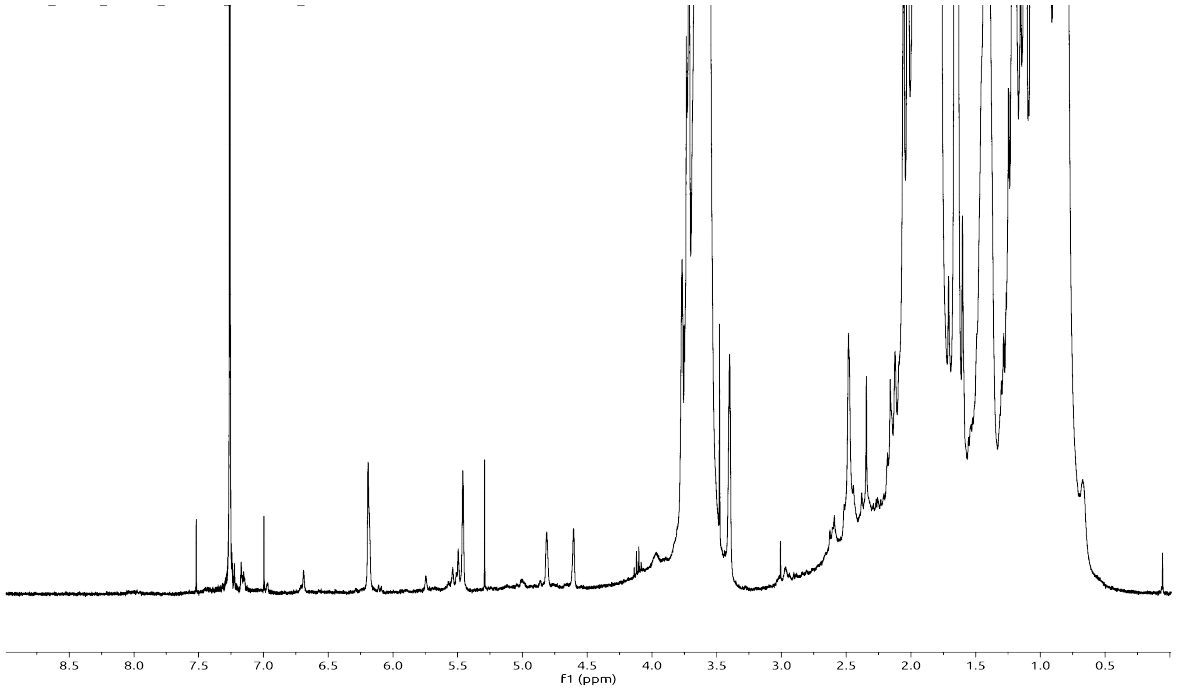

Figure E.7: ^{1}H-NMR spectrum of PMMA milled using stainless steel.

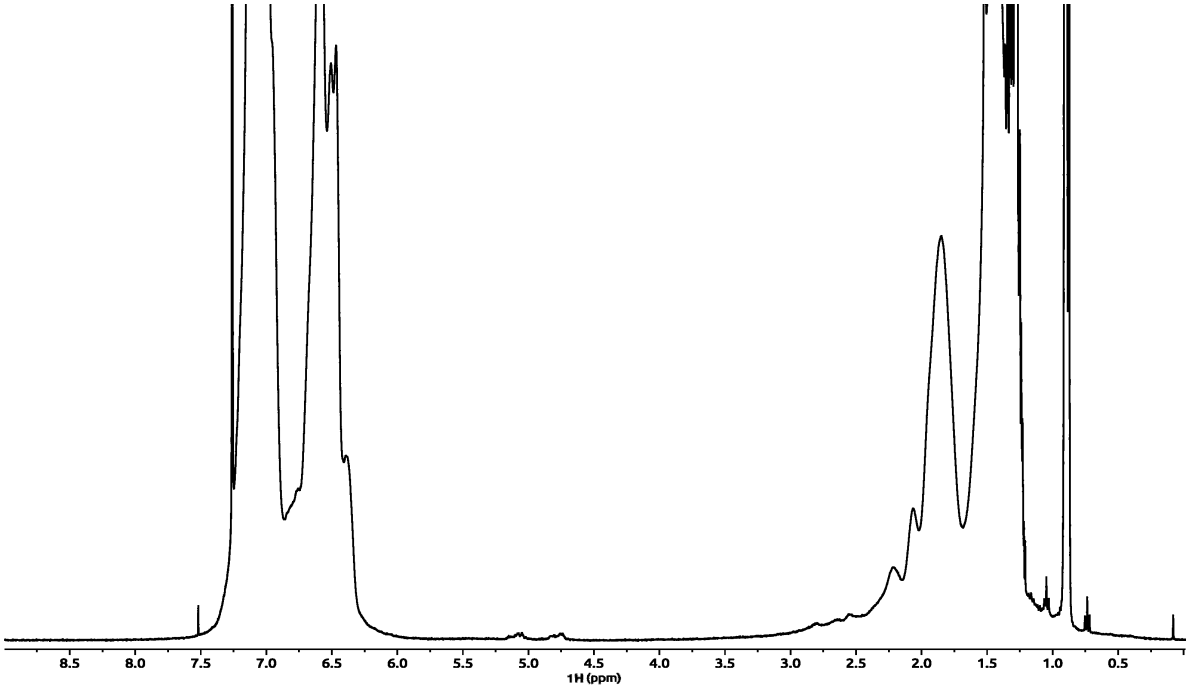

Figure E.8: ^{1}H-NMR spectrum of PS using stainless steel.

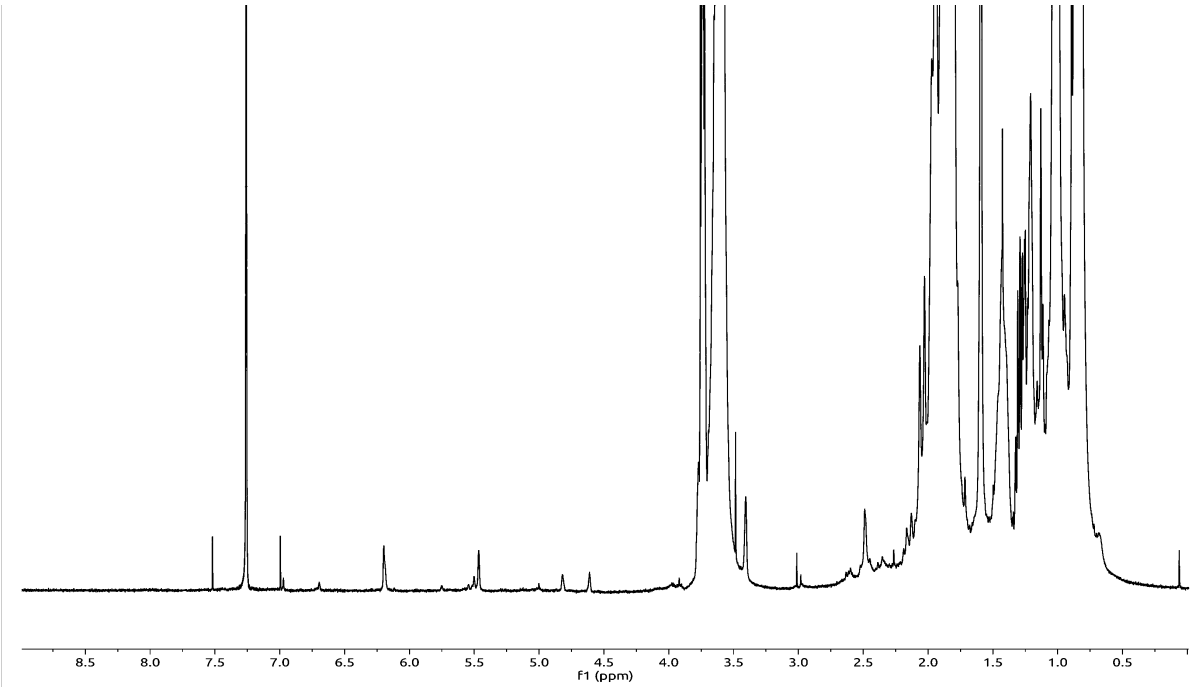

Figure E.9: ^{1}H-NMR spectrum of PMMA milled using ZrO_2.

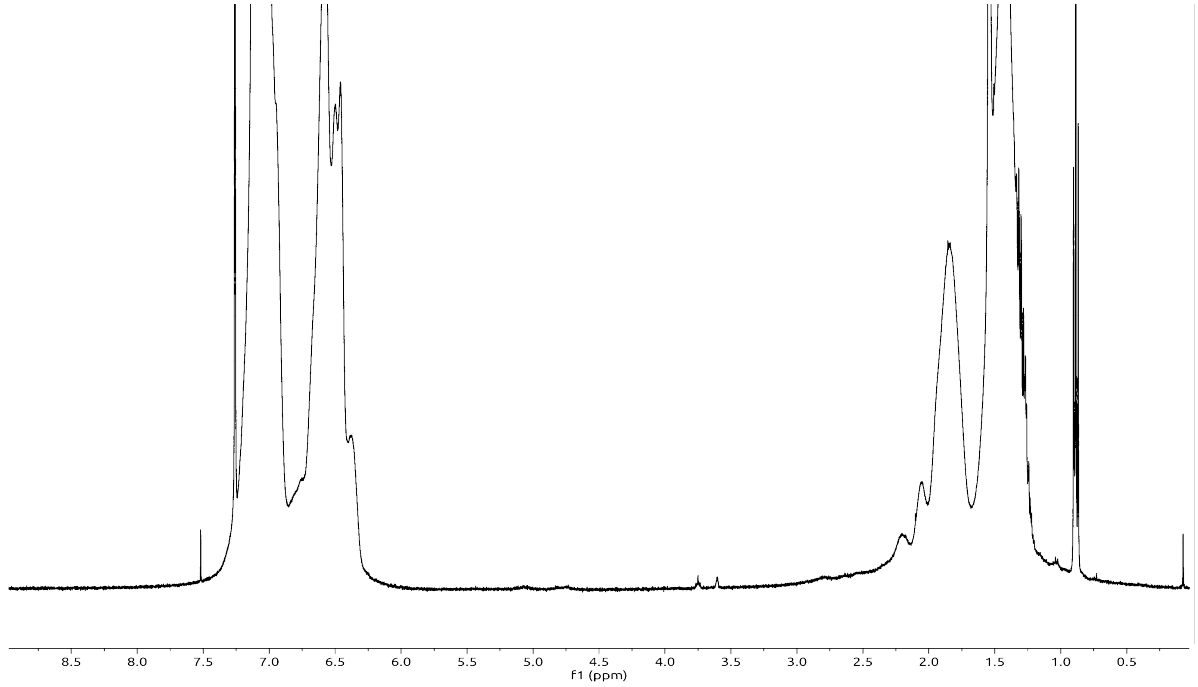

Figure E.10: ^{1}H-NMR spectrum of PS milled using ZrO_2.

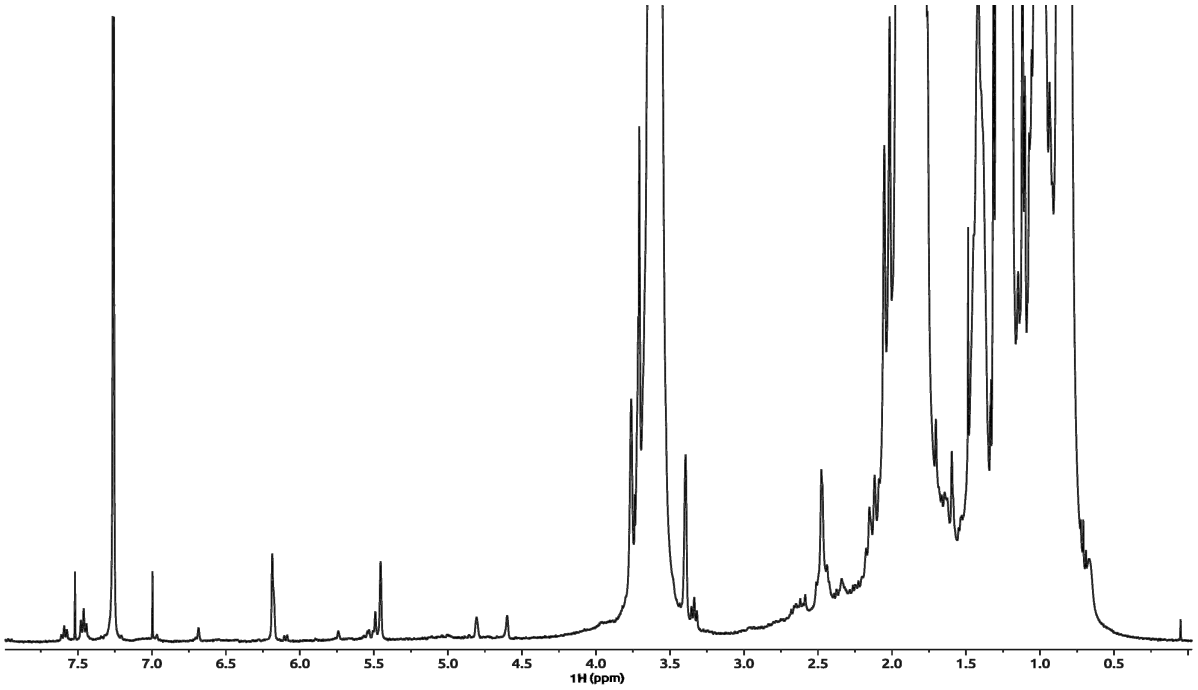

Figure E.11: ^{1}H-NMR spectrum of PMMA milled with BDTC using stainless steel.

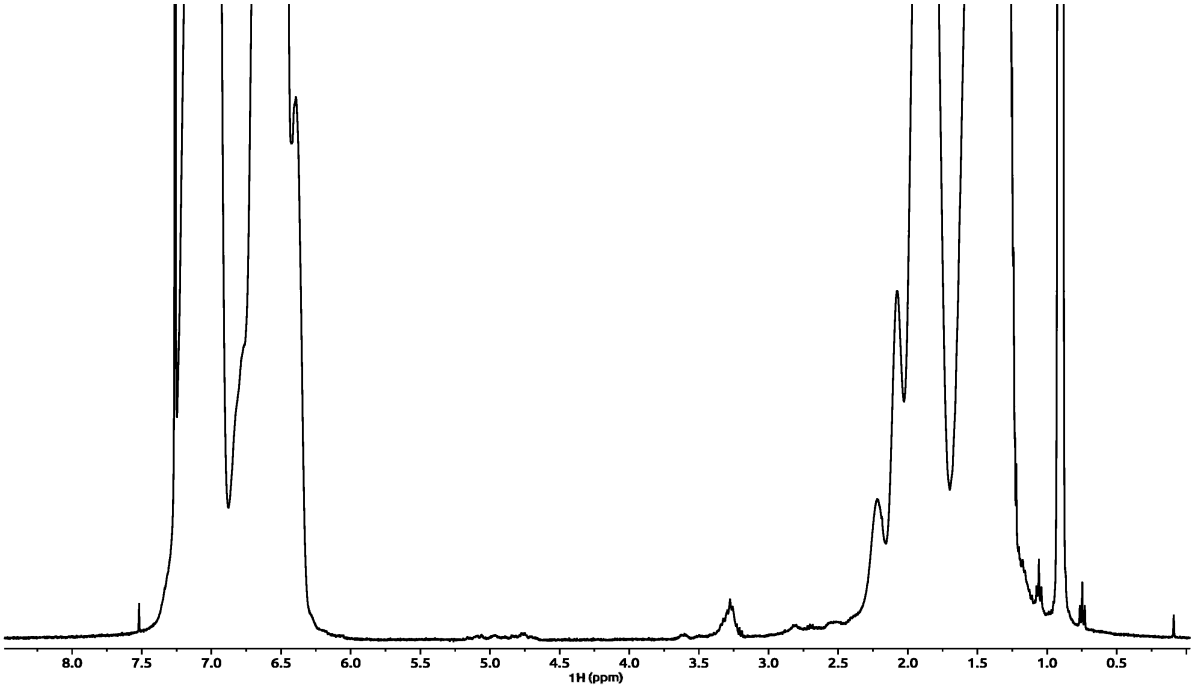

Figure E.12: ^{1}H-NMR spectrum of PS milled with BDTC using stainless steel.

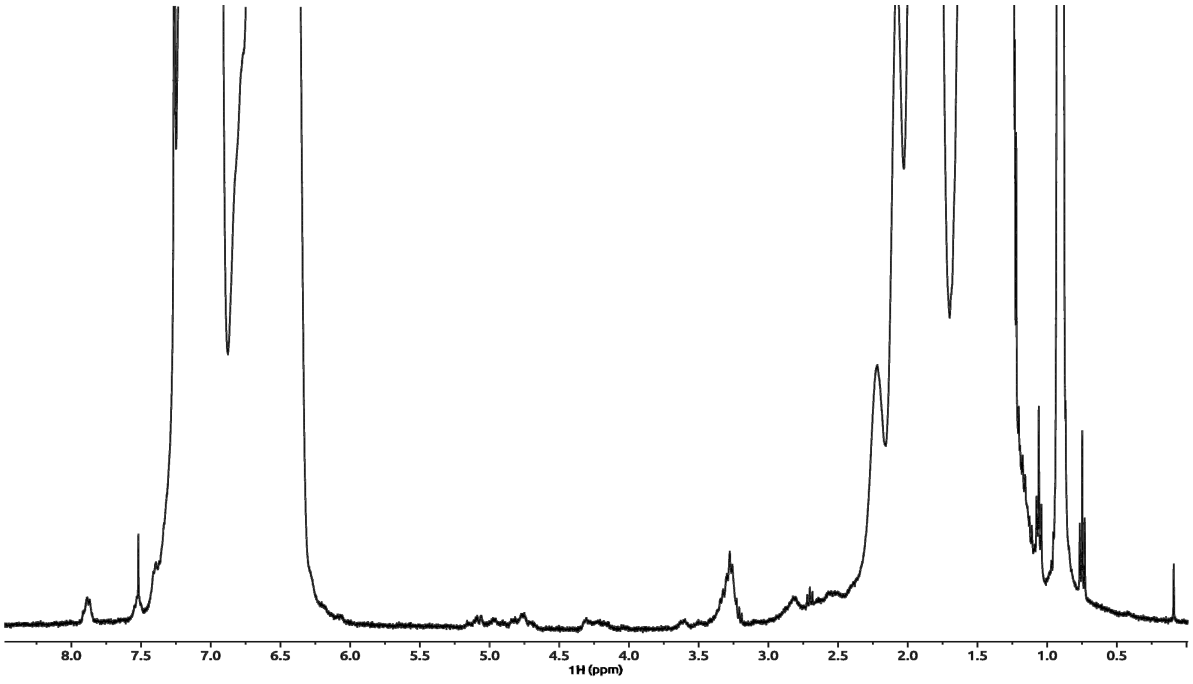

Figure E.13: ^{1}H-NMR spectrum of EPS milled with BDTC using stainless steel.

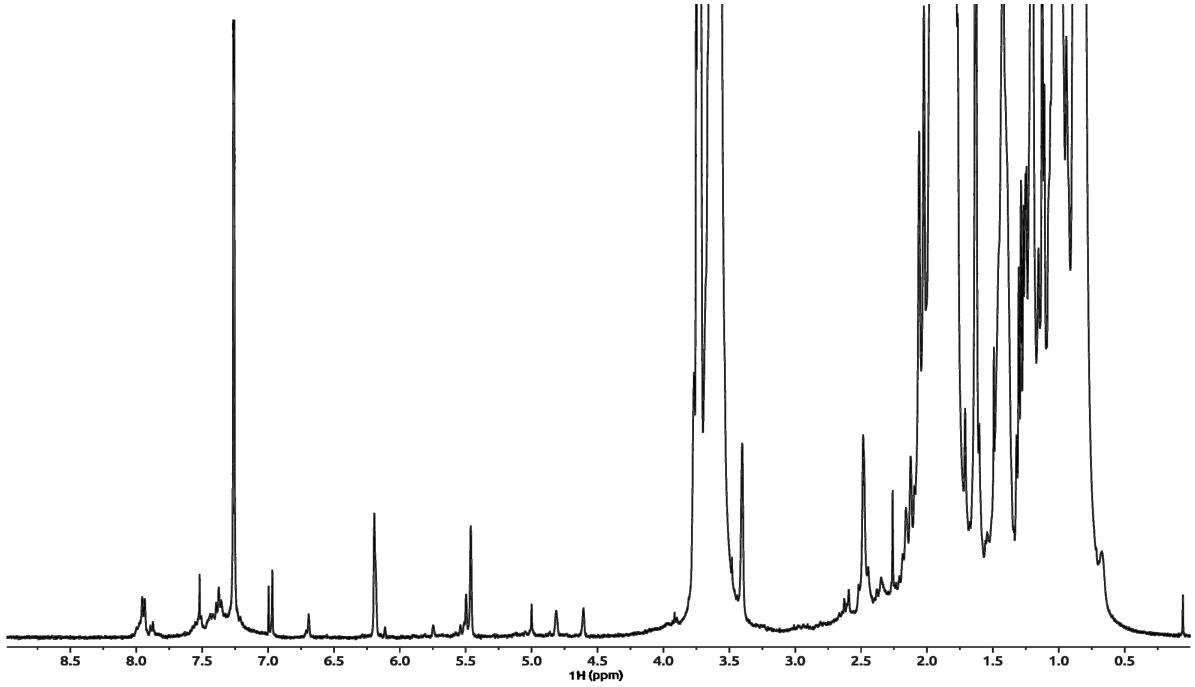

Figure E.14: ^{1}H-NMR spectrum of PMMA milled with BDTB using stainless steel.

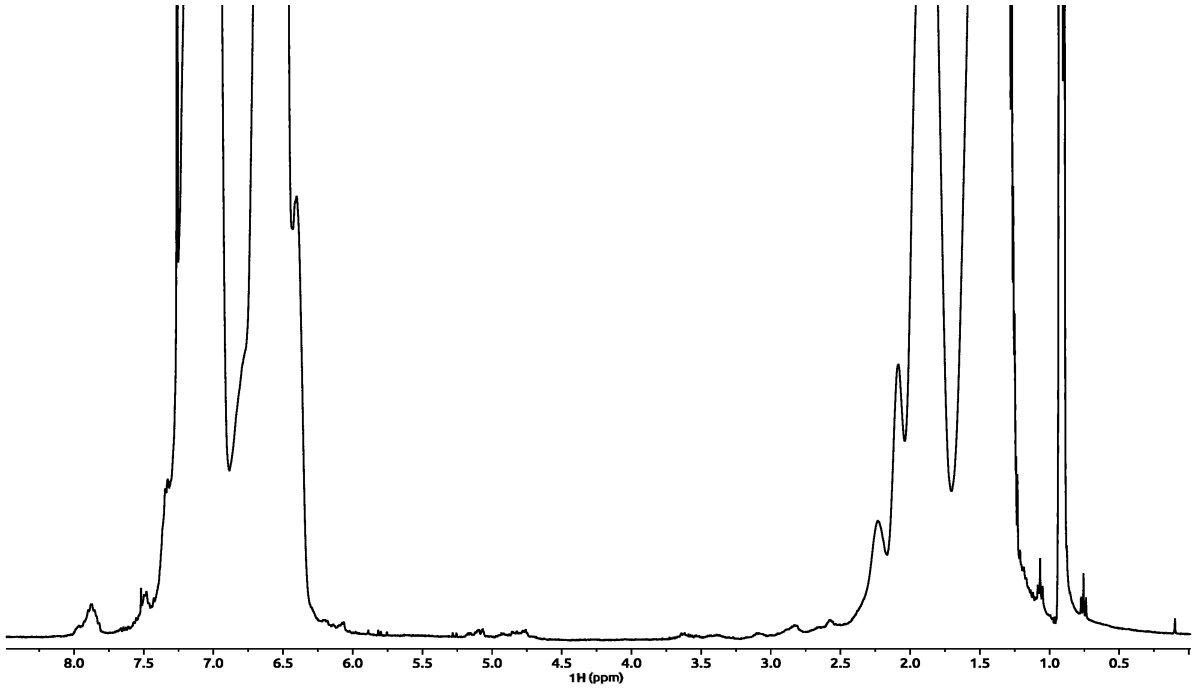

Figure E.15: ^{1}H-NMR spectrum of PS milled with BDTB using stainless steel.

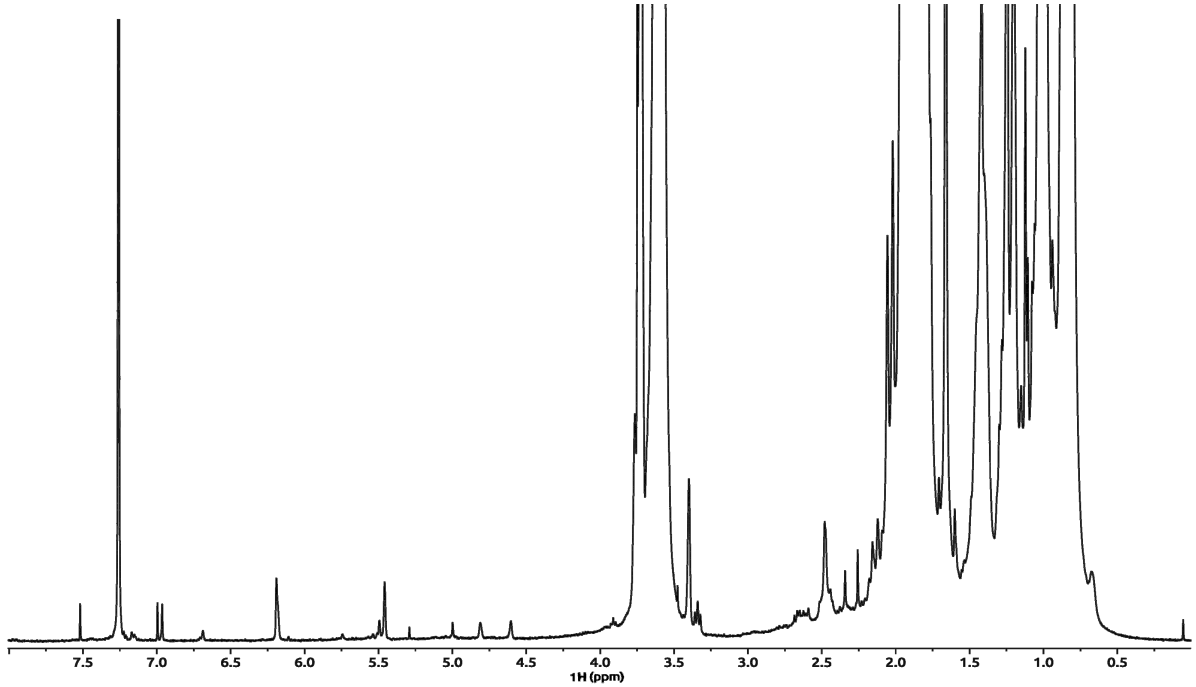

Figure E.16: ^{1}H-NMR spectrum of PMMA milled with BDTC using ZrO_2.

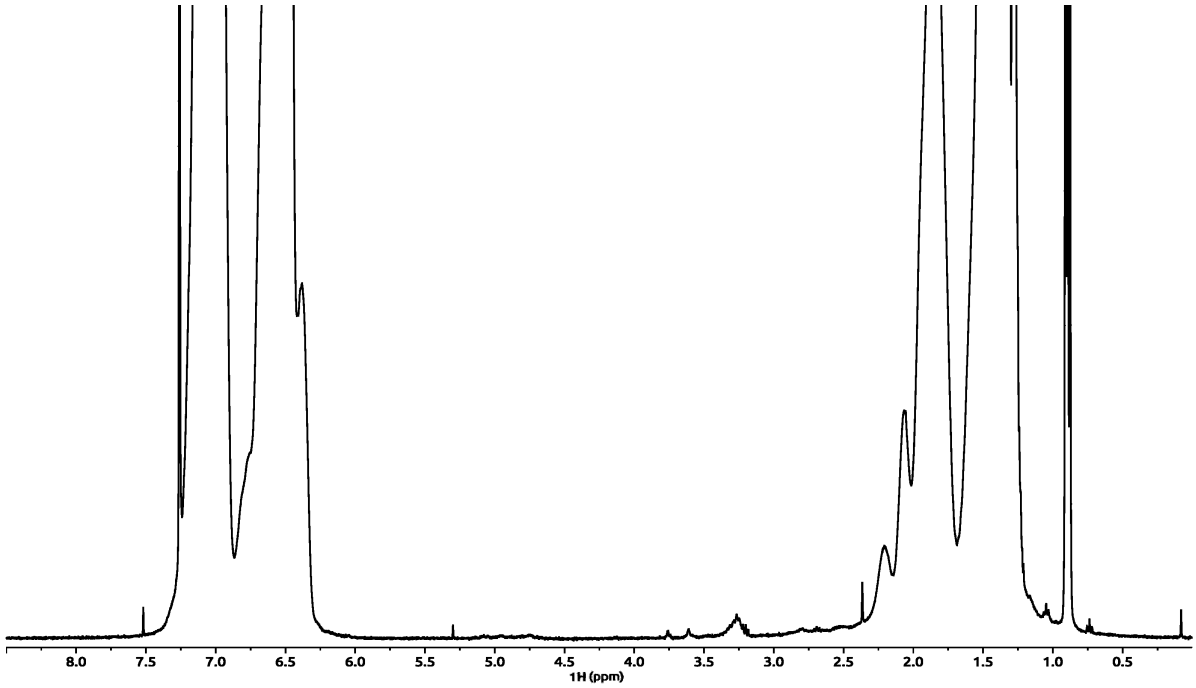

Figure E.17: ^{1}H-NMR spectrum of PS milled with BDTC using ZrO_2.

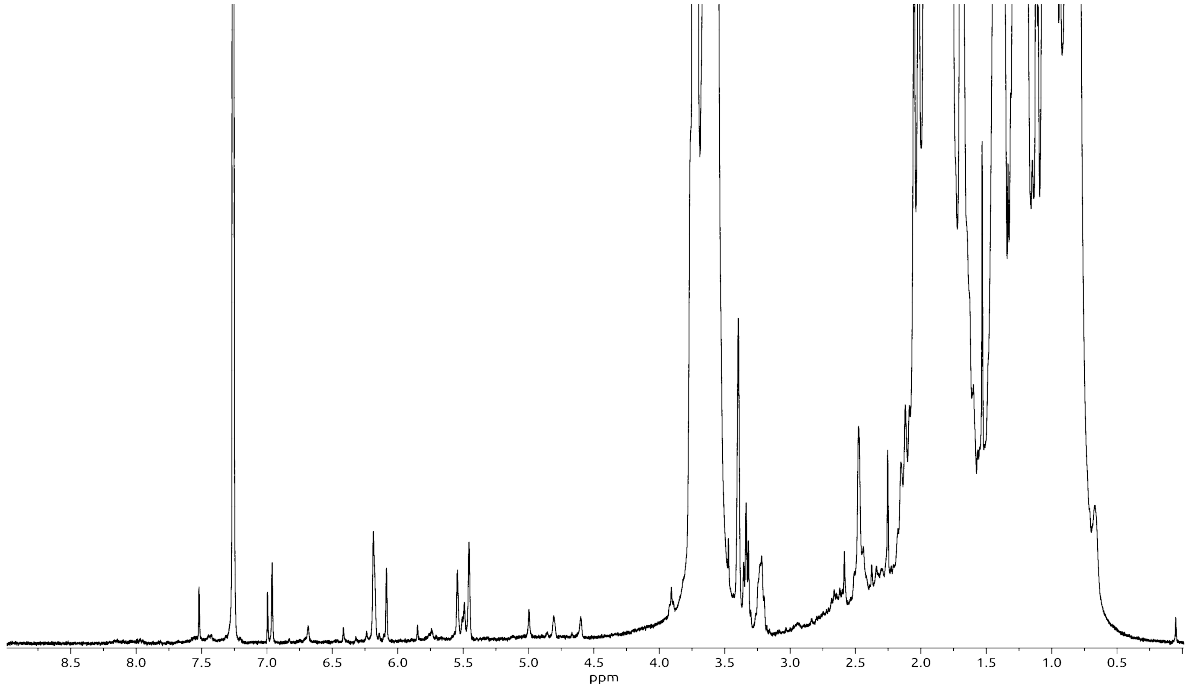

Figure E.18: ^{1}H-NMR spectrum of PMMA milled with CPDTC using stainless steel.

F

UV-Vis Absorption Spectra

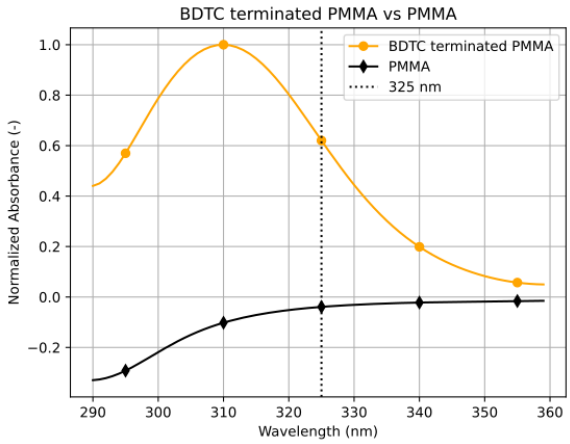

Figure F.1: Slice of a normalized UV-Vis absorption spectrum of BDTC terminated PMMA and bare PMMA.

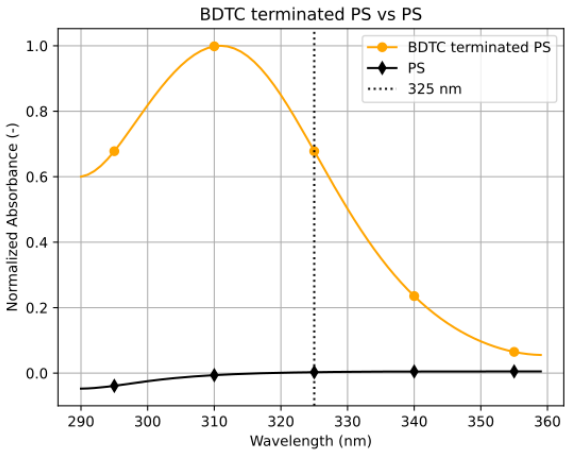

Figure F.2: Slice of a normalized UV-Vis absorption spectrum of BDTC terminated PS and bare PS.

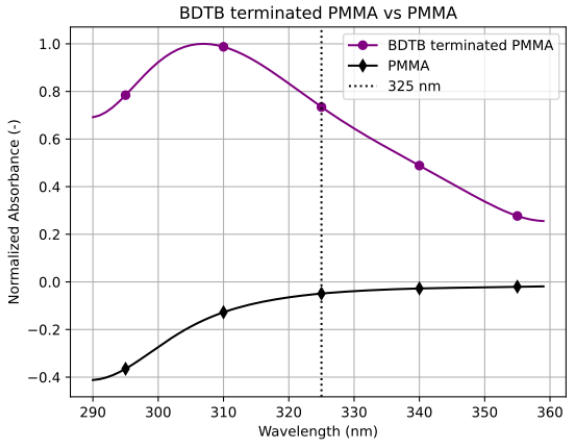

Figure F.3: Slice of a normalized UV-Vis absorption spectrum of BDTB terminated PMMA and bare PMMA.

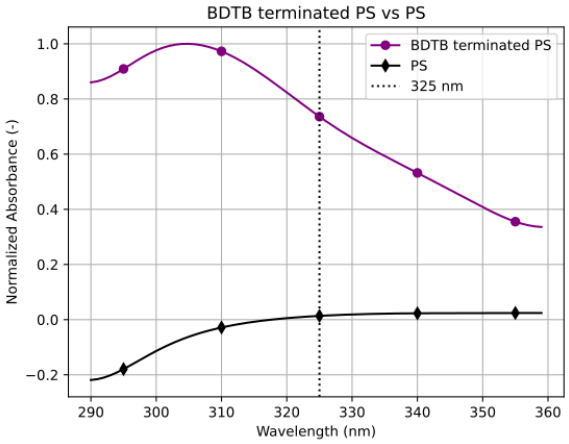

Figure F.4: Slice of a normalized UV-Vis absorption spectrum of BDTB terminated PS and bare PS.

G

DSC Heating Curves

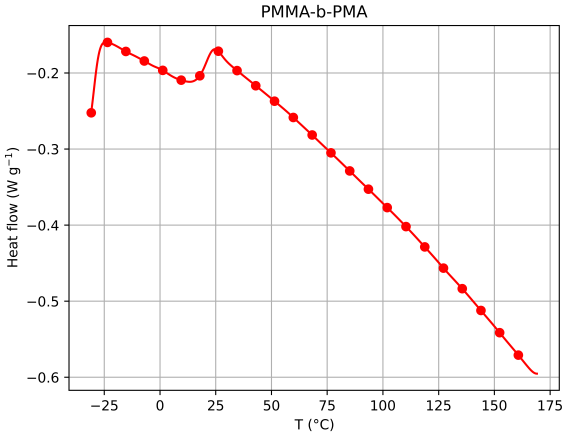

Figure G.1: Differential Scanning Calorimetry (DSC) heating curve of PMMA-b-PMA. Heating from -30 °C to 170 °C at a heating rate of 10 °C min^{-1}.

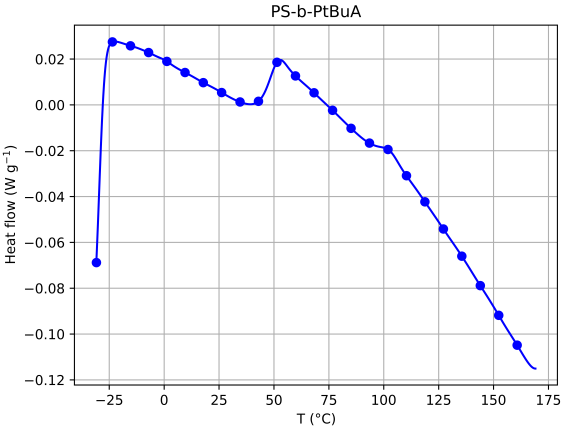

Figure G.2: Differential Scanning Calorimetry (DSC) heating curve of PS-b-PtBuA. Heating from -30 °C to 170 °C at a heating rate of 10 °C min^{-1}.

H

Atomic Force Miscoscopy Imaging

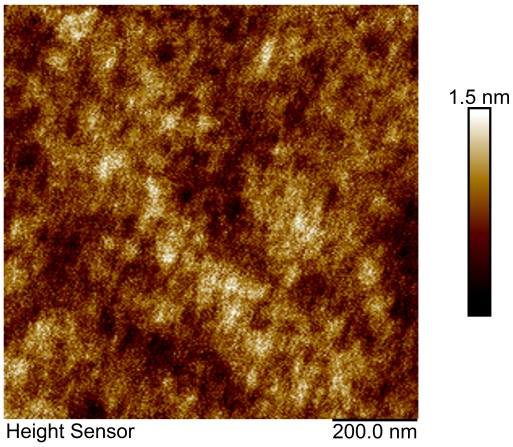

Figure H.1: Atomic Force Microscopy (AFM) height results for the PMMA-b-PMA block copolymer at a 1 µm scale.

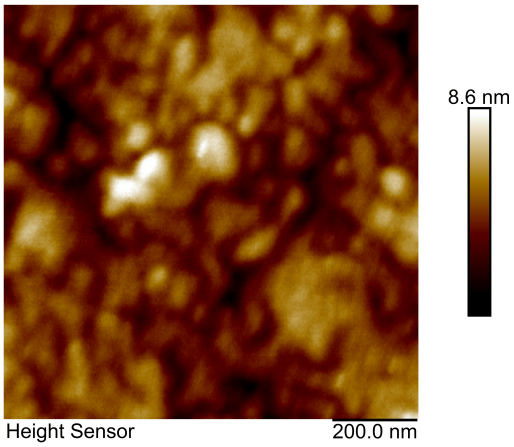

Figure H.2: Atomic Force Microscopy (AFM) height results for the PS-b-PtBuA block copolymer at a 1 µm scale. There are small microdomains formed of approximately 150 nm in size, with larger domains surrounding it. This is indicative of phase separation.

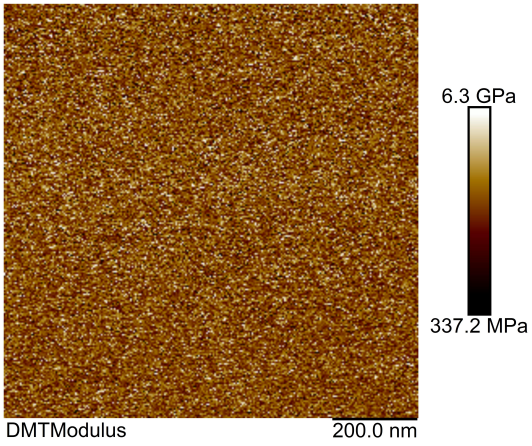

Figure H.3: Atomic Force Microscopy (AFM) nanoindentation results (measuring Young's Modulus E) for the PMMA-b-PMA block copolymer at a 1 µm scale. As is shown here, there is essentially only noise, meaning no microdomains form and therefore no phase separation is detected.

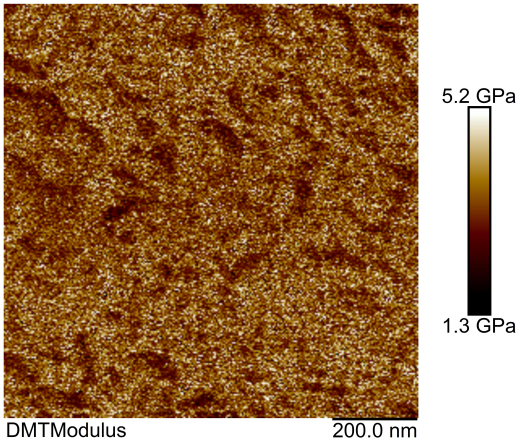

Figure H.4: Atomic Force Microscopy (AFM) nanoindentation results (measuring Young's Modulus E) for the PS-b-PtBuA block copolymer at a 1 µm scale. There are small microdomains formed of approximately 150 nm in size, with larger domains surrounding it. This is indicative of phase separation.